BULKY CYCLOPENTADIENYL CHROMIUM COMPLEXES AS ETHENE TRIMERISATION CATALYST PRECURSORS

A THESIS PRESENTED IN PARTIAL FULFILMENT OF THE DEGREE

MASTER OF SCIENCE

IN THE DEPARTMENT OF CHEMISTRY,
UNIVERSITY OF CAPE TOWN

BY

BURGERT BLOM (JR.)

BSc (Mathematics) University of Pretoria; BSc (HONS), University of Cape Town.

Department of Chemistry

University of Cape Town
Rondebosch
7701
South Africa.

August 2004.

BULKY CYCLOPENTADIENYL CHROMIUM COMPLEXES AS ETHENE TRIMERISATION CATALYST PRECURSORS

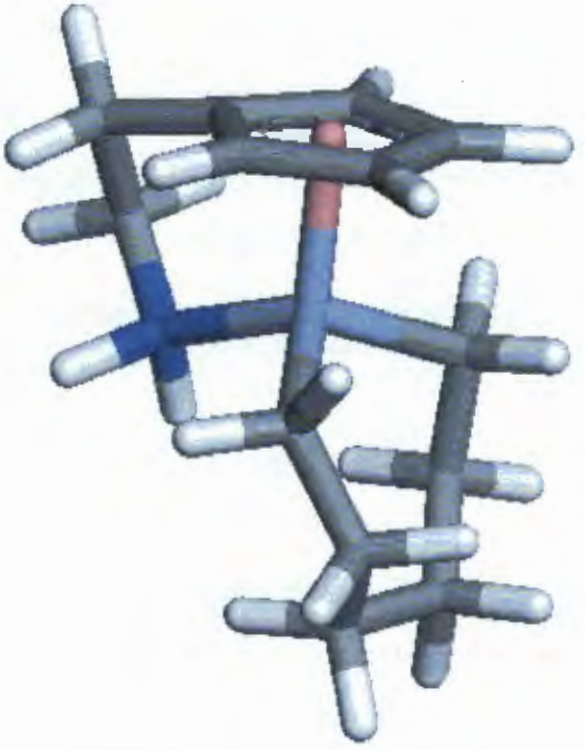

A model of a metallacycle of chromium, isolated by Jolly and co-workers. A key intermediate in this project.

BURGERT BLOM (JR.)

BSc (Mathematics) University of Pretoria; BSc (HONS), University of Cape Town.

Look around,
The grass is high,
The fields are ripe,
It's the springtime of my life.

Excerpt from "A Hazy shade of Winter"
Paul Simon, 1966

Abstract

The process of ethene trimerisation to 1-hexene, has recently attracted considerable interest, in light of the usefulness of 1-hexene industrially.

In this project the process of catalytic ethene trimerisation, using bulky cyclopentadienyl chromium complexes was investigated. Firstly, a series of known and novel bulky cyclopentadiene ligands, of the type, C_5Ph_4RH (R = H, alkyl, aromatic or substituted aromatic group) were synthesised. Four routes were investigated. (i) Making use of an *in situ* generated *bis*-lithium intermediate, resulting in the formation of 1,2,3,4,5-pentaphenyl cyclopenta-1,3-diene and 1,2,3,4-tetraphenylcyclopenta-1,3-diene. (ii) The attempted use of a metallation / alkylation route which was unsuccessful. (iii) The use of tetracyclone as starting material, reacted with alkyl likthium reagents, or alkyl Grignard reagents which resulted in the formation of ligands, of the type C_5Ph_4R, with R in the 5 position of the ring (R = *n*-butyl, *tert*-butyl, hexyl). Unexpected side reactions afforded the isolation of two ligands of the type C_5Ph_4R, R = 1-propeneyl and ethyl, both with the terminal alkene function, saturated. (iv) The use of a Pd catalysed route, making use of Cp_2ZrCl_2 as source of cyclopentadiene, resulted in the successful isolation of the cyclopentadiene, C_5Ar_5H (Ar = $C_6Me_2H_3$). All new compounds were successfully characterised using NMR, IR, MS and elemental analysis. A stable Fe(II) model complex, *bis*-tetraphenylcyclopentadienyl iron, was prepared and cyclic voltametry conducted on it, to investigate the effect of phenyl substituents on a Cp ligand in the reduction / oxidation potential of the iron(II) centre. This study showed that phenyl rings on a cyclopentadiene ligand have a significant effect on the redox potential of Fe(II); this trend could possibly be expected with other metals, in particular chromium.

Possible trimerisation catalyst precursors of the type $[(C_5Ar_nH_{5-n})CrCl_2]_2$ (Ar = Ph or $C_6Me_2H_3$), were next synthesised. A route making use of a radical to form target dinuclear Cr complexes was looked at, but was not particularly successful. A convenient route using $CrCl_3(thf)_3$ and a sodium or potassium salt of the ligands prepared resulted in the isolation and characterisation of $[(C_5Ph_5)CrCl_2]_2$, $[(C_5Ph_4H)CrCl_2]_2$, $[(C_5Ar_5H)CrCl_2]_2$ (Ar = $C_6Me_2H_3$) , all dinuclear *pseudo*-octahedral Cr(III) complexes. EPR spectroscopy on $[(C_5Ph_5)CrCl_2]_2$ and $[(C_5Ph_4H)CrCl_2]_2$ in weakly co-ordinating dichloromethane, at low temperatures demonstrated the presence of an equilibrium between the dinuclear complex and the monomer. EPR spectra showing signals typical of mononuclear Cr(III) with S = 3/2 were observed, supporting this dissociation hypothesis. The X-ray crystal structure of $CrCl_3(thf)_3$ was determined with an R value of 3.3 %.

High pressure testing of a catalytic system containing the cyclopentadiene ligands; together with Cr-2-ethyl hexanoate, triethylaluminium and hexachloroethane was investigated. Catalytic testing of one of the model complexes, $[(C_5Ph_5)CrCl_2]_2$, demonstrated not only catalytic activity towards ethene trimerisation, but a link between the activity and selectivity of the model complex, and the *in situ* system. This result has shed light on the nature and structure of the catalytic precursor.

Density Functional Theory (DFT) studies were also conducted on a representative catalytic precursor species, $CpCrMe_2$, using Materials Studio™. In the first instance, the role of the alkylating agent (typically triethylaluminium) was neglected, and a series of geometry optimisations and transition state searched conducted on the catalytic process starting from $CpCrMe_2$. The process was investigated in a stepwise fashion until formation of the product, 1-hexene. High energy barriers were identified along the pathway, particularly in the last step of the process, where an energy barrier of 88 $kJ.mol^{-1}$ was identified. The addition of an alkylating agent was also investigated, at two key high energy stages. It was found on both occasions that the presence of an alkylating agent significantly reduces the energy barriers, by providing a more stable transition state, and hence a lower energy pathway. In this instance, the oxidation state of the chromium was four, as opposed to three looked at in all our earlier calculations. Finally, the system, CpPhCr was investigated. It was found that the addition of a phenyl ring onto the Cp moiety has a significant effect on sequential ethene binding energies. Hence, the importance of the phenyl rings in the catalytic ethene trimerisation process was highlighted.

List of Abbreviations

General (including DFT work)

Cp	–	cyclopentadienyl
Cp*	–	pentamethylcyclopentadienyl
CpPh	–	phenylcyclopentadienyl
CV	–	cyclic voltametry
DFT	–	Density Functional Theory
dg	–	diglyme
DMF	–	dimethylformamide
$E_{1/2}$	–	half wave potential
EI	–	electron impact
E_{pa}	–	anodic peak potential
E_{pc}	–	cathodic peak potential
FAB	–	fast atom bombardment
MeOH	–	methanol
mp	–	melting point
m/z	–	mass to charge ratio
MS	–	mass spectrometry
n-BuLi	–	n-butyllithium
NEB	–	nudged elastic band
R_f	–	ratio of movement of solute to solvent in TLC
tert-BuLi	–	*tertiary*-butyllithium
TEA	–	triethylaluminium
TMA	–	trimethylaluminium
THF	–	tetrahydrofuran
TLC	–	thin layer chromatography
TS	–	transition state

Infra-red spectroscopy (IR)

br	–	broad band
m	–	medium band
s	–	strong band
v	–	very strong band
w	–	weak band

Nuclear Magnetic Resonance Spectroscopy (NMR)

Ar	–	signals arise from aromatic group
d	–	doublet
dd	–	doublet of doublets
^{IV}C	–	quaternary carbon atom
m	–	multiplet
t	–	triplet
^{x}J	–	Coupling over x bonds
Ph	–	signals arising from phenyl group specifically

Conference contributions and manuscripts for publication

1. G. Klatt, B. Blom and J. R. Moss, Computational investigation of a CpCr ethene trimerisation system, *1st Cape Organometallic Symposium,* Morgenhof, poster presented, 2003.

2. B. Blom and J. R. Moss, Bulky cyclopentadienyl chromium ethene trimerisation, *1st Cape Organometallic Symposium, Morgenhof,* oral presentation, 2003.

3. B. Blom and J. R. Moss, EPR investigation of bulky cyclopentadienyl chromium ethene trimerisation catalyst precursors, *37th SACI Conference,* Pretoria, oral presentation, 2004.

4. B. Blom, J. R. Moss, E. Nordlander and A. Magnusson, Chemistry of complexes of the type $[(C_5Ph_nH_{6-n})CrCl_2]_2$ in weakly coordinating solvents, *Manuscript in preparation,* 2004.

5. G. Klatt, B. Blom and J. R. Moss, Computational investigation of ethene trimerisation catalysed by chromium complexes, *Manuscript in preparation,* 2004.

6. B. Blom, M. J. Overett and J. R. Moss, Late transition metal imine complexes, *Dalton Discussion 6, York University, York, UK,* 2003.*

7. B. Blom, J. R. Moss, A. Bollmann and J. Dixon, Catalytic trimerisation of ethene using bulky cyclopentadienes, *Manuscript in preparation,* 2004.

8. B. Blom, J.R. Moss and M. J. Overett, Late transition metal imine complexes, *Inorganic 2003 Conference,* poster presentation, 2003.*[1]

[1] * Earlier work presented during the course of *this* project.

Acknowledgements

A research project of this magnitude is not ones own doing. I would like to take this opportunity to thank some people for their input, guidance and support through out this degree.

Firstly, my supervisor, Prof. John Moss, thanks for everything. What I have learnt from you has become indispensable in my career as a scientist. Then, Dr. Ebbe Nordlander and Prof. Susan Jagner, who were most gracious hosts and mentors whilst on the exchange program in Sweden. This too was a wonderful experience, and I managed to obtain data not possible in South Africa. To Dr. Gunter Klatt, an "un-official" supervisor – thanks for the help, time and effort with the Molecular modeling. Of course, my industrial supervisors deserve a huge thank-you, Dr Annette Bollmann, and Dr Johntho Dixon. Sasol, the company that funded this research, and took the interest to invest in my future deserves a lot of credit for this work. Also, to Bjorn, Viktor and Katja (from Sweden) – you have all become friends of mine.

Then, to the technical staff of the department, Noel, Pete, Sweetness, the list is endless – many thanks. The people in the Organometallics lab over the years, my first mentor, Dr. Matthew Overett, who has also become a close friend, thanks. Reinout, we had our disagreements, but I learned a lot from you too (and had some great parties in Obs !!). Also, to Prof. Alan Hutton, for supporting me and encouraging me – thanks Prof ! There are so many wonderful people in this department that I must thank for being there and supporting me in my darkest hours, Pamela, Kirsten, Siya, Claire, Meredith, Sonja, Chas, Karen – the list is endless: you have all become very special to me, thanks guys !

To Prof. Danita de Waal, for running the FT-IR spectra of the Cr complexes – thanks. To Dr. Sjoerd Harder, for the collaborative work on some of the ligand design, and Cr complex synthesis, I learned a great deal from you, and will remember our day sailing in Simon's town fondly! I would also like to thank Dr. Hong Su for solving the crystal structure reported here.

There are some other special people in my life that I must also thank. These are people who are not scientists, but very special to me. Firstly, my best friend Karin – what would I do without you ? Then, Catherine, Arthur and Quintin (all who live in London) – you are and always will be special – thanks for the support. Kaja, how could I forget all your input (and our December holiday in Cape Town !) – thanks !

Finally, my parents, to which I dedicate this thesis. Thanks for your great parenting – this thesis is thanks to all your stimulation and support in my youth.

List of compounds in this thesis

Number of Compound	Materials Studio *Model*	Structure / Formula / Shorthand representation	Characterisation
2.1	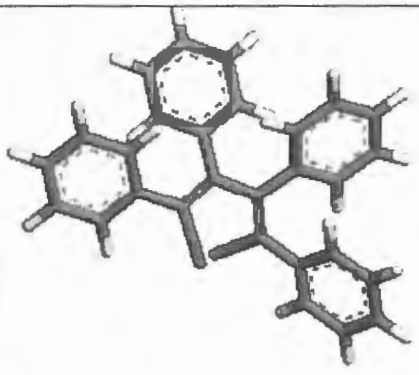	$C_4Ph_4Li_2$	^1H NMR
2.2	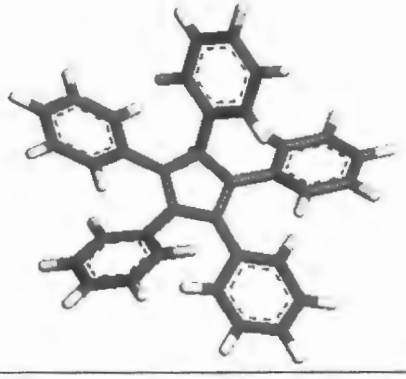	C_5Ph_5H	^1H , ^{13}C NMR
2.3	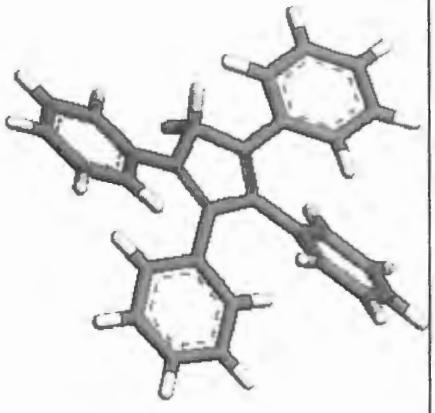	$C_5Ph_5H_2$	^1H , ^{13}C NMR

2.4	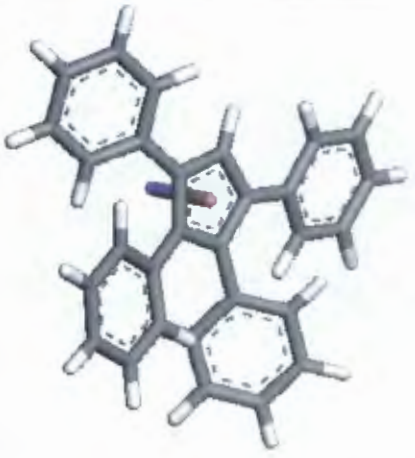	$Na[C_5Ph_4H]$	^{1}H , ^{13}C NMR
2.5	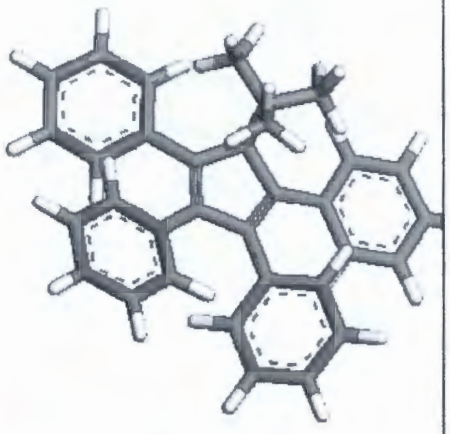	$C_5Ph_4(^{t}Bu)H$	^{1}H , ^{13}C NMR, IR, MS, EA.
2.6	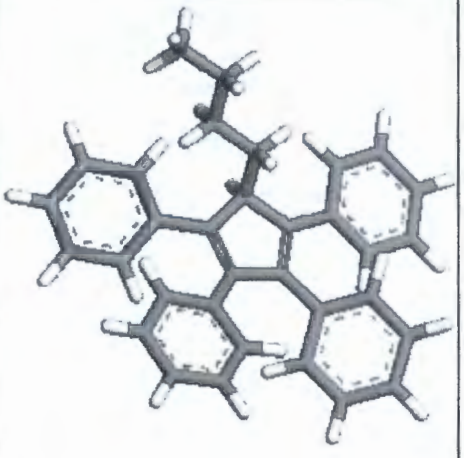	$C_5Ph_4(^{n}Bu)H$	^{1}H , ^{13}C NMR, IR, MS, EA.

2.7	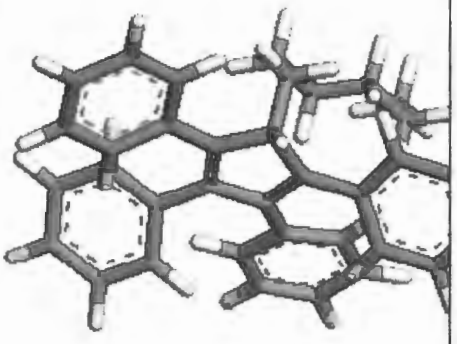	$C_5Ph_4(C_6H_{13})H$	^1H , ^{13}C NMR, IR, MS, EA.
2.8	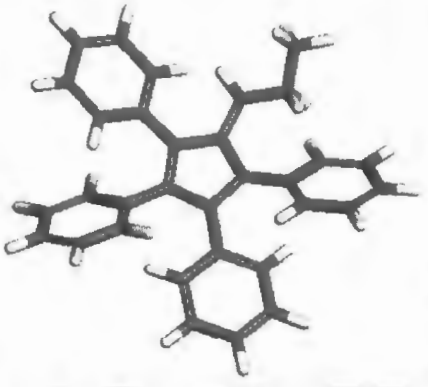	$C_5Ph_4(C_3H_6)H$	^1H , ^{13}C NMR, IR, MS, EA.
2.9	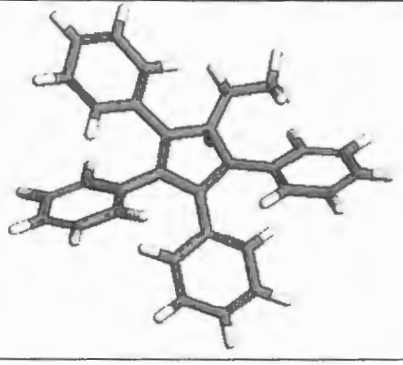	$C_5Ph_4(C_2H_6)H$	^1H , ^{13}C NMR, IR, MS, EA.

2.10	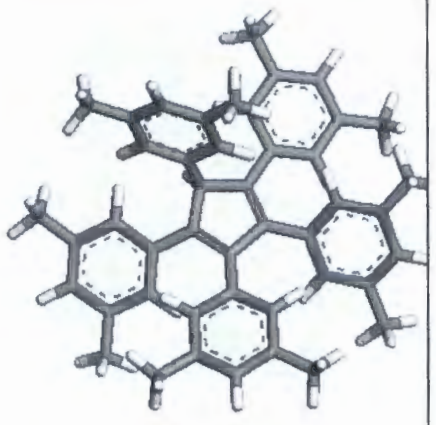	C_5Ar^*H, $Ar^* = C_6Me_2H_3$	^1H , ^{13}C NMR
3.1	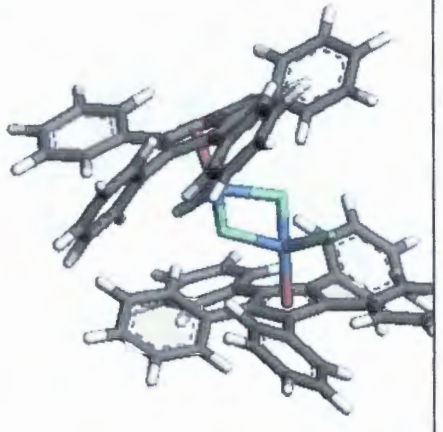	$[(\eta^5 C_5Ph_5)CrCl_2]_2$	^1H , ^{13}C NMR, IR, MS, EPR, EA
3.2	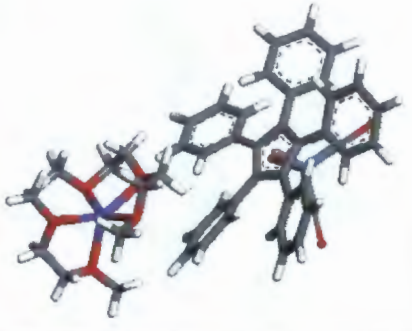	$[Na(dg)]_{3/2}$ $[(\eta^5 C_5Ph_5)Cr(CO)_3]$	IR

3.3		$CrCl_3(thf)_3$	IR
3.4	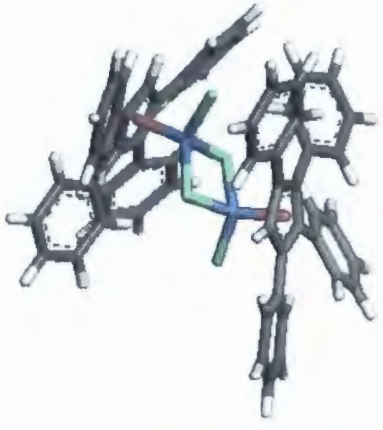	$[(\eta^5 C_5Ph_4H)CrCl_2]_2$	^1H , ^{13}C NMR, IR, MS, EA, EPR
3.6	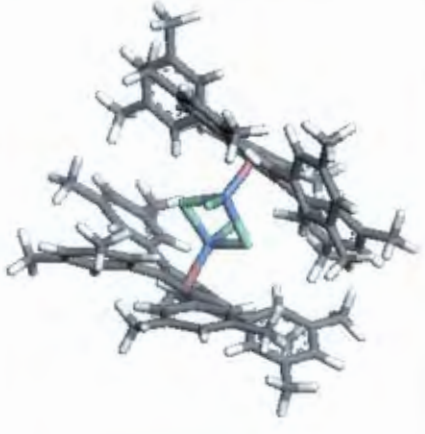	$[(\eta^5 C_5Ar^*_5)CrCl_2]_2$	^1H , ^{13}C NMR, IR

3.8	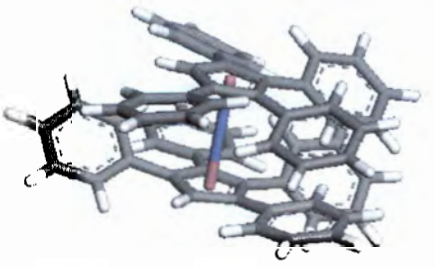	(η^5 $C_5Ph_4H)_2Fe$	NMR, MS, EA, CV.

Table of Contents

Topic	Page number
Abstract	i
Abbreviations	iii
Conference proceedings	v
Acknowledgements	vi
Index of Compounds Synthesised in this project	vii
Chapter 1 : Introduction and Overview	1
1.1 Organometallic compounds in selective alkene oligomerisation	1
1.2 Examples of selective ethene trimerisation catalysts	3
1.3 System of focus in this dissertation	6
1.4 Succinct overview of dissertation	8
Chapter 2 : Synthesis of bulky cyclopentadienes	10
2.1 A brief introduction to cyclopentadienes as ligands in organometallic chemistry	10
2.2 Bulky Cyclopentadienyl ligands	12
2.2.1 Increased steric crowding	13
2.2.2 Increased stability of otherwise sensitive complexes	13
2.2.3 Conjugation effects	14
2.3 Synthetic routes	15
2.3.1 The use of a dilithium reagent	15
2.3.2 The use of a metallation / alkylation pathway.	17
2.3.3 The use of an alkyl lithium or Grignard reagent	19
2.3.4 The use of palladium-catalysed reactions of metallocenes with aryl bromides	24

2.4 Summary and conclusions of this chapter 25

Chapter 3 : Synthesis of Model Complexes to shed light on the ethene trimerisation process 26

3.1 Introduction 26

3.2 Another look at the system focused on in this project 26

3.3 Synthesis of Chromium Cyclopentadieneyl model complexes 27

3.4 Characterisation of the model complexes 32

3.4.1 FT-IR Spectroscopy. 32
3.4.2 Raman Spectroscopy 34
3.4.3 Electron-spin paramagnetic resonance spectroscopy (EPR). 34

3.5 NMR studies on Cr(III) model complexes 38

3.6 Discussion of EPR and NMR data of Cr(III) model complexes 41

3.7 Elemental analysis 41

3.8 Mass Spectrometry 41

3.9 Synthesis of other transition metal model complexes 41

3.9.1 Preparation of Bulky Iron(II) sandwiches 42

3.10 Single Crystal X-Ray Diffraction Studies 45

Chapter 4 : Catalytic Studies on Model Complexes and Cyclopentadieneyl Ligands 52

4.1 Introduction and overview 52

4.2 Catalytic results 54

4.3 Discussion 56

Chapter 5 : Density Function Theory and Transition State Theory : An Introduction 58

5.1 Introduction and background to DFT (Density Functional Theory) 58

5.2 DFT Methods at a glance 59

5.3 Computational Accuracy and Performance 61

5.4 The transition state theory (TS) 62

Chapter 6 : Molecular Modeling Studies on CpCr(III) Trimerisation System 65

6.1 Introduction to molecular modeling 65

6.2 Finding minimum energy configurations of molecules 65

6.2.1 DFT (Density functional theory) approach. 67
6.2.2 Catalyst precursor activation. 70
6.2.3 Catalyst precursor generation (neglecting the role of the alkylating agent). 70
6.2.4 The catalytic process 72

6.3 Transition state (TS) searches 73

6.3.1 DFT Approach 73
6.3.2 Transition states in the catalyst precursor generation step 79
6.3.3 Transition states in the catalytic process 79

6.4 The role of the alkylating agent 79

6.5 The role of the phenyl groups 82

6.6 Free energy profile of catalyst precursor generation and catalytic cycle 87

6.7 Discussion and conclusion of DFT work 89

Chapter 7 : Conclusions Discussion and Future Work 90

7.1 Brief summary of thesis results : global perspective 90

7.2 The synthetic approach in a "nut shell" 90

7.3 The catalytic studies in a "nut shell" 91

7.4 The molecular modeling investigation in a "nut shell" 91

7.5 Future work 92

7.5.1 Additional Synthetic work 92
7.5.2 Additional Catalytic work 94
7.5.3 Additional Molecular Modeling 94

Chapter 8 : Experimental 95

8.1 General experimental details 95

8.2 Solvents and materials 95

8.3 Instrumentation 96

8.4 Experimental details pertaining to Chapter 2 97

8.5 Experimental details pertaining to Chapter 3 103

8.6 Catalytic reaction conditions and work-up 107

Chapter 9 : References 108

Appendix 113

A1 - Additional Crystal Data 113

A2 – Tabulated Catalytic Results 121

Chapter 1

Introduction and a review of selective ethene oligomerisation.

"All paid jobs absorb and degrade the mind."
Aristotle

1.1 Organometallic compounds in selective alkene oligomerisation

The discovery of Ziegler-Natta type catalysis in the late 1950s[1] heralded a new era in the polymerization of ethene. Research into catalysts that polymerise ethene and other alkenes, has attracted considerable attention, industrially and academically.[2] In the last two decades, research into homogeneous catalysts (more specifically metallocene catalysts) has been fostered by the desire to engineer catalysts that are capable of tailoring new products (See Figure 1.1).[2]

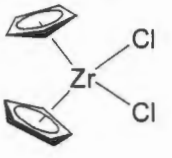

Figure 1.1 A classical zirconium metallocene catalyst used industrially as a polymerisation catalyst precursor.

In the case of Ziegler-Natta and metallocene catalysed polymerization of ethene, the widely accepted Cossee-Arlmann mechanism [3] is believed to be responsible (Scheme 1.1). Recently, studies on model complexes by Casey *et al.*, resembling proposed intermediates in the Cossee-Arlmann mechanism, have lent further support to this mechanism. [4] Here, metal-alkyl-alkene Y and Zr complexes were studied, and the rate of alkyl migration to the coordinated alkene determined (See Figure 1.2).

Figure 1.2 Model complexes prepared by Casey *et al.* that lend support to the Cossee-Arlmann mechanism.

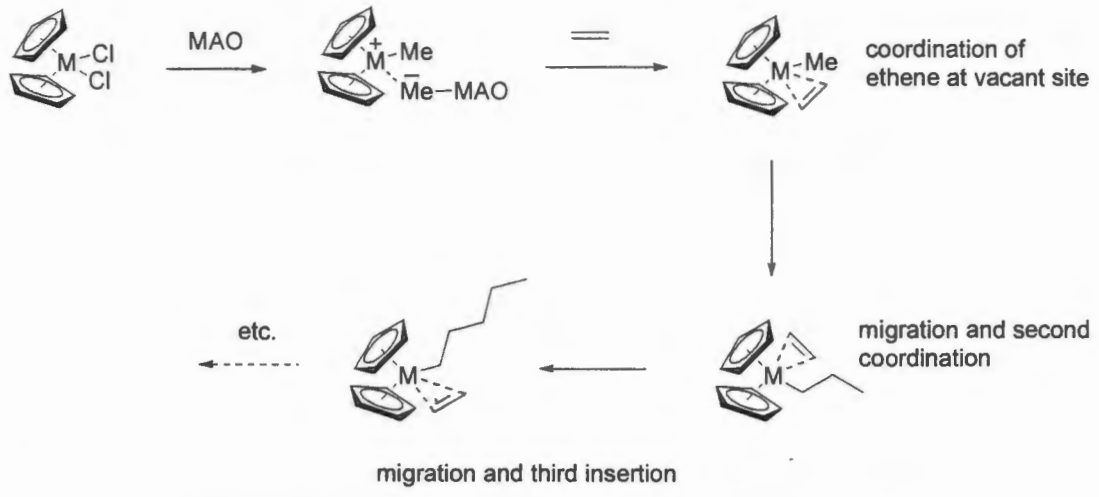

Scheme 1.1 Cossee-Arlmann mechanism: activation and insertion steps of group 4 metallocene catalysed polymerization with MAO (methylalumoxane) as co-catalyst.

Polymerization is a process that has become vitally important in the modern world. Modified metallocene systems are currently used industrially to synthesise a wide array of modified polymers. More recently, research into *oligomerisation* has become increasingly more important. This is in view of the possibility of adding high value to alpha olefins under such a process. Oligomerisation of alpha olefins that is selective to desired products is not only an important goal academically, but industrially as well.

Oligomerisation is the process by which an alkene (usually ethene or propene) is catalytically, or by some other means linked to form intermediate chain lengths of alkene hydrocarbons. In many such systems, however, there exists only a small degree of control over the product distribution. A recent example of this is the system prepared by Brookhart *et al.*,[5] in which a late transition metal complex, with a co-ordinated *bis*-imine behaves as the catalytic precursor.

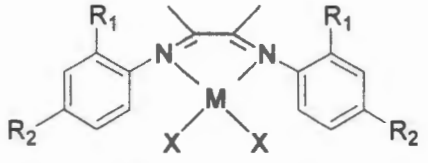

X = Br, Cl
M =Late transition metal
R_1, R_2 = Bulky group

Figure 1.3: The Brookhart type catalyst

In general, a lack of a bulky substituent in the *ortho* position of the phenyl ring (R_1) in Figure 1.3, results in a so called, Schulz-Flory distribution.[6] A Schultz-Flory distribution is observed when the

rate of chain propagation relative to chain transfer is constant. This can be expressed in terms of α, a propagation constant as :

α = rate of propagation / rate of propagation + rate of chain transfer

$$= \frac{molesC_{n+2}}{molesC_n}$$

where C_n refers to the alkene in question.

In the case of the Brookhart system, a substituent in the *ortho* position tailors the α value.

The ability of late-transition metal catalysts to form dimers or oligomers, does not only depend on the ligand system present, but also on other effects. In another paper, the use of late transition metal based catalysts as oligomerisation, or a dimerisation catalyst is highlighted, in general as a result of competing β-hydride elimination.[7] The above system, does however illustrate that it is possible to tailor the distribution of oligomer products of ethene.

1.2 Examples of selective ethene trimerisation catalysts

Industrially a need exists for a highly selective process of oligomerisation. These oligomers (for example 1-hexene in *trimerisation* of ethene) can be used as co-monomers in the preparation of linear low density polyethylene (LLDPE), or as starting materials for other desired products, such as epoxides. *This key process, i.e. ethene trimerisation was the key focus area of this research project.*

Several ethene trimerisation systems have been developed such as the Phillips chromium pyrrolide system (Reagan *et al.*) [8] and the BP chromium PNP system (Carter *et al.*) [9] which have been reported to both give very high weight percentages of 1-hexene. Other systems have also been investigated, such as a cyclopentadienyl-arene titanium system by Deckers *et al.* [10] which has also shown potential as an ethene trimerisation catalyst.

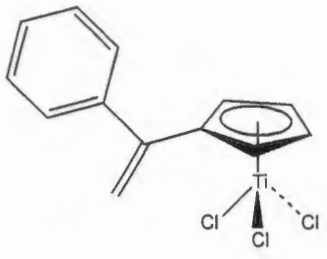

Figure 1.4 : A cyclopentadienyl-arene titanium pre-catalyst, prepared by Deckers *et al.* [10]

Recently, cyclopentadienyl chromium systems have shown potential as ethene trimerisation catalysts.[11] In these systems, substituted cyclopentadiene ligands are combined with Cr(III) hexanoate, and a halogen source (typically hexachloroethane), and ethene gas. The product distribution shows a high selectivity towards trimers, and 1-hexene in particular, that approach the Phillips [8] and BP systems.[9]

Key intermediate species involved in this ethene trimerisation process are believed to be metallacycles, resulting in the high selectivities reported for the formation of 1-hexene. [12] This is shown in Scheme 1.2 below.

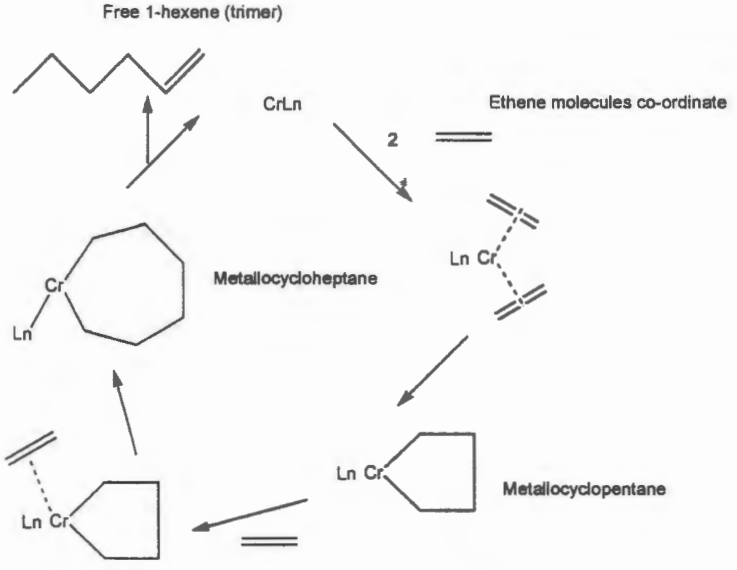

Scheme 1.2 : A proposed catalytic cycle for the trimerisation of ethene, producing 1-hexene.

Evidence to support the existence of a metallacyclic intermediate stems from the preparation of model metallacyclic compounds by Emrich *et al.* [13] In this investigation chromium cyclopentadienyl metallacyclic systems were isolated and characterized. See Figure 1.5.

Other related chromium metallacycles have been isolated and characterised by Heinemann *et al.* [14]

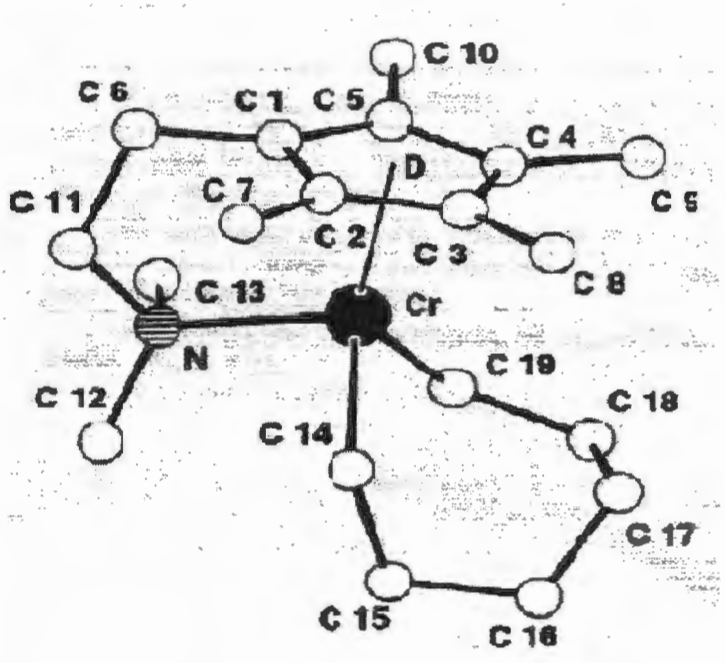

Figure 1.5: Structure of the chromium metallacycle isolated and characterized by Heinemann *et al.* [14]

The isolation of the metallacycle by Emrich *et al.* lends support to the proposal that the trimerisation of ethene by a chromium based system proceeds via a metallacyclic pathway (Scheme 1.1). Isotope labeling studies have also been conducted on chromium-diphosphine trimerisation systems by Agapie *et al.*,[15] lending further support to the metallacyclic mechanism.

Another example of an ethene trimerisation system is that by Carter *et al.*[16] This system makes use of a diphosphine ligand, and a chromium source and results in high selectivities of 1-hexene (ca. 99 % wt.)

A more recent example of a chromium ethene trimerisation system, is that by McGuiness *et al.* [17] A SNS (sulphur, nitrogen, sulphur) ligand is reacted with $CrCl_3(thf)_3$ to form the catalytic precursor.

A selective ethene trimerisation system, which makes use of a $Cr[N(SiMe_3)_2]_3$ with isobutylalumoxane as co-catalyst, supported on silica has also been reported by Monoi and Sasaki.[18] A mechanism is also reported here, which again makes use of the metallacyclic intermediates. In this report, the active catalytic species is supported on silica.

Another ethene trimerisation system containing a chromium source (Cr-2-ethyl hexanoate), a 2,6 disubstituted phenol and an aromatic ether as solvent, has also been reported by Morgan *et al.*[19] Here, high C_6 weight percentages are reported, and 1-hexene selectivities greater than 90 percent in most cases.

Finally, a trimerisation system, that makes use of triazacyclohexane complexes of chromium, activated by MAO has also been reported by Kohn *et al.* [20] An explaination is given here for the formation of other isomers, by making use of 1-hexene as feed for the catalytic process. The metallacyclic mechanism is also mentioned in this paper.

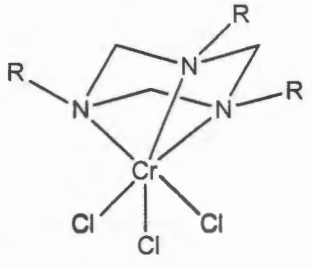

R = *n*-octyl or *n*-dodecyl

Figure 1.6 Structure of trimerisation catalyst precursor studied by Kohn *et al.*[20]

From this brief review it is clear that although selective ethene oligomerisation (trimerisation) catalysts are known and many studies have alluded to the presence of metallacyclic intermediates, the process has not been fully elucidated, partially due to the intractability of the complexes.

1.3 System of focus in this dissertation

1.3.1 Introduction and background

Similar to the pyrrole Phillips system,[8] the system focused on in this research project is one containing a bulky cyclopentadiene source, a chromium source, an alkylating agent (TEA – Tri

ethyl aluminium) a halogen source (hexachloroethane) and ethene gas. This system was pioneered by researchers at SASOL in the late 1990s. [11, 40] It was found that high weight percentages of 1-hexene are obtained from a system containing the components above, with various bulky cyclopentadienes (ca. 75 – 80 %). These reactions were carried out under high pressures of ethene, and the reactions were allowed to run for 40 minutes. The experimental setup is represented in Figure 1.7.

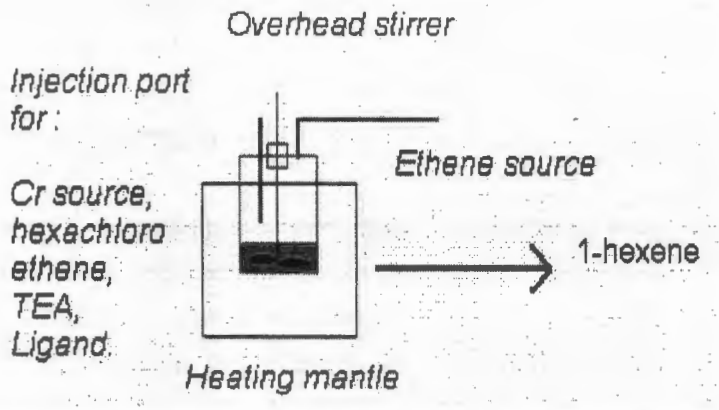

Figure 1.7 Schematic representation of catalytic ethene trimerisation using the SASOL cyclopentadiene system.

Very little light had been shed on this process, and the understanding of the chemistry involved hindered by the intractability of the intermediates and precursors involved. This was the departure point of the project:

to investigate this process, from a catalytic, and fundamental point of view; to investigate the structures of possible intermediates and precursors, and to gain an overall understanding of this process.

1.3.2 Approaches used in this project

In order to gain insight into the ethene trimerisation process using the cyclopentadiene/Cr system, the project was investigated on several fronts :

1.3.2.1 Synthetic Approach

In order to quantify and shed light on the trimerisation process, and the factors affecting selectivity and activity to 1-hexene, several new and existing bulky cyclopentadienyl ligands were

prepared, in addition to chromium model complexes that showed catalytic activity as ethene trimerisation catalysts.

1.2.2.2 Catalytic Approach

In order to understand, and quantify the steric and electronic effects of the ligands in the trimerisation process, catalytic work was carried out on the ligands, and the complexes. Some work has been done using this approach, but in order to quantify it further, catalytic screening of several more ligands was required.

1.3.2.3 DFT (Molecular Modeling) Approach

A detailed array of DFT calculations was performed to evaluate the energy requirements of the catalytic system. Activation steps, and the subsequent catalytic cycle was looked at by geometry optimizations and TS (transition state searches). Published work using this approach is at a minimum, restricted to tantalum and titanium. Only recently, has a theoretical paper been published in which the study of the Phillips system was undertaken. (A full discussion will follow in the pertinent chapter).

1.4 Succinct overview of dissertation

Chapter 2 details the various synthetic approaches used in the preparation of a number of bulky cyclopentadiene ligands. Characterisation of these ligands are discussed, using an array of techniques. Plausible explanations for failure of certain attempted routes is also discussed.

Chapter 3 documents the preparation, characterization and fundamental chemistry of transition metal complexes used to understand the ethene trimerisation process. A number of routes to the preparation of the Cr(III) model complexes is detailed, in addition to EPR (Electron Spin Resonance Spectroscopy) conducted on these compounds. Cyclic voltametry is discussed for Fe(II) sandwich compounds as a method to evaluate electronic influences of ligands on a metal centre.

Chapter 4 discusses the catalytic testing and screening of the ligands, and the metal Cr(III) complexes prepared.

Chapter 5 provides a brief overview and theoretical introduction to the various aspects of DFT (density functional theory). The mechanics and mathematical background of DFT are introduced, and a comparison of various DFT methods detailed.

Chapter 6 details the array of DFT calculations performed on the model system, $CpCrCl_2$. The activation step is looked at in detail, in addition to the catalytic mechanism itself. Calculated free energies of stationary states are documented, in addition to free energies of TS (transition states). Enthalpic values for all species involved are also documented.

Chapter 7 discusses the experimental procedures involved in the project.

Chapter 8 Conclusion, future work.

Chapter 9 References.

Chapter 2

Synthesis of Bulky Cyclopentadienyl Derivatives

"Arguments are to be avoided; they are always vulgar and often convincing."
Oscar Wild

2.1 A brief introduction to cyclopentadienes as ligands in organometallic chemistry

Since the serendipitous discovery of ferrocene in 1951 by Pauson and Kealy [21] a vast number of organometallic compounds, containing the cyclopentadienyl moiety have been prepared. The non-classical bond of a cyclopentadienyl ligand with a metal centre was studied, amongst others, by Wilkinson and Woodward.[22,23] Many such cyclopentadienyl containing complexes have uses in medicine, for example as currently investigated anti-malarial agents [24] and catalysis, of which numerous examples exist. [25]

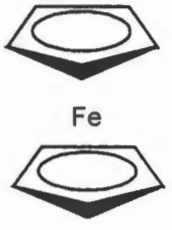

Figure 2.1 : Ferrocene, discovered in 1951. The compound observed to have non-classical, so-called "η^5" Cp co-ordination resulting in a "sandwich". This was the first isolated metallocene.[21]

The non-classical bonding of the Cp rings with the iron center in ferrocene is best described by molecular orbital theory.[23] A so-called orbital correlation scheme of ferrocene is presented in Figure 2.2. For most other similar systems (with different metal centers) this diagram can be used and adapted, in the description of the bond. The molecular orbital model of ferrocene describes experimental observations most satisfactorily. The frontier orbitals are neither strongly bonding or antibonding, permitting complexes to exist that do not obey the 18 electron.[27] Some examples of these complexes are given in Table 2.1.

Complex	Valence electrons
$V(C_5H_5)_2$	15
$Cr(C_5H_5)_2$	16
$Co(C_5H_5)_2$	19
$Ni(C_5H_5)_2$	20

Table 2.1 Sandwich compounds deviating from the 18 electron rule. (Adapted from ref. 27).

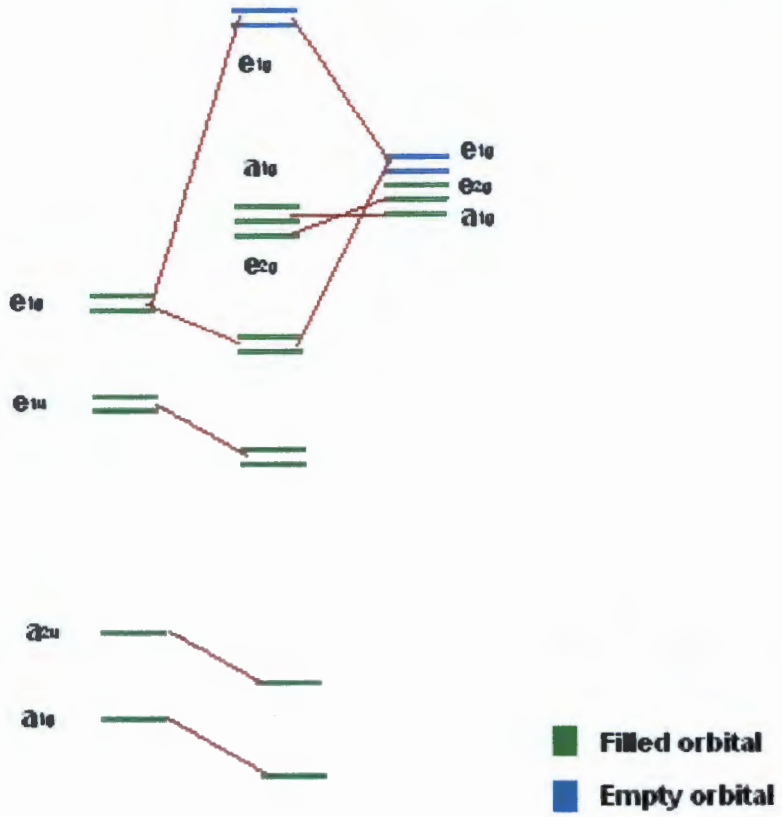

Figure 2.2 : An orbital correlation scheme of ferrocene.[26]

In addition to having sandwiches resembling that of the ferrocene molecule, so-called bent sandwiches, containing tilted cyclopentadienyl rings, also exist. Half sandwich compounds, containing only one cyclopentadienyl moiety have also been prepared.[27] Some half sandwich compounds are referred to as "piano-stool" complexes. In general, these complexes can contain a strong π acid ligand, in which case the 18 electron rule can be applied. In the case of a weak π acceptor ligand, the 18-electron rule does not always apply. Some examples of each type are presented in Figure 2.3.

Half sandwiches with strong π-acid ligands

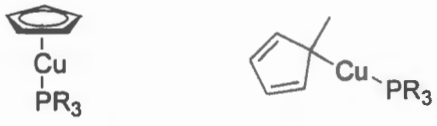

Half sandiwches with poor π-acceptor ligands

Distorted 14 electron Cu complex.

Figure 2.3 Some examples of 'half sandwiches' (From ref. 27).

It became possible to synthesise more exotic cyclopentadienyl metal systems of which Cp* or pentamethylcyclopentadiene is an example. [28] With five methyl groups replacing five hydrogen atoms of the cyclopentadiene, differences in properties of the metal complexes was noted.[29] In the mid 1980s high yielding routes to the synthesis of decamethyl osmocene, and ruthenocene was reported by Albers *et al.* [30]

It stands to reason that changing the substituents on a Cp ring to even larger aromatic or sterically demanding aliphatic substituents, could further change the chemical and physical properties of complexes. This idea gives precedence to the research of more bulky cyclopentadienes.

2.2 Bulky Cyclopentadienyl ligands

Schumann and Janiak, define a bulky cyclopentadienyl ring as one that contains at least three substituents larger than a methyl group. [31] Several known examples of such systems exist and are illustrated in Figure 2.4.

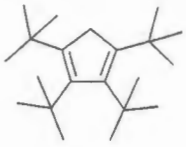

1,2,3,4-tetra *tert*butylcyclopenta-1,3-diene

1,2,3,4,5-Pentaphenylcyclopenta-1,3-diene

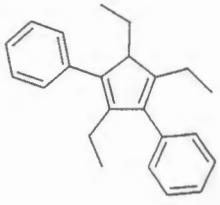

2,4,5-triethyl-1,3 diphenylcyclopenta-1,3-diene

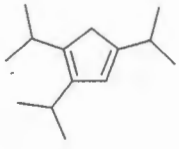

1,2,4-triisoprpoylcyclopenta-1,3-diene

Figure 2.4 Some examples of "bulky" cyclopentadiene ligands.

Several motivations exist for the synthesis of these compounds :

2.2.1 Increased steric crowding

When the bulky ligand is co-ordinated to a metal center a marked increase in steric crowding around that center is noted. This could be advantageous in a catalytic or other process. An example of extreme crowding around a metal center is found in decaphenyl stannocene first reported by Heeg *et al.* [32] The steric demand is so great, the arrangement of the ligands around the metal center is dictated by the steric requirements rather than by electronic requirements.

2.2.2 Increased stability of otherwise sensitive complexes

The increased steric crowding also provides a stabilizing effect on metal centers susceptible to oxidation. Even Cr(III) radical species have been isolated, containing a pentaphenyl cyclopentadienyl ligand. [33] In this case, the cyclopentadienyl analogue of this radical is far more sensitive.

2.2.3 Conjugation effects

A computer generated model of pentaphenyl cyclopentadiene shows that the phenyl rings are not co-planar to the cyclopentadiene ring. Regardless of this, one can argue some degree of "charge delocalisation" arising from the electron rich phenyl rings, attached to the cyclopentene nucleus. This is reflected in the dramatic colour changes seen in Fe(II) complexes of the pentaphenyl cyclopentadiene (red), compared with that of ferrocene (orange). A model of a bulky cyclopentadienyl Iron(II) complex is shown in Figure 2.5.

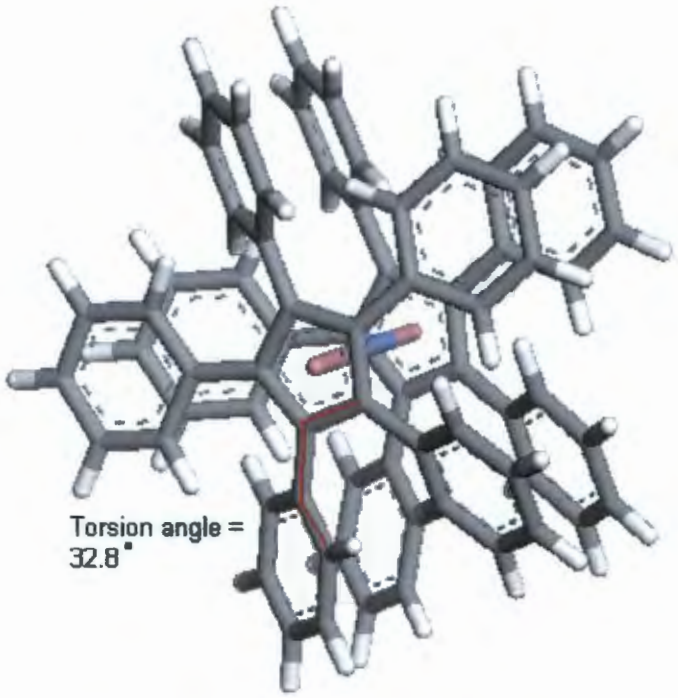

Figure 2.5 A Materials Studio model of bis-pentaphenylcyclopentadiene Fe(II). One of the torsion angles is shown.

The remainder of this chapter will deal with routes explored in the synthesis of the bulky cyclopentadienes, for potential use in the catalytic trimerisation of ethene to 1-hexene. These routes, though similar to those used in the case of less substituted Cp rings, have synthetic difficulties arising from the extreme steric crowding that arises in some cases.

2.3 Synthetic routes

2.3.1 The use of a dilithium reagent

The first route reported by Braye *et al.* in 1961, [34] makes use of an *in-situ* generated di-lithium intermediate that can rapidly react with a geminal dihalide electrophile to undergo ring cyclisation, and form a bulky cyclopentadiene. This route is shown to be used to synthesise heterocyclic systems, containing metals, such as gold. This reaction pathway is represented in Scheme 2.1

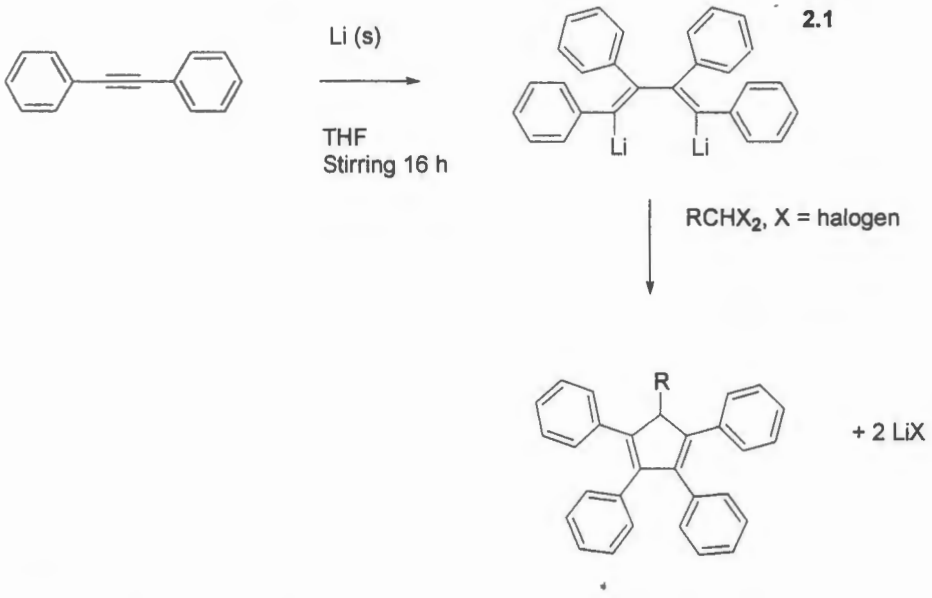

Scheme 2.1 The use of a dilithium reagent in the synthesis of bulky cyclopentadienes.

The dimerised dilithium reagent (**2.1**) was isolated and characterized by NMR spectroscopy. It was possible to use integration values to calculate the number of coordinated THF molecules to the lithium centres. A more accurate structural assignment for (**2.1**) from the NMR spectrum is $C_4Ph_4Li_2.0.4$ THF. The ^1H spectrum of (**2.1**) is shown in Figure 2.6.

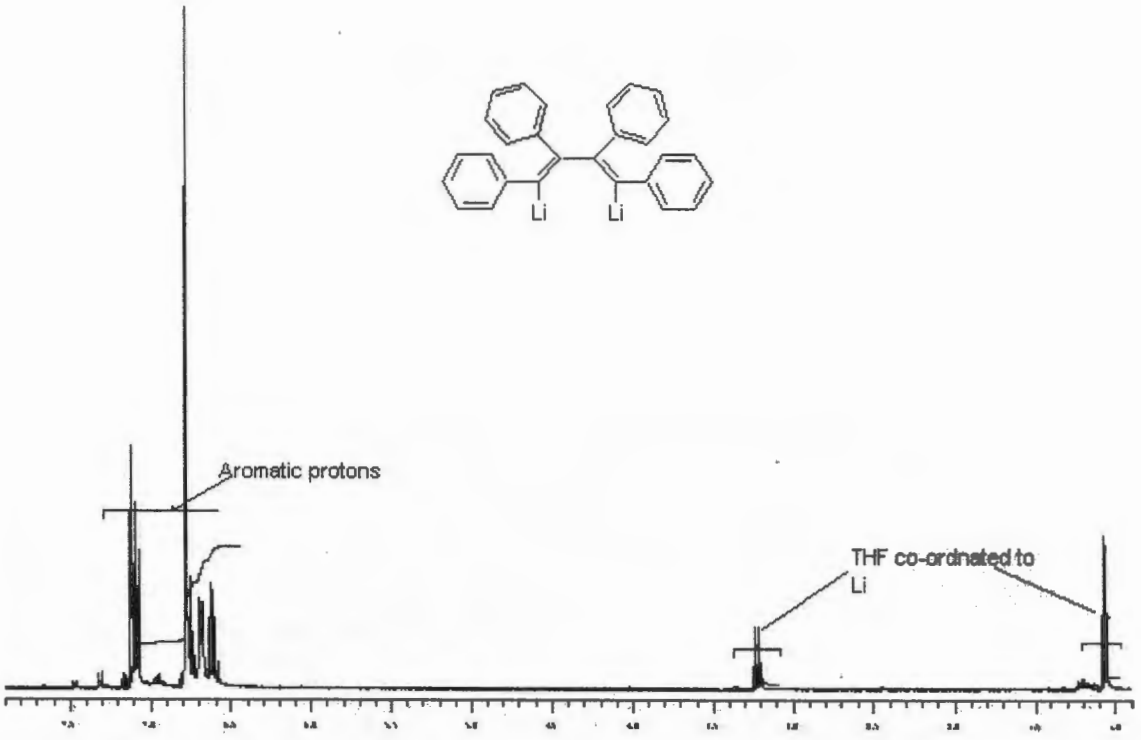

Figure 2.6 ^{1}H NMR spectrum of (**2.1**) in C_6D_6. The amount coordinated THF to the Li can be estimated from the NMR spectrum. In this case it is 0.4.

1,2,3,4,5-pentaphenylcyclopenta-1, 3-diene (**2.2**) and 1,2,3,4-tetraphenylcyclopenta-1,3-diene (**2.3**) was synthesized in low yields (*ca.* 15 – 20 %) using this route. The low yields can be attributed to the formation of some linear products in the synthesis.

It was noted, however, that these bulky ligands had poor solubility in common solvents, such as chloroform, and toluene. Hence, it was decided to attempt a synthesis of an alkyl tetraphenyl cyclopentadiene using an alkyl tail to solubilise the ligand.

This route was initially explored in the generation of such a species, but none of the expected product was isolated. A larger geminal dihalo species (1,1-dibromoheptane) was synthesized, using a route reported by Hoffmann and Bovicelli [35] and reacted with the dilithium reagent, but expected ring closure was not observed. This limitation can be explained in terms of preferential attack on the β position, as opposed to the expected geminal position.

Development of this route by attempting to generate other dilithium intermediates also failed. Instead of reacting diphenyl acetylene with lithium to form the bis-lithium-1,2,3,4-tetraphenyl-1,3-butadiene, hexyne and butyne was reacted with lithium in an attempt to form other dilithium

intermediates. The desired dimerisation was not observed, possibly due to the lack of aromatic stabilization that exists in the dilithium tetraphenyl butadiene system. This synthetic attempt is presented in Scheme 2.2.

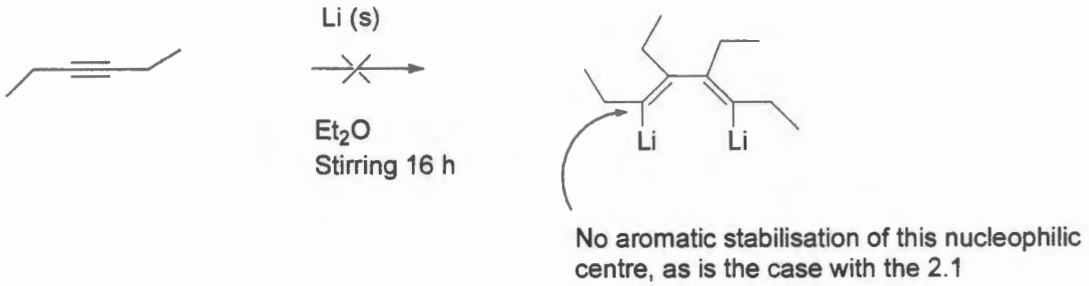

Scheme 2.2 Attempted dimerisation of 3-hexyne with lithium.

2.3.2 The use of a metallation / alkylation pathway.

The observed lack of solubility of the tetraphenyl cyclopentadiene, prompted the need for attachment of an alkyl chain in the 1-position of the cyclopentadiene ring (see Figure 2.6 later). Since the modification of route 2.3.1 for such a target was unsuccessful, this route was next investigated. Here, a lithium, sodium or potassium salt of the tetraphenyl cyclopentadiene is each reacted with an alkyl halide to form the desired product. This route, has been reported for the synthesis less bulky cyclopentadienes. A scheme of a so-called metallation/alkylation reaction is shown in Scheme 2.3.

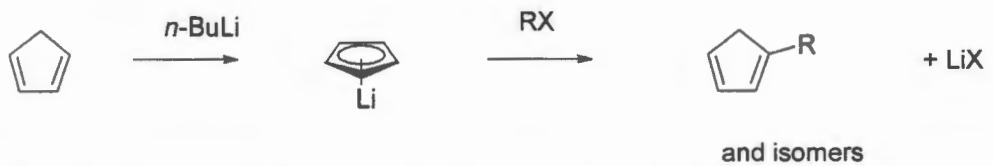

Scheme 2.3 Metallation/Alkylation pathway, reported for the synthesis of less bulky cyclopentadienes.

An example of the use of this pathway is in the synthesis of 1,3,5-tri(*tert*-butyl)cyclopentadiene from the sodium salt of 1,3-di(*tert* butyl)cyclopenta-1,3-diene. [36] Only a 9 % yield is reported for this reaction as a consequence of the competing elimination of HI from ^{t}BuI. Despite this observation in the literature, it was decided to attempt to synthesise ligands of the type C_5Ph_4RH, where Ph = phenyl, R = alkyl or other group. Attempts were made to react $Na[C_5Ph_4H]$ with several alkyl iodides, such as hexyl iodide, pentyl iodide, and butyl iodide. In each case, none of

the desired product could be isolated. A schematic representation of this attempt is shown in Scheme 2.4.

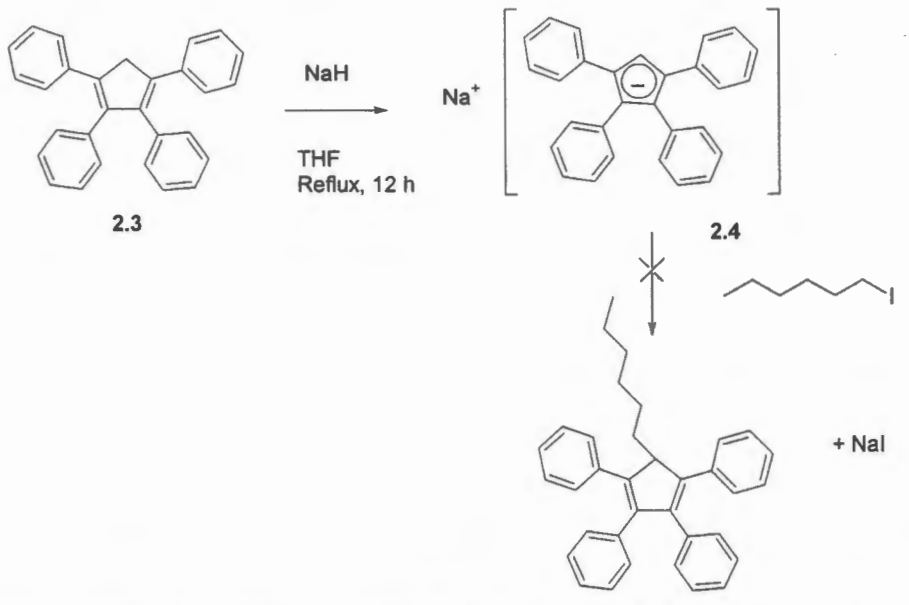

Scheme 2.4 Attempted Metallation/Alkylation to form 5-hexyl-1,2,3,4-tetraphenyl cyclopenta-1,3-diene.

Compound (**2.4**) was isolated and charactersied by ^{1}H NMR to prove proton abstraction in (**2.3**). This spectrum in shown in Figure 2.7. By making use of the integration values of the aromatic resonances relative to the Cp*H* resonance, the relative integration values can be determined.

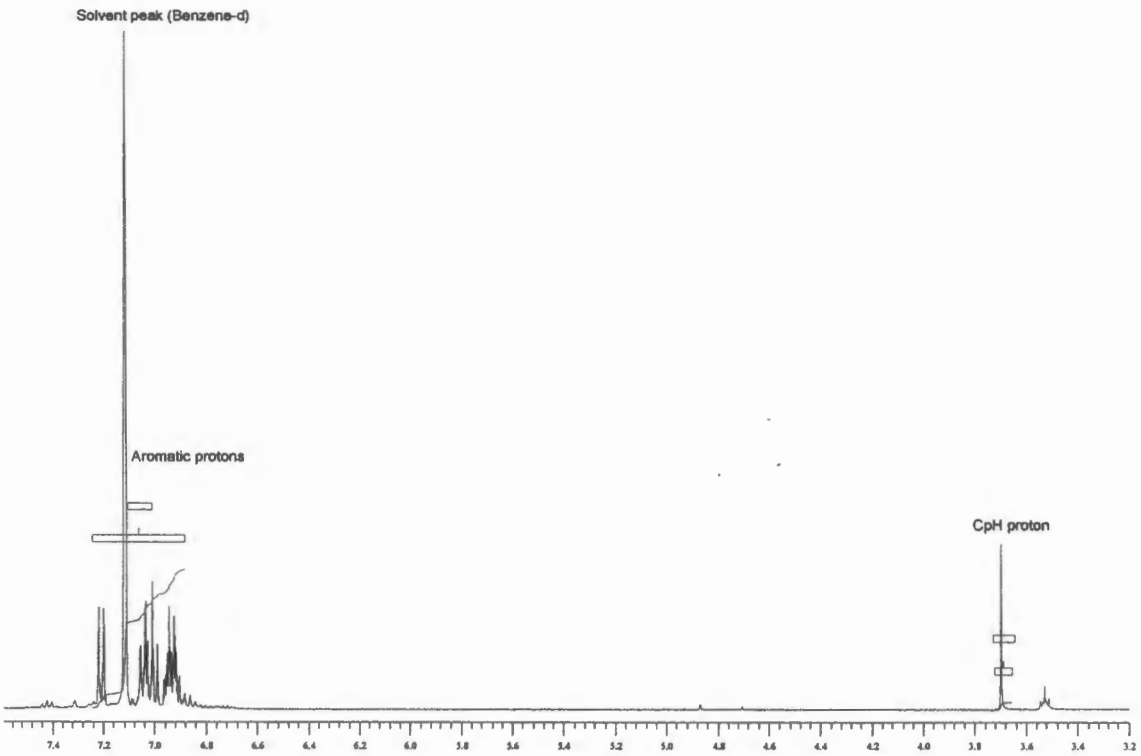

Figure 2.7 ^{1}H NMR spectrum of $Na[C_5Ph_4H]$ in C_6D_6. An integration of 20:1 (Ar*H* to Cp*H*) is noted as expected denoting complete proton abstraction to form the anion.

The fact that the desired product could not be isolated can be explained in terms of reactivity and steric bulk. Compound (**2.4**) is less reactive as a nucleophile than less bulky analogues, due to the "smearing out" of the negative charge into the phenyl rings. Also the steric considerations hinder the possibility of attack on the electrophillic carbon, adjunct to the iodide in the alkyl iodide. These arguments, satisfactorily explain the failure of the Metallation/Alkylation pathway in the synthesis of the desired ligand types in this project.

2.3.3 The use of an alkyl lithium or Grignard reagent

In this synthetic pathway, the starting material, tetracyclone, is readily available and inexpensive, which makes this an attractive synthetic route. Here, the tetraphenylcyclopentadienone (tetracyclone) is reacted with either a Grignard reagent, or an alkyl lithium reagent, to form a substituted cyclopentadienol. This in turn can be reduced, using AcOH and HBr to form species of the type, C_5Ph_4RH, where R is derived from RLi, or RMgBr. This route has been reported in the literature.[37,38,39] This route was applied to synthesise a wide array of new cyclopentadiene ligands, described in this dissertation. This is shown in Scheme 2.5.

2.3.3.1 Unexpected side reactions

In the attempted synthesis of 5-allyl-1,2,3,4-tetraphenylcyclopenta-1,3-diene and 5-vinyl-1,2,3,4 tetraphenylcyclopenta-1,3-diene unexpected products were isolated instead of the expected targets. Tetracyclone was reacted with allyl Grignard in an attempt to prepare the former mentioned product. Vinyl Grignard was reacted with tetracyclone in an attempt to prepare the latter mentioned product above. In both cases, however, it was noted spectroscopically (by NMR) that hydrogenation of the terminal double bond took place. In the case of the attempted synthesis of 5-allyl-1,2,3,4-tetraphenylcyclopenta-1,3-diene, a conjugated triene, 5-(1-propenyl)-1,2,3,4 tetraphenylcyclopenta-1,3-diene, was isolated. In the case of the attempted preparation of 5-vinyl 1,2,3,4-tetraphenylcyclopenta-1,3-diene, 5-ethyl-1,2,3,4-tetraphenylcyclopenta-1,3-diene was isolated as the major product.

A mechanistic rationalization for this observation is shown in Scheme 2.6.

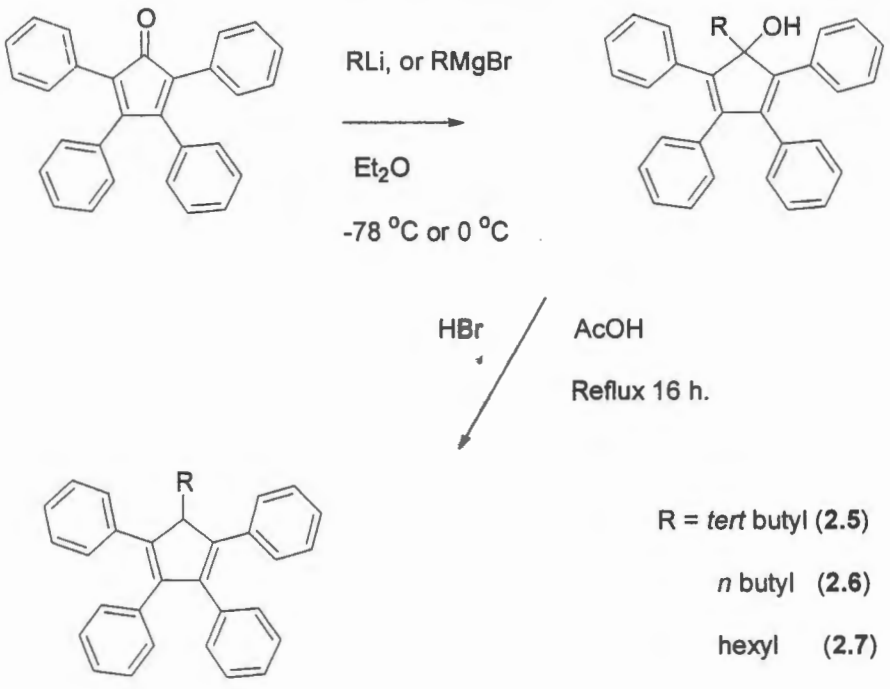

Scheme 2.5 Ligands synthesised using route 2.3.3.

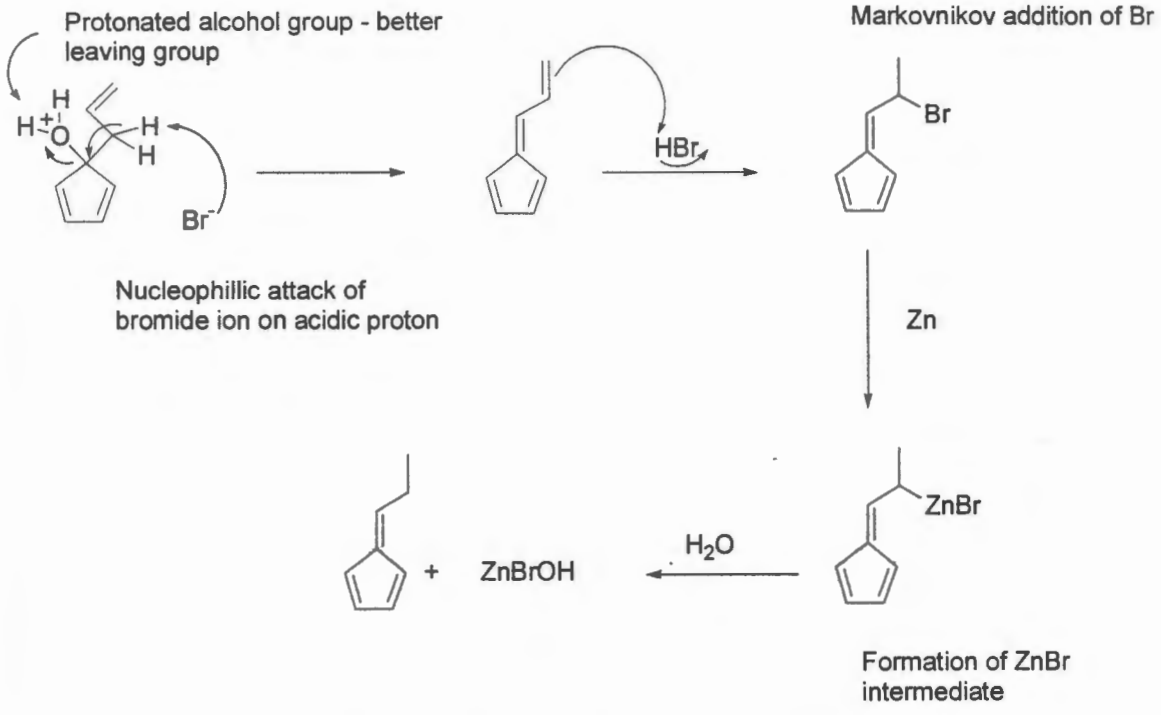

Scheme 2.6 A possible pathway to account for the unexpected formation of compound (**2.8**). A similar explanation can be used to account for the formation of the 5-ethyl analogue. The phenyl rings are omitted.

All ligands were fully characterised, using NMR, IR, FAB-MS, EA and mp. An example of an NMR spectrum of the 5-hexyl-1,2,3,4-tetraphenylcyclopenta-1,3-diene ligand (**2.7**) is shown in Figure 2.8. Figure 2.9 shows the triplet of the Cp*H* proton, with hyperfine ^3J coupling.

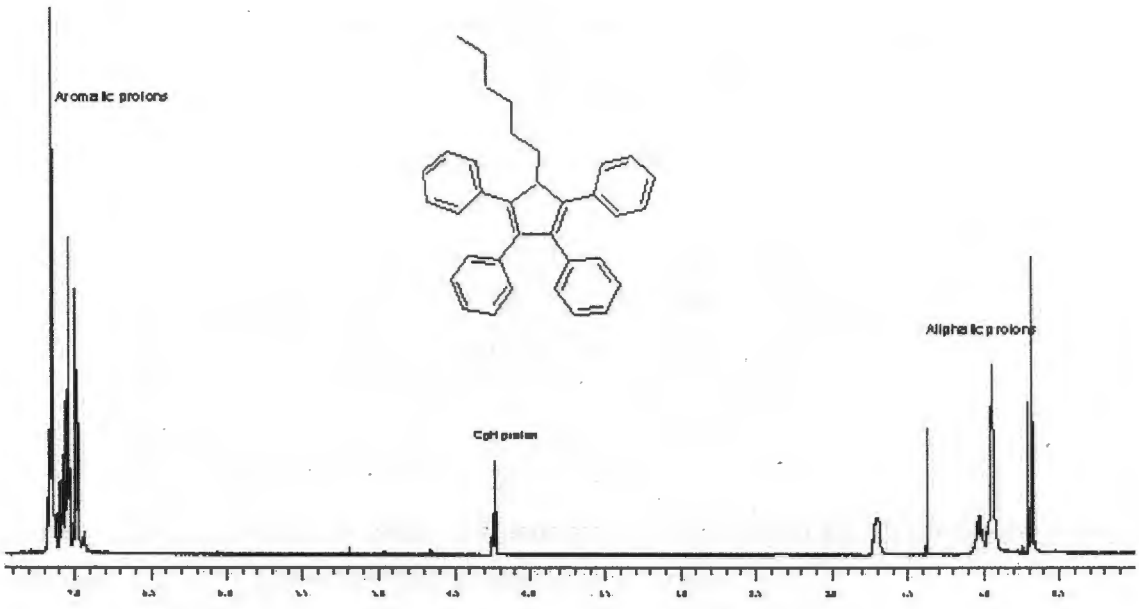

Figure 2.8 : ^{1}H NMR spectrum of 5-hexyl-1,2,3,4- tetraphenylcyclopenta-1,3-diene.

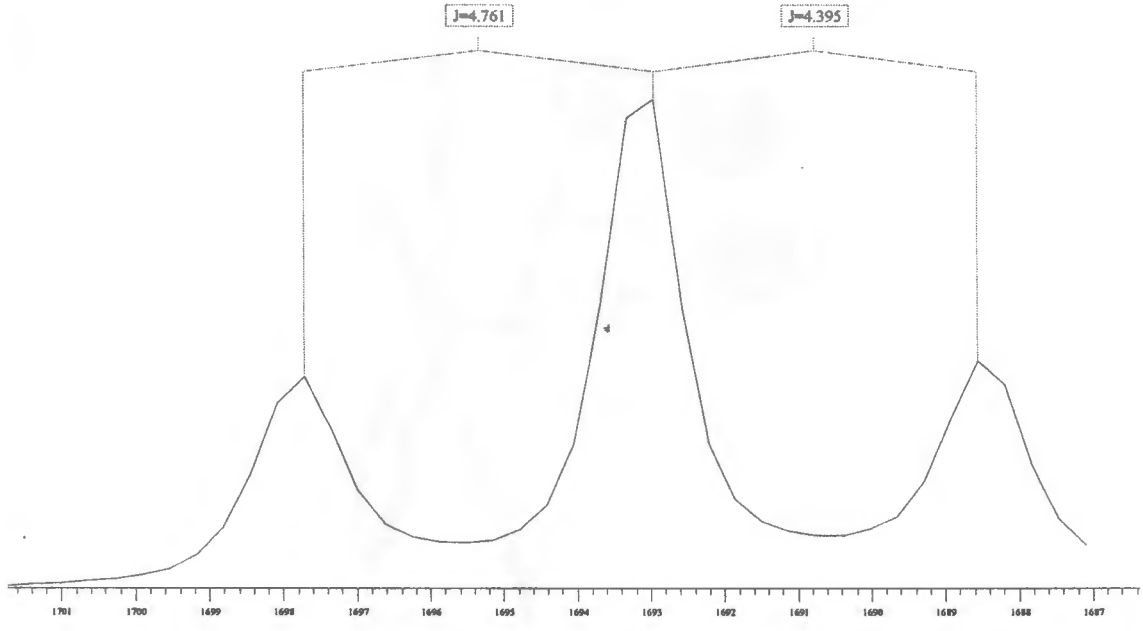

Figure 2.9 : Expansion of Cp*H* proton at δ = 4.25 ppm , showing coupling constants.

Characteristic features in the NMR spectra of these ligands, is the presence of the Cp*H* proton. In general, with this class of bulky cyclopentadiene, it occurs at ppm 4 – 5, with downfield or upfield shifting, depending on the R group present on the specific carbon atom. For example, $C_5Ph_4H_2$ has it's Cp*H* protons resonating at ppm = 4.05. An expansion of this Cp*H* proton is

shown in Figure 2.9 and a table summarizing these shifts of the Cp*H* protons is shown in Table 2.1.

R group on Cp ring	ppm of Cp*H*
hexyl	4.25
1-propeneyl	-
ethyl	4.25
butyl	4.22
^{t}butyl	4.47
H	4.05*

Table 2.2 Cp*H* chemical shift values of ligands synthesised by route 2.3.3. (* this is the value for the ligand $C_5Ph_4H_2$). (solvent shifting is neglected in this case).

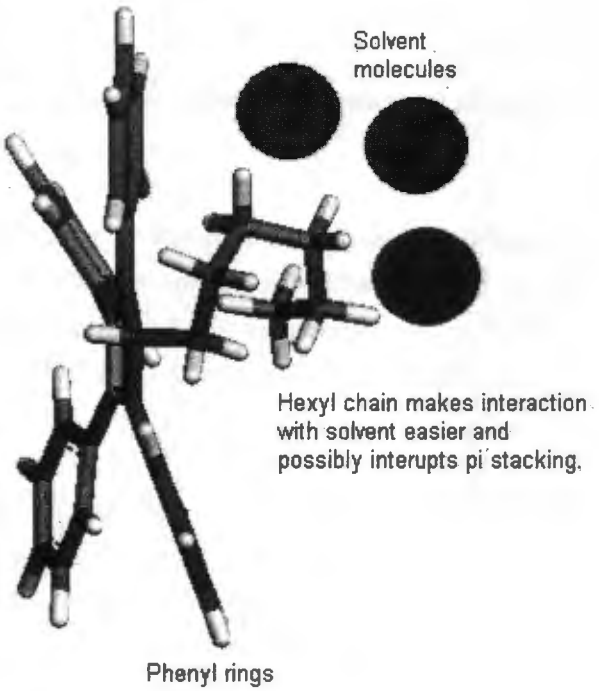

Figure 2.10 Idealized representation of the 5-hexyl-1,2,3,4-tetraphenylcyclopenta-1,3-diene. The alkyl chain makes interaction with solvent, and ultimately solubility more possible.

This route proved significantly more successful than the previous two routes investigated, but the low yields provided some impetus to explore another route.

2.3.4 The use of palladium-catalysed reactions of metallocenes with aryl bromides.

To synthesise even more exotic, and bulky cyclopentadienes, in higher yields that was reported by the previous three routes investigated, a new route reported by Giesbrecht *et al.*[40] was used. (originally reported by Dyker *et al.* [41]) This pathway makes use of $(\eta^5C_5H_5)_2\ ZrCl_2$ as a source of the cyclopentadiene, and a palladium catalysed coupling reaction of an aryl bromide, yields the substituted product in good yield. This pathway is represented in Scheme 2.7.

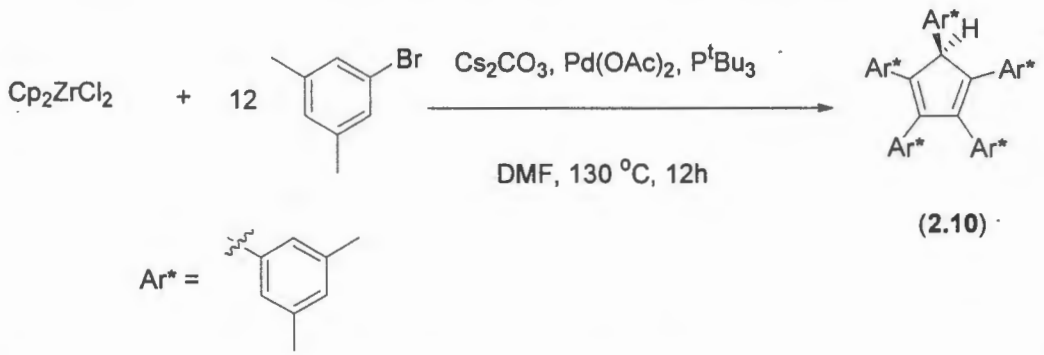

Scheme 2.7 Representation of the route reported by Giesbrecht *et al.*, and Dyker *et al.* [40, 41] The zirconium byproduct is omitted for clarity.

This route was used successfully to synthesise the known so-called "superbulky" cyclopentadiene represented above (**2.10**), which was consequently characterised by NMR. With much more steric bulk that the other ligands prepared, this ligand could supply insight into the steric effects of these ligands in catalysis. Table 2.2 is a summary of all ligands prepared, their yields and melting points.

Ligand	Mp. (°C)	Appearance	% Yield
2.2	247 - 249	Pale yellow solid	7
2.3	185 - 186	Pale yellow solid	10
2.5	200 - 204	Pale Yellow solid	24
2.6	163 - 166	Pale yellow solid	25
2.7	125 - 127	Pale yellow solid	26
2.8	150 - 153	Bright orange solid	23
2.9	164 - 167	Pale yellow solid	14
2.10	203 - 206	Pale off-white solid	78

Table 2.2: Summary of ligands, their yields and melting points (uncorrected).

2.4 Summary and conclusions of this chapter

Finding a reliable synthetic route to synthesise these bulky cyclopentadienes was challenging, and of paramount importance. Using route 2.3.1, two known ligands (**2.2**) and (**2.3**) were prepared. In the end the route most successful, was that of 2.3.3, involving the use of tetracyclone as a starting material. Several new ligands were prepared this way (**2.5**), (**2.6**), (**2.7**), (**2.8**), (**2.9**). Finally, a superbulky ligand (**2.10**) was prepared using a palladium-catalysed reaction, and Cp_2ZrCl_2 as the source of cyclopentadiene.

Notwithstanding the importance, from an organic chemistry point of view of these ligands, they were to be used to synthesise bulky cycopentadienenyl model complexes (chapter 3), and to be used in the catalytic trimerisation of ethene to 1-hexene (chapter 4).

Chapter 3

Synthesis of model complexes to shed light on the ethene trimerisation process.

"An education isn't how much you have committed to memory, or even how much you know. It's being able to differentiate between what you do know and what you don't."
Anatole France

3.1 Introduction

In order to make improvements on a multi-component catalyst system it is important to *understand* the process from a fundamental point of view. Probing into the fundamental chemistry of a process would enable one to tailor the selectivities and activities of a given system. This is not always a simple task, especially if the system contains intractable precursors and intermediates. In the case of a chromium based system, this is indeed the case. The difficulties associated with defining the chemistry of the system investigated in this dissertation lie in the paramagnetic nature of chromium(I) and (III), which essentially makes nuclear magnetic resonance (NMR) spectroscopy an unattractive characterization technique. NMR can however be used with limited success to characterize some Cr(III) complexes. Alternatively, electron paramagnetic resonance (EPR) spectroscopy can be used. The sensitivity of the chromium system is a also problematic, as it is air and moisture sensitive. To understand the catalytic process, a method had to be developed to shed light on it.

3.2 Another look at the system focused on in this project

This multi-component system, has similarities to the Phillips ethene trimerisation system. A "black-box" process that has the following components :[42]

(a) "Cr source" : Cr-2-ethyl hexanoate is used. This is a commercially available compound.

(b) Halogen source : C_2Cl_6, also commercially available.

(c) Ligand source : Bulky cyclopentadienyl ligands, either commericially available or synthesized.

(d) Alkylating agent : TEA (Tri-ethyl aluminium), commercially available.
Pressurised ethene gas : Pure and purified and commercially available.

Very little understanding exists for this process, except that it is thought to possibly proceed via a metallacyclic pathway. This has been shown to be the case with a chromium diphosphine system conclusively,[15] but not for the system investigated in this thesis. [43] Similar CrCp (Cp = C_5H_5) systems are used extensively in industry as polymerization catalysis, but have not been reported to trimerise ethene.[44, 45, 46, 47] In the case of a bulky Cp ligand, trimerisation of ethene is observed. What was therefore required was the synthesis of model compounds, that possibly mimic the intermediates and precursors in the actual reaction.

3.3 Synthesis of Chromium Cyclopentadieneyl model complexes

Group VII(a) complexes exist, and have been reported, that contain a metal centre, terminal halogen atoms, and a bulky cyclopentadiene moiety. [48] These complexes, in the case of tungsten(V), and molybdenum(V), present themselves as "piano stool" monomeric complexes. These compounds could be isomorphic to the chromium precursors, involved in this catalytic process. An example of such a "piano-stool" complex is represented in Figure 3.1.

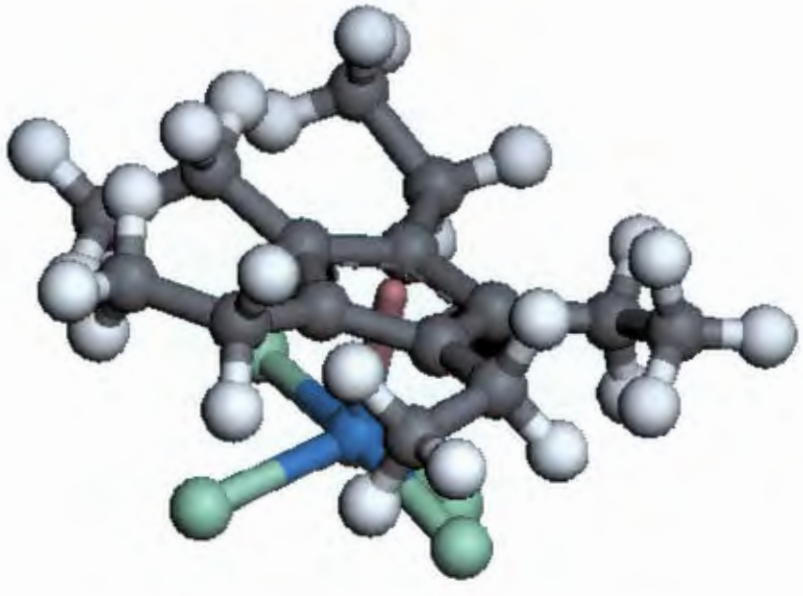

Figure 3.1 A Materials Studio model of the "piano-stool" tungsten complex - (η^5-C_5Et_5)WCl_4.

It was necessary to prepare a model compound that resembles or mimics the system investigated in this dissertation. In other words, it needed to have a chromium(III) centre, a halogen (chlorine), and a bulky cyclopentadiene. Such a system has been reported in the literature, [49] in which the

complex exists as a dimer in the solid state, with bridging chlorine atoms and no Cr-Cr bond. This compound indeed contains all the components of the catalyst system, and was earmarked as a possible model precursor compound.

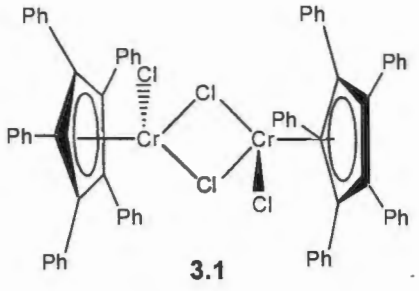

3.1

Figure 3.2 Structure of possible model catalyst precursor.

It was decided to synthesise the compound. Several routes are possible. Firstly, a route involving the preparation of the radical species, $(C_5Ph_5)Cr(CO)_3^{\bullet}$, [50] was attempted. In this pathway, the ligand (C_5Ph_5H – (**2.2**)) is reacted with NaH in THF , resulting in the sodium salt form of the ligand. This is represented in Scheme 3.1.

$$C_5Ph_5H + NaH \xrightarrow{THF} Na[C_5Ph_5] + H_2$$

Scheme 3.1 Abstraction of Cp*H* proton with NaH.

The $Na[C_5Ph_5]$ is isolated, rinsed with pentane, using centrifuge procedures, and dried under vacuum. This highly reactive salt, is next reacted with $Cr(CO)_6$ in tetraglyme, a high boiling linear ether under harsh reflux conditions (ca. 200 °C) for 2 hours. A yellow intermediate, $[Na(diglyme)_{3/2}][(C_5Ph_5)Cr(CO)_3]$ (**3.2**) develops, after recrystallisation. This reactive salt is then oxidized with $AgBF_4$ or $AgPF_6$ to form the blue free radical, $(C_5Ph_5)Cr(CO)_3^{\bullet}$, which can be dissolved in a halogenated solvent to yield the product, (**3.1**). A schematic representation of this is given in Scheme 3.2.

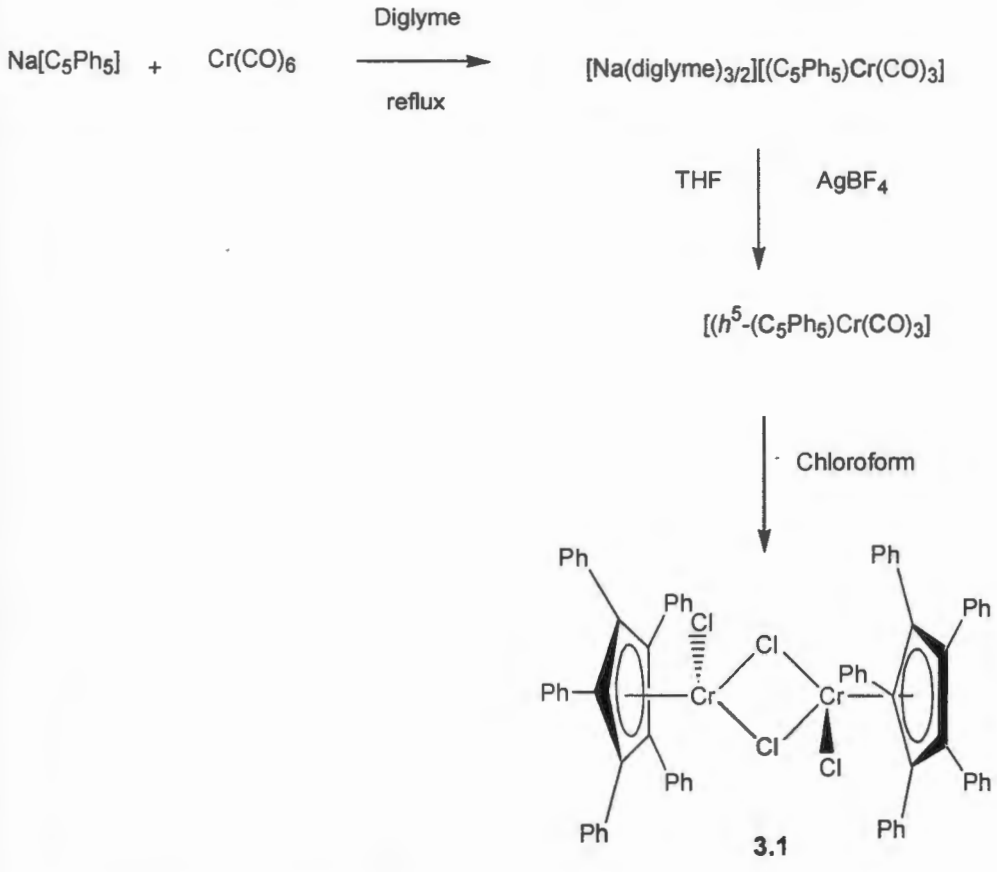

Scheme 3.2 Synthetic pathway to prepare (**3.1**), a possible model catalyst precursor.

It was found that this route, when attempted, was tedious and complicated by the instability of the intermediate salt (**3.2**), although it was possible to isolate and obtain spectroscopic evidence of (**3.2**). The target model compound (**3.1**), was however not isolated using this route in our laboratory.

A more attractive and simpler route to the target model compound, (**3.1**) was a route involving the reaction of $Na[C_5Ph_5]$ with $CrCl_3(thf)_3$ (**3.3**). [51] Compound (**3.3**) was synthesised using a convenient preparation by Shamir, and characterized by IR. [51] The bright purple adduct, (**3.3**) was reacted under reflux with $Na[C_5Ph_5]$, washed with pentane using centrifuge techniques, and the desired target, (**3.1**) was isolated as a bright green powder. This reaction is presented in Scheme 3.3.

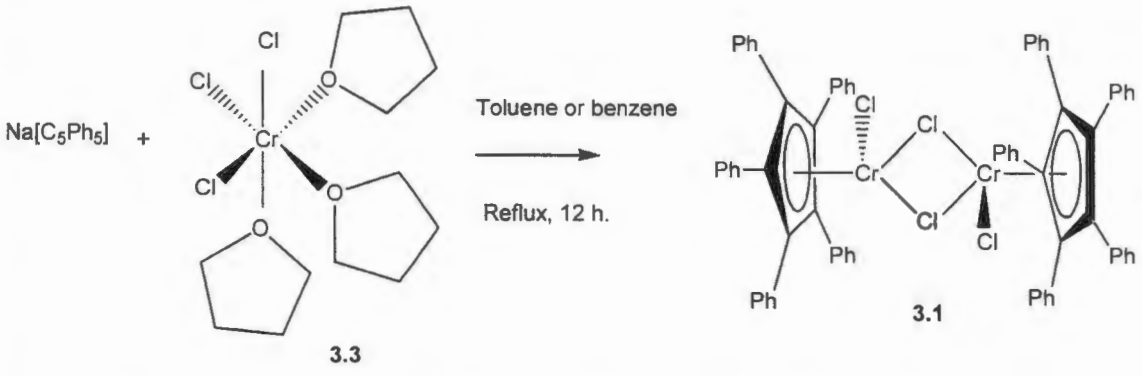

Scheme 3.3 Convenient route to the preparation of (**3.1**), the target model complex. Stoichiometric constants are omitted.

This route proved to be most convenient, and was used to prepare the tetraphenylcyclopentadienyl analogue of (**3.1**) in the same way. i.e. $[(C_5Ph_4H)CrCl_2]_2$, (**3.4**).

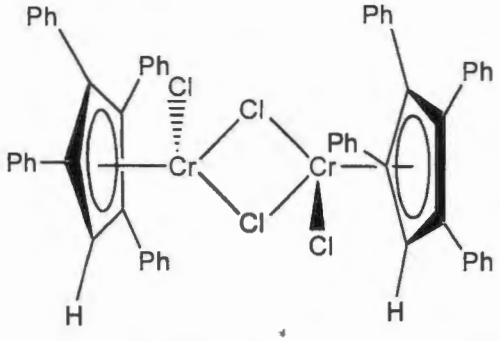

Figure 3.3 Structure of complex (**3.4**), tetraphenylcyclopentadienyl analogue of (**3.1**), synthesized using the same route.

A third model complex, resembling that of the previous two dimeric chromium complexes, was also prepared using a different route. The "superbulky" cyclopentadiene prepared (see chapter two), (**2.10**) was reacted with $KN(TMS)_2$ to generate the potassium salt form of the ligand (**3.5**). The motivation behind generating a potassium rather than a sodium (as before) or lithium salt is the marked increase in reactivity and nucleophilicity of the anion. This, in theory, enables milder reaction conditions and a similar methodology has been used by Heigl *et al.* to synthesise $[(t\text{-BuCp})CrCl_2]_2$.[52] The use of *n*-BuLi to abstract the Cp*H* proton, and form the lithium salt of the anion, is not always desired as a result of inaccurate concentration determination of the active species. $KN(TMS)_2$, however, is a salt, which can be weighed more accurately.

The potassium salt, (**3.5**) is then reacted with the $CrCl_3(thf)_3$ (**3.3**) in THF at room temperature to yield a dark blue solid. This blue solid, is possibly an intermediate complex, with co-ordinated THF to the chromium centre. After drying under high vacuum at 50°C, the colour slowly changes to olive green, as with the other model complexes, to form the target dimer, (**3.6**).

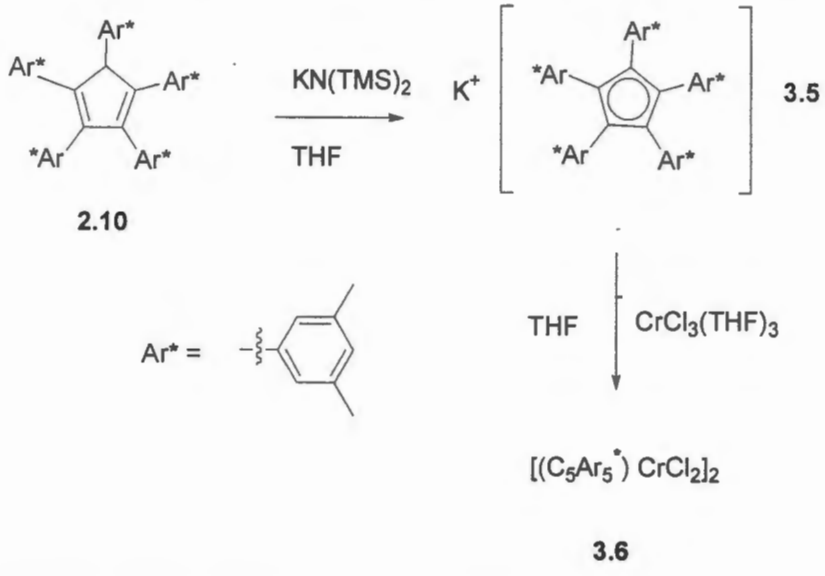

Scheme 3.4 Synthetic pathway to the preparation of complex (**3.6**).

Target (**3.1**) was also prepared using an analogous route as shown in Scheme 3.4. This route had similar yields to that found by Castellani *et al.*[50], but enabled milder reaction conditions, and reaction completion to be reached in a shorter time span. This is in light of the increased nucleophilicity of the $K[C_5Ph_5]$ compared with $Na[C_5Ph_5]$. This reaction Scheme is presented in Scheme 3.5.

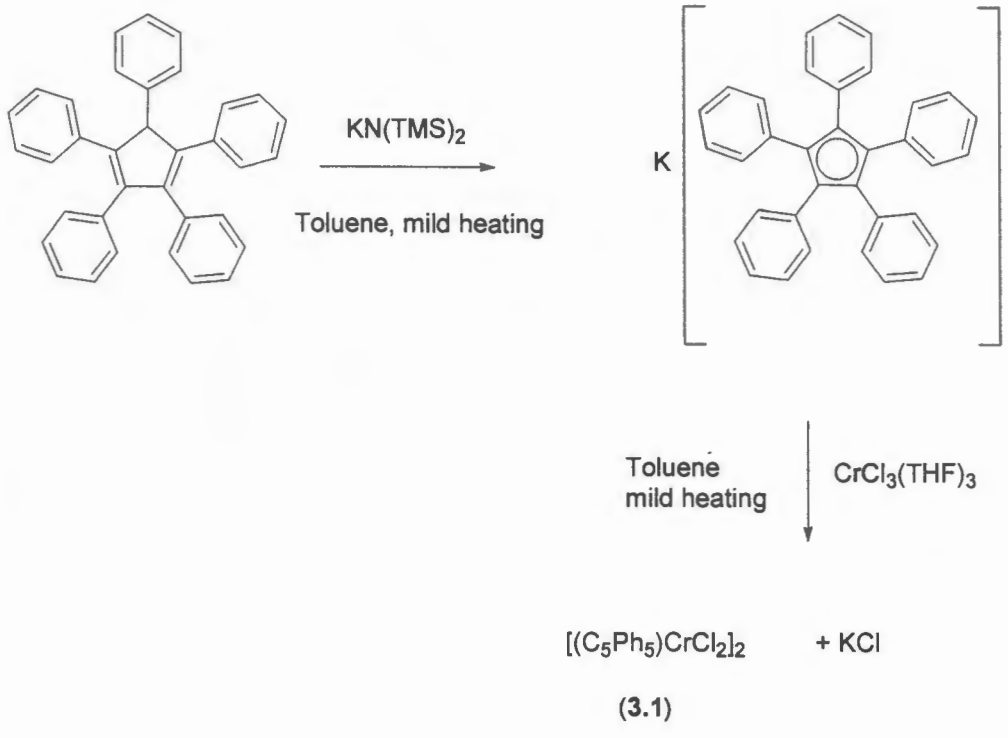

Scheme 3.5 Alternative route to target dimer (**3.1**).

Model complexes (**3.1**), (**3.4**), (**3.6**) are themselves rather intractable reaction products, and characterization of these complexes was a challenging exercise. Attempts at growing crystals for single crystal X-Ray diffraction, also failed. Hence, Fourier Transform Infra red spectroscopy, elemental analysis and electro-paramagnetic resonance (EPR) spectroscopy was used to characterize these complexes partially.

3.4 Characterisation of the model complexes

3.4.1 FT-IR Spectroscopy.

In order to validate the presence of bridging halides (chlorine atoms) in the solid state of the complexes, FT-IR was used. Terminal and bridging chlorines have a different characteristic absorption regions. The Cr-Cl stretching frequency usually occurs between 319 - 497 cm^{-1}. [53] The frequency for a metal-halogen bridge is usually lower that a terminal stretch.[54] Lattice vibrations of crystalline compounds influence the stretching position of infra red absorptions. Despite this, it was possible to make assignments of the FT-IR spectra. Stretches for (**3.6**), (**3.1**) and (**3.4**) was seen in the region 151 – 297 cm^{-1} corresponding to the ν(Cr-Cl-Cr). Another series of frequencies, ranging from 1027 – 1185 cm^{-1} corresponds to the ν (Cr-Cl) terminal stretches.

Similarly, stretches occurring in the range 1417 – 1499 cm^{-1} can be assigned to the aromatic residues (ν(Ar-H)), and absorptions at 3026 cm^{-1} can be assigned to ν(C-H). Aromatic stretches also exist at 1578 – 1619 cm^{-1}. Figure 3.4 and 3.5 depicts this.

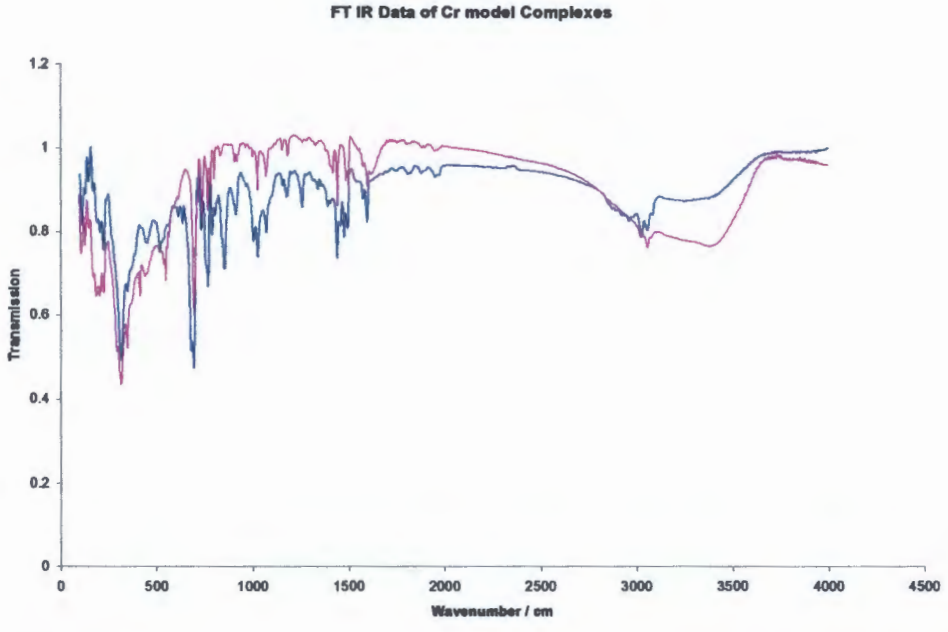

Figure 3.4 FT-IR spectrum of the (**3.1**) and (**3.4**), collected as KBr pellets or polyethylene pellets.

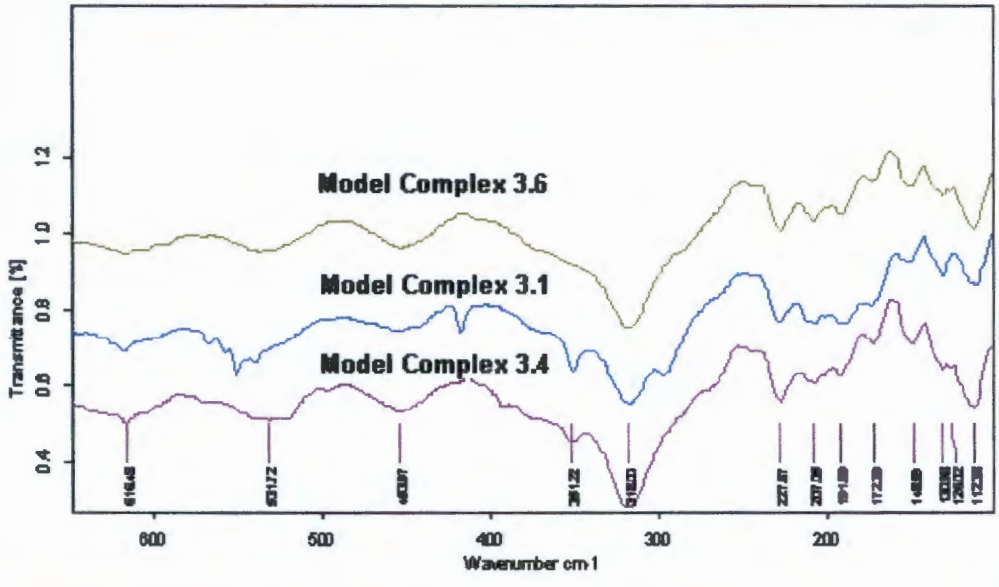

Figure 3.5 Comparison of Cr(III) complexes in the far infra-red region. Polyethylene pellets were used in this range.

3.4.2 Raman Spectroscopy

Although these compounds have been characterized in the literature by Raman spectroscopy, attempts made at doing this failed in our case. The samples dissociated under the 514 nm laser line, and attempts at diluting the sample in a KBr matrix and using a 10 x objective with a low laser power, also failed. A reliable spectrum could not be recorded, and the use of this technique was hence abandoned. This might be in light of florescence associated with the complex,due to the presence of aromatic rings, which hindered the use of this technique.

3.4.3 Electron-spin paramagnetic resonance spectroscopy (EPR). [55]

Complexes of the type $Cr_2X_9^{3-}$ exist and have been shown to be paramagnetic. This observation can easily be explained in terms of the lack of any bond that exists in this species. [56] In the case of the W and Mo analogues of these compounds, the compounds are diamagnetic, due to the existence of multiple bonds between the metals. A literature X-ray crystal structure of (**3.1**)[50] shows a Cr-Cr bond length of 3.375 Å. Despite this antiferromagnetic coupling is possible, probably through the Cl bridges. Previous magnetic susceptibility studies, have shown a presence of antiferromagnetic coupling at room temperature. These studies, also show a calculated *g* value of 2.1, slightly higher than the expected value of 2.0.

In order to probe the actual structure of the model complexes in solution, EPR spectroscopy was conducted at low temperatures in dichloromethane. Using this technique, the paramagnetic nature of possible dissociated forms of the model complexes could used to gain insight into the possible chemistry in solution of these complexes, as possible catalyst precursors; and aid in characterization of these intractable reaction products. This study was conducted on (**3.1**) and (**3.2**).

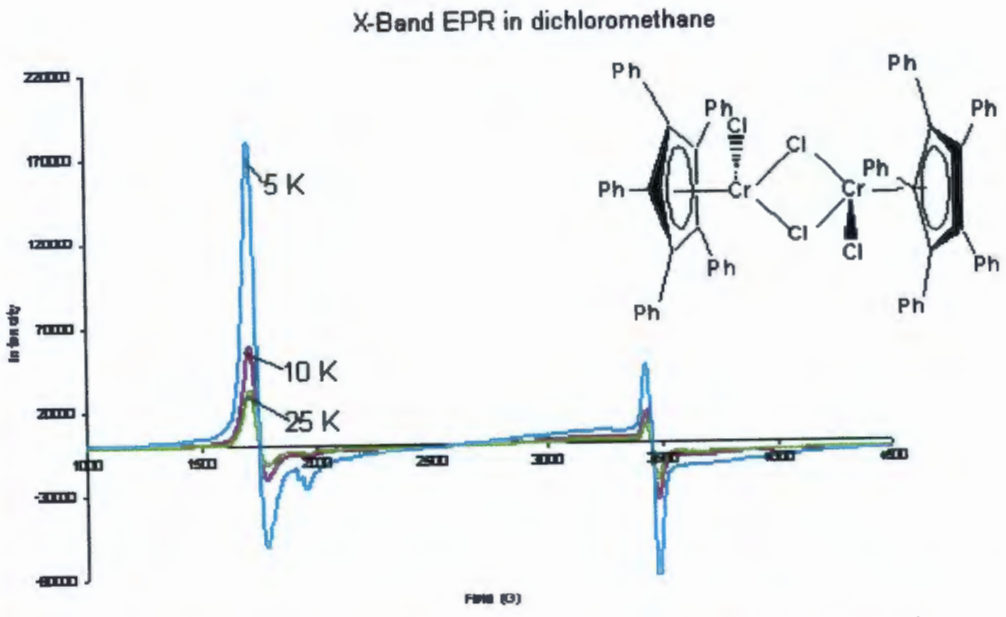

Figure 3.6 EPR spectrum of model complex (**3.1**) in dichloromethane glass at several temperatures at 1 mW power.

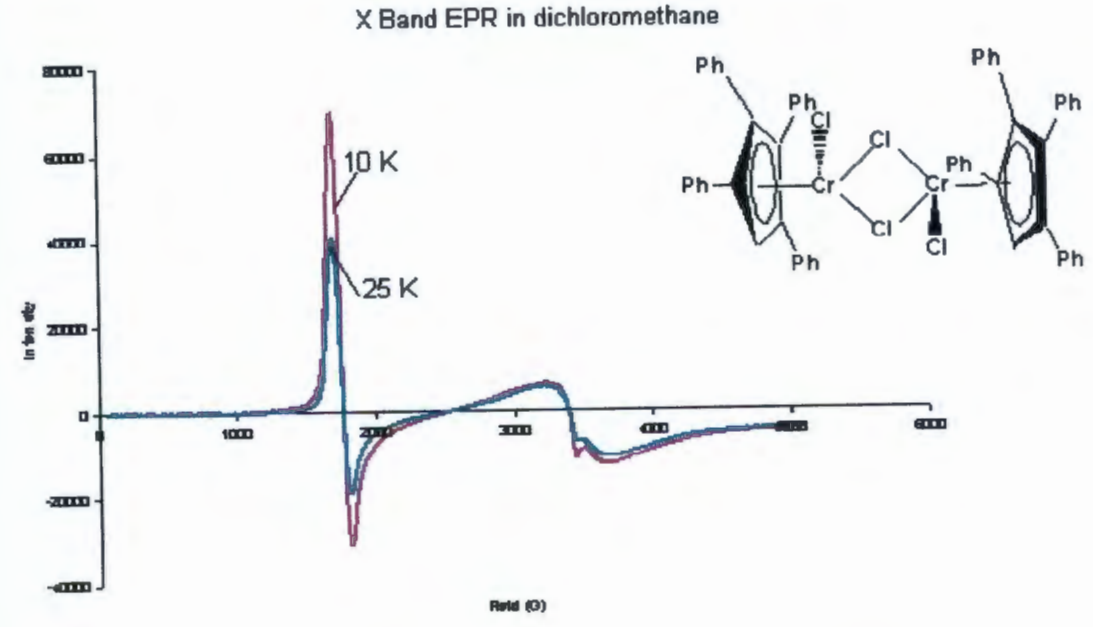

Figure 3.7 EPR spectrum of model complex (**3.4**) in dichloromethane glass at 10 K and 25 K at 1 mW power.

Clearly, from the above spectra, it is seen that at constant power (1 mW power), the signal intensity is inversely proportional to the temperature. The observed intensity is proportional to the difference in the population of the α and β spin energy levels. The ratio of the populations is summarized by the relation,

$N_\alpha / N_\beta = \exp(-2\mu_B B/kT)$, **(eq 3.1)**

where, T is the temperature at which the sample is run, k is the Boltzmann constant, B is the field strength, and μ_B the Bohr magneton, in the direction of the field. The difference in population of α and β spin energy levels is after some algebra approximately,

$= \mu_B B/kT$ **(eq. 3.2)**

This important relation shows, very simply, that a *lower* sampling temperature will yield a greater difference in population of the spin states and hence a *greater* intensity of the signal. This explains the observed trends seen in both spectra.

Another important parameter in the analysis of these spectra, is signal broadening. By using the Heisenberg uncertainty principal, the following inequality is obtained,

$\Delta W \, \Delta t \geq h / 2\pi$ **(eq. 3.3)**

where, Δt can be thought of as the T_1 relaxation time, the spin-lattice relaxation time. A small T_1 value, will consequently, result in a large ΔW value, and line broadening will be observed in the spectrum. The converse is also true. In Figure 3.7, significant line broadening is noted in the downfield region. This implies a shorter relaxation time than for the analogue complex in Figure 3.6. A speculative suggestion can be explained in terms of the additional phenyl ring on the Cp fragment, which alters the relaxation time. In the case of (**3.1**) molecular modeling reveals an average torsion angle of 28.3 degrees for all the phenyl rings to the Cp ring. In the case of (**3.2**), the average torsion angle is significantly more, 33.8 degrees (by computer model). This implies greater conjugation in the former case, with the metal, which could influence the relaxation time, and cause less line broadening.

It is unlikely that the two signals seen in each spectrum correspond to a hyperfine coupling, the difference in field strength is too much, and the signal does not resemble that of a coupled EPR signal. In general, for mononuclear S=3/2 Cr(III) species, a signal with a *g* (parallel) and a *g* (orthogonal) component exists at 2 and 4 respectively.[57] This is reflected in each EPR spectrum

of (**3.1**) and (**3.4**). EPR spectroscopy conducted on mononuclear Cr(III) complexes have been reported in the literature. In one such case, reported by Bryliakov *et al.*, Cr^{III}(salen)Cl complexes, yielded spectra with g values of around 4 and 2. It is noted here that this is typical of electronic spin S=3/2 complexes.[58] Another study by Shaham *et al.* investigates the EPR spectra of $(H_2O)_5Cr^{III}$alkyl complexes. Again, similar spectra are obtained as observed in our work, with spectra having g factor values of around 4 and 2, and a spin of 3/2 is again assigned.[59] Analogous monomeric Cr(III) species that have a similar magnetic resonance values to those seen here (approx 3550 G) have also been reported.[60] The effect of the temperature is noted, as the intensity of the signal improves at lower temperatures as expected. It is likely that a dissociation equilibrium takes place, in solution, between the EPR silent dimeric species and EPR active the monomeric species. This is shown in Scheme 3.6.

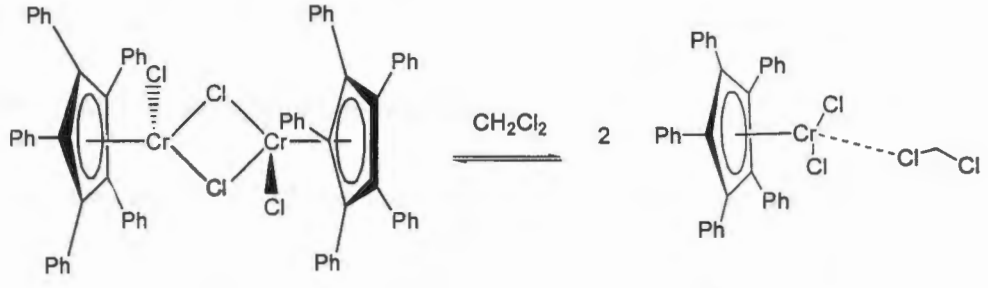

3.7

EPR Silent at low temperatures

Possible EPR active species

Scheme 3.6 Possible dissociation equilibrium of (**3.1**) to form the solvated mononuclear Cr(III) complex with associated dichloromethane.

It is likely that (**3.7**) and the tetraphenyl analogue (**3.8**) is stablised by the weakly coordinating solvent (dichloromethane) especially at the low temperatures that the EPR spectra were run at. Numerous examples of Cr(III) monomeric complexes exist, that can be isolated and are moderately stable, such as $(C_5Ph_5)Cr(CO)_3$•. Piano-stool complexes for Mo and W are generally "four-legged" while for Cr "three-legged" [61], hence the proposed structure of (**3.7**), which is responsible for the EPR signals obtained (pseudo-octohedral).

The resonance condition can be re-written in terms of *g*, a dimensionless parameter that depends on the species under investigation. This value is a function of the frequency of the laser beam used ν, the Bohr Magneton, μ_B; and the field strength at the centre of absorption. (eq **3.4**)

$g = h\nu/\mu_B B$ **(eq. 3.4)**

Table 3.1 illustrates the calculated *g* values for each complex in the specified magnetic field.

Model Complex	$g_{orthogonal}$	$g_{parallel}$
3.1	3.92	1.99
3.4	3.87	2.02

Table 3.1 Calculated *g* values for EPR resonances in each model complex (**eq 3.4**).

Respective g values, calculated from the resonance condition, and the EPR spectra for each model complex. The expected values of around 4 and 2 are noted in each case, as expected for a mononuclear Cr(III) species, with S = 3/2 spin state (as discussed above and referenced).

3.5 NMR studies on Cr(III) model complexes

NMR work done on $[Cp^*CrCl_2]_2$ has shown it to be paramagnetic, with excessive shifting effects on the methyl protons as a result of the Cr(III) paramagnetic centre. [62,63] More recently, NMR work on cationic and neutral phosphido–bridged dimeric Cr(III) compounds has demonstrated ^{1}H NMR silence of Cp* protons in normal NMR spectroscopy, but resonances from protons in far proximity of the Cr(III) centre, visible in the expected regions. [64] No NMR work has been conducted on the complexes of the type investigated in this project, and in view of the distance of the protons in the aromatic rings (on the Cp ligand) from the Cr(III) centre a muted line broadening effect could be anticipated. Each complex was submitted for NMR spectroscopy, deliberately in a non coordinating solvent to ensure a lack of previously observed dissociation of these dimeric complexes, and subsequent paramagnetic broadening. A lack of paramagnetic broadening, lends a certain amount of support to the hypothesis above that in a non coordinating solvent, no dissociation is observed. The fact that no (or little) line broadening is observed suggests dimeric or diamagnetic properties. This is *however* speculative, as a lack of line broadening could simply be a consequence of the distance between the aromatic protons and the paramagnetic centers, as observed in ref. 59. See Figure 3.8.

[i] $g_e = 2.00$ for a free electron.

^4J coupling of H* and Cr(III) centre

^3J coupling of H* with Cr(III) centre

Figure 3.8 Possible explanation for lack of line broadening in (**3.1**), (**3.4**) and (**3.6**) (top), compared with the literature case, where line broadening and shifts are observed (bottom). In the former case, the distance between the paramagnetic centre is one bond length further than in the latter, literature case.

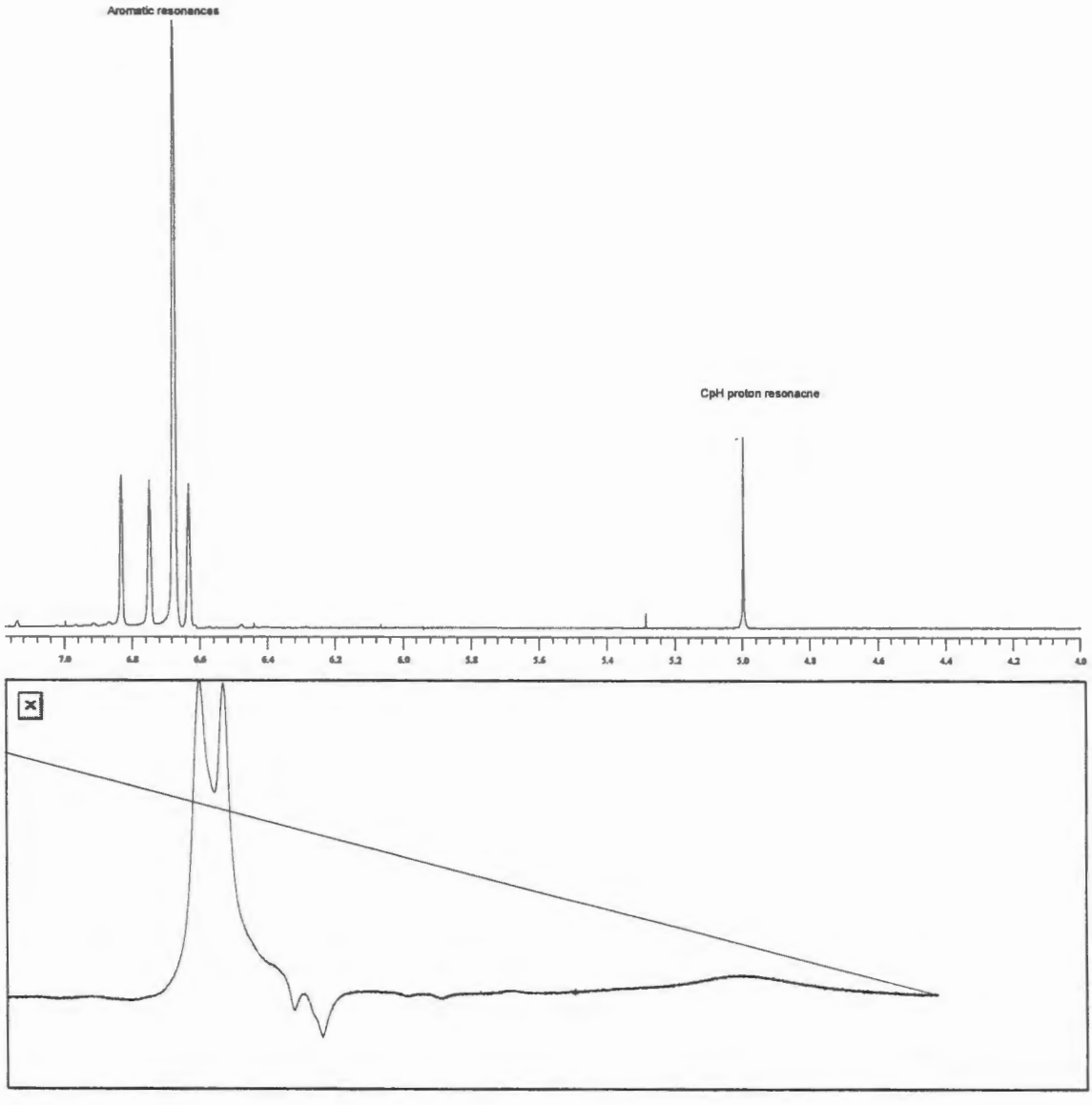

Figure 3.9 Comparison of ^{1}H NMR of ligand (**2.10**) (in $CDCl_3$) (top) with complex (**3.6**) in toluene-d_8 (bottom).

The above spectra clearly show the distinction between the protonated ligand and the complex. An absence of the Cp*H* proton resonance is noted in the complex (as expected), and a shift in the aromatic region is also noted. Similar trends were observed for the other complexes. Slight signal broadening is noted in Figure 3.9, but to a lesser extent than other paramagnetic species.

3.6 Discussion of EPR and NMR data of Cr(III) model complexes

As combined techniques, NMR and EPR enabled insight into the behavior of the Cr(III) model complexes, that are catalytically active as ethene trimerisation precursors (See chap 4). The EPR data suggests, that in a weakly coordinating solvent, paramagnetic Cr(III) mononuclear complexes are generated, suggesting dissociation to possibly a distorted tetrahedral system (**3.7**). The NMR studies revealed that in a non coordinating solvent (such as toluene – d_8) there is no paramagnetic line broadening present and hence the spectra could reflect that of the dimeric species present (which are reported to have antiferromagnetic interactions between the Cr(III) centres). *Alternatively*, in light of the distance between the aromatic protons and the Cr(III) centres (which themselves are paramagnetic), line broadening could be significantly reduced, or not observed at all. These results are significant, since what they are suggesting is that the choice of solvent, affects the solution dissociation of the dimeric complexes. A non coordinating solvent (such as toluene) does not promote dissociation, and the dimeric complexes are observed. A moderately coordinating solvent (such as CH_2Cl_2) promote reversible dissociation of the Cr(III) complexes, whereas strongly coordinating solvents (such as THF) promote irreversible dissociation of the dimeric species present (as suggested by literature).

3.7 Elemental analysis

For the targets (**3.1**), (**3.4**) and (**3.6**), elemental analysis proved problematic. This has been noticed before for (**3.1**) and other halo Cr(III) dimeric complexes. [65] This is possibly in light of incomplete combustion of the compounds (especially the quaternary carbon atoms) , which in general yield analyses that are not publishable or repeatable. Despite this, elemental analysis on these compounds was carried out, and an oxidant (V_2O_5) added to the samples to aid in the combustion of the sample. Even so, results obtained were not within the required margin of error. Attempted elemental analysis on compound (**3.6**) showed a complete lack of repeatability in light of the labile nature of the complex.

3.8 Mass Spectrometry

In the case of (**3.1**) and (**3.4**) FAB-MS was attempted. No parent peak was obtained in either case. The only peaks that could be tentatively assigned in both cases was that of the Cp^+ peak and that corresponding to the species $[CpCrCl]^+$ [In the case of (**3.1**) Cp = C_5Ph_5; (**3.4**) Cp = C_5Ph_4H]. MALDI-TOF Mass Spectrometry of (**3.1**) was attempted in a THF matrix (consisting of THF and benzyl alcohol) and attempts at obtaining an M^+ peak were again unsuccessful.

3.9 Synthesis of other transition metal model complexes

The Cr(III) model complexes enabled a better understanding of the catalytic process in terms of understanding the chemistry of the Cr centre better, when catalysis was carried out. In order to quantify and understand the role of the bulky cyclopentadieneyl ligand in the process, more model complexes had to be prepared.

It is known that CrCp systems, where Cp = C_5H_5 are precursors to polymerization catalysts,[66] however, in the case of bulky cyclopentadiene ligands, such as 1,2,3,4,5 pentaphenyl cyclopenta-1,3,-diene, high mass percentage 1-hexene is observed as product. This could be as a result of the *steric* properties of the phenyl rings present on the Cp moiety, but could also be as a result of *electronic* influences.

As stated in Chapter 2 – physical properties, such as colour, of known metal complexes, of the type, Cp_2Fe, with bulky ligands are different from those only containing the Cp ligand. This idea could be of importance in the catalytic process under investigation. In order to quantify this idea, an Fe(II) model complex, containing the bulky Cp ligand was prepared, and compared to ferrocene. Cyclic voltametry was used to probe the change in oxidation/reduction potential at a metal centre with these ligands, which could shed light on the electronic influence of the ligands on other metals (in particular chromium).

3.9.1 Preparation of bulky iron(II) sandwiches

Preparation of more bulky Fe(II) sandwich compounds usually follows the use of $FeCl_2$ with a Cp anion. This is represented schematically in Scheme 3.7.

M = Li, Na, K

Scheme 3.7 General preparation of Fe(II) "sandwiches".

The compound, $(C_5Ph_4H)_2Fe$, (**3.8**) has been reported [67] and in light of it's stability was earmarked as a complex to explore the electronic effects of the phenyl rings on the metal centre. In order to probe this parameter, we employed cyclic voltametry.

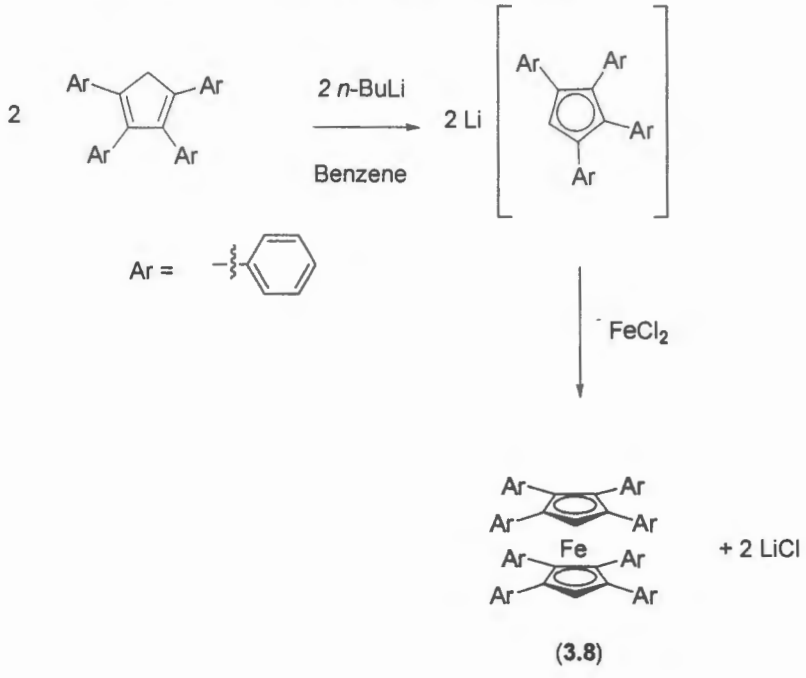

(3.8)

Scheme 3.8 Schematic representation of pathway used to synthesise target (**3.8**), in accordance with the method by Castellani *et al.* [67]

The cyclic voltamogram of ferrocene,$(C_5H_5)_2Fe$, was compared with that of (**3.8**) in order to establish the electronic influence of the aromatic rings on the metal centre. Although (**3.8**) is known, and CV has been conducted on it [67] the solvent used was CH_2Cl_2. Our CV data was obtained in CH_3CN as solvent with Bu_4NBF_4 (0.1 M) as supporting (background) electrolyte. In light of the poor solubility of (**3.8**) in CH_3CN, a more sensitive scan setting was used than was required with ferrocene, which was used as standard.

The cyclic voltamograms are presented in Figure 3.10. In both cases a reversible wave is observed. This is in light of the cathodic / anodic current ratio being close to unity. The electrochemical process in both cases is Cp_2Fe -> $[Cp_2Fe]^+$ (where Cp = C_5H_5 or C_5Ph_4H).

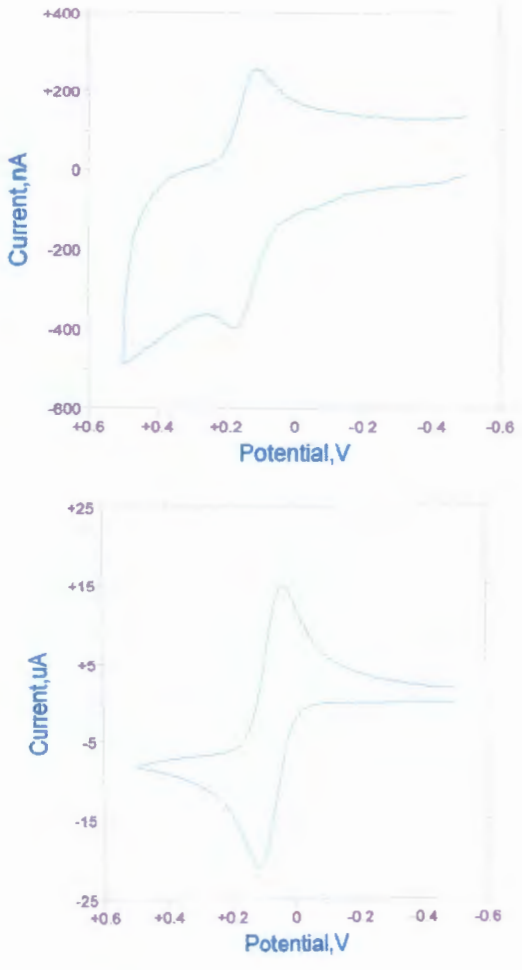

Figure 3.10 CV in CH_3CN with Bu_4NBF_4 (0.1 M) as supporting electrolyte for (**3.8**) (top) and ferrocene (bottom).

Complex	$E_{1/2}$	Ratio i_a/i_c	Corrected $E_{1/2}$ (to ferrocene)
Ferrocene	0.075 V[ii]	0.99	0
(3.8)	0.14 V[ii]	1.22	0.065
Decaphenyl ferrocene	0.74 V[iii]		0.665

Table 3.2 Summary of obtained electrochemical parameters for the model complex (**3.8**) and ferrocene in CH_3CN.

[ii] This work
[iii] Previous work (ref.69)

An increase in the half wave potential is noted in the case of the model complex (**3.8**) compared with ferrocene. This observation has also been noted in CH_2Cl_2 solvent for this complex, and other analogues such as that of V, Cr, Co, Ni. [68]

Previous cyclic voltametric investigations on the pentaphenylcylopentadienyl complex i.e. $(C_5Ph_5)_2Fe$ [69] in CH_3CN has demonstrated a half wave potential of 0.74 V. From our determination of the $E_{1/2}$ for $(C_5Ph_4H)_2Fe$ in CH_2CN it would appear that a shift in a positive potential direction indicates increased difficulty to form the $[(C_5Ph_4H)_2Fe]^+$ compared with ferrocene. In the case of $(C_5Ph_5)_2Fe$ this shift is almost an order of magnitude more positive than ferrocene. These results demonstrate a direct relationship between the number of phenyl rings on the cyclopentadiene ligand and the $E_{1/2}$. This essentially implies the greater the number of phenyl rings on the cyclopentadienyl ligand, the more difficult is the process of oxidation. This observation can be steric or more likely, electronic. It demonstrates a "withdrawal" of electron density from the Fe(II) centre to the phenyl rings, resulting in a more electron deficient metal centre. These results are plotted (Figure 3.11).

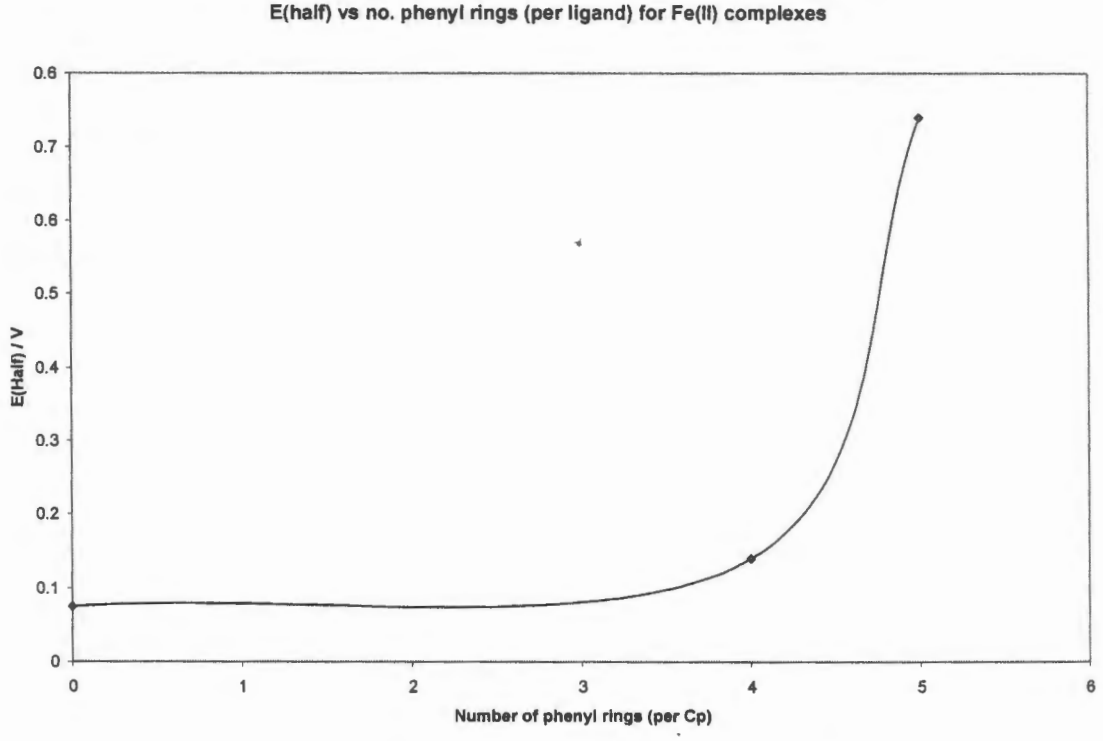

Figure 3.11 Uncorrected plot $E_{1/2}$ for Ferrocene, octaphenyl ferrocene (**3.8**) and decaphenyl ferrocene.

The observed trend sheds light on the electronic role of the phenyl rings in bulky cyclopentadienyl complexes. From the CV results, it can be concluded that the phenyl rings withdraw electron density from the metal centre, a trend that could logically be extended to any other transition metal analogues of these ligands.

This work may shed light on the role of the phenyl rings on the catalysis, from an electronic point of view. By using stable Fe(II) model complexes, the electronic influences could be probed by CV. By applying these results to the Cr(III) catalyst system, an increase in the electronic withdrawal from the Cr centre results in an electron deficient metal that possibly promotes catalytic activity.

3.10 Single Crystal X-Ray Diffraction Studies

In an attempt to obtain crystals of the mononuclear Cr(III) complex (i.e. $(C_5Ph_4H)CrCl_2X$, where X is a co-ordinating solvent, such as THF), suitable for X-ray diffraction studies, a sample of (**3.4**) was dissolved in THF and left in the glove-box. Over a period of *ca.* 4 weeks, the development of X-Ray quality crystals were observed and sent for X-ray analysis. The structure was solved, but was $CrCl_3(thf)_3$, as opposed to the expected monomer. Possibly, this observation is as a consequence of the THF not only cleaving the dimeric parent, but occupying the three vacant co-ordination sites of the Cp ring, on the Cr, possibly formed by a planar $CrCl_3$ intermediate, that enables the formation of the observed *mer* stereochemistry. Scheme 3.8 depicts a possible, but speculative route to the formation of the $CrCl_3(thf)_3$ from the parent dimer. In all likelihood, it is possible that the crystals obtained could also be starting material.

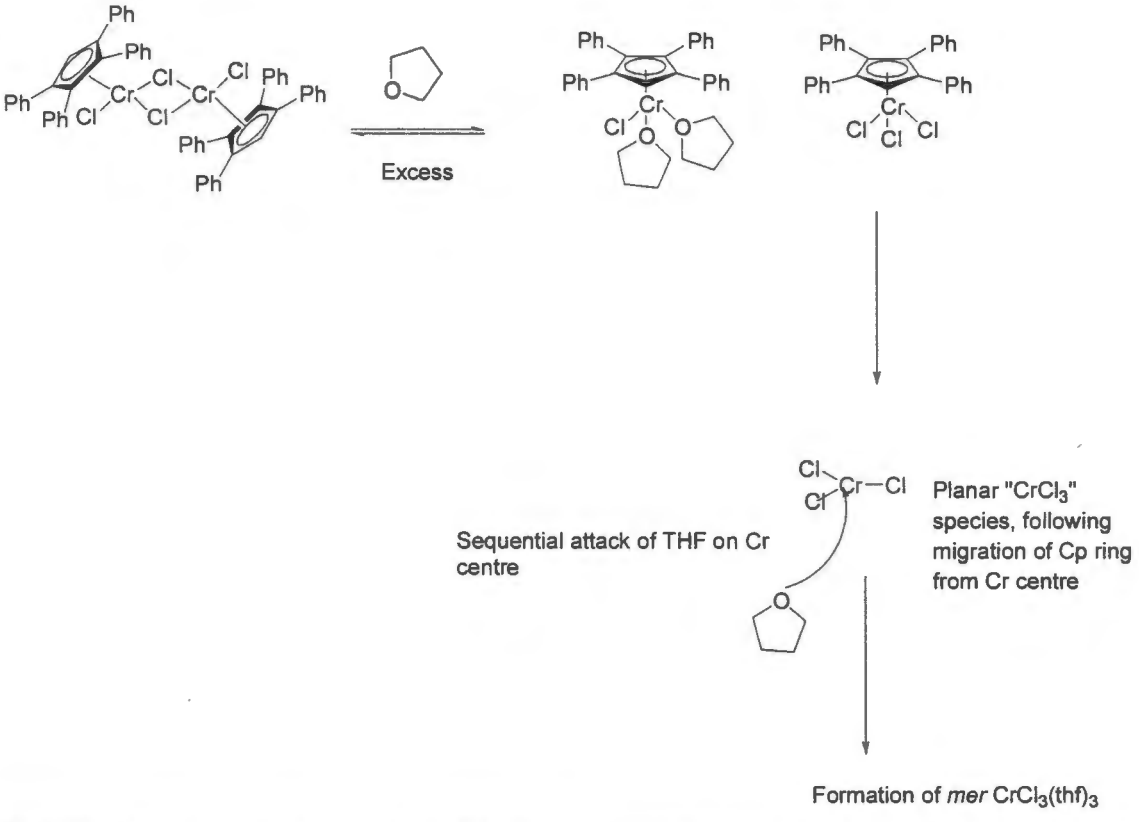

Scheme 3.8 Speculative formation of the observed product from the dimer. To account for the stereochemistry of the product, it is likely to pass through a planar "transition state". Charges are omitted.

X-Ray crystallographic studies of this complex were reported by Cotton *et al.*, in 1986. [70] The data was collected, in this case, at room temperature (295 K). The data collection in our case was done at low temperatures (113 K), and the structure solved. Despite the fact that the structure has been solved before, our crystallographic results can be compared with those previously reported, and any deviations, or differences attributed to a temperature effect.

Empirical formula	$C_{12}\ H_{24}\ Cl_3\ Cr\ O_3$	
Formula weight	374.66	
Temperature	113(2) K ;	278 K[a]
Wavelength	0.71073 A	
Crystal system, space group	Monoclinic, $P2_1/c$	
Unit cell dimensions	a = 8.01240(10) A alpha = 90 deg.	
	b = 12.44290(10) A beta = 92.6030(10) deg.	
	c = 16.3678(5) A gamma = 90 deg.	
Volume	1630.14(6) A^3 ;	1684(1) $Å^3$ [a]
Z, Calculated density	4, 1.527 Mg/m^3	
Absorption coefficient	1.194 mm^{-1}	
F(000)	780	
Crystal size	0.20 x 0.15 x 0.15 mm	
Theta range for data collection	4.30 to 26.75 deg.	
Limiting indices	-10<=h<=10, -15<=k<=15, -20<=l<=20	
Reflections collected / unique	44881 / 3457 [R(int) = 0.0301]	
Completeness to θ=	26.75 99.4 %	
Max. and min. transmission	0.8413 and 0.7962	
Refinement method	Full-matrix least-squares on F^2	
Data / restraints / parameters	3457 / 0 / 173	
Goodness-of-fit on F^2	1.048	
Final R indices [I>2σ(I)]	R1 = 0.0332, wR2 = 0.0803 ; R1 = 0.059[a], wR2 = 0.086[a]	
R indices (all data)	R1 = 0.0405, wR2 = 0.0853	
Extinction coefficient	0.0022(8)	
Largest diff. peak and hole	1.644 and -0.525 e/ $Å^3$	

Table 3.3 Crystal data (this work). [a] Reported by Cotton *et al.*[70]

Most of the parameters are similar for our crystal determination, compared well with that of Cotton *et al.*

As expected, the unit cell volume is slightly smaller in our case, than that reported by Cotton *et al.* This can be attributed to the fact that the data was collected at significantly lower temperatures, in our case, than originally by Cotton *et al.* An improvement on the R factor is also noted in our solved structure, with a value of 3.3 % compared with 5.9 % by Cotton *et al.* This can be attributed to the fact that the data was collected at a much lower temperature in our case, which leads to less disorder in the structure, and hence a lower R value.

Some diagrams of our solved structure will follow, along with crystal packing diagrams showing clearly the space group's ($P2_1/c$) symmetry elements.

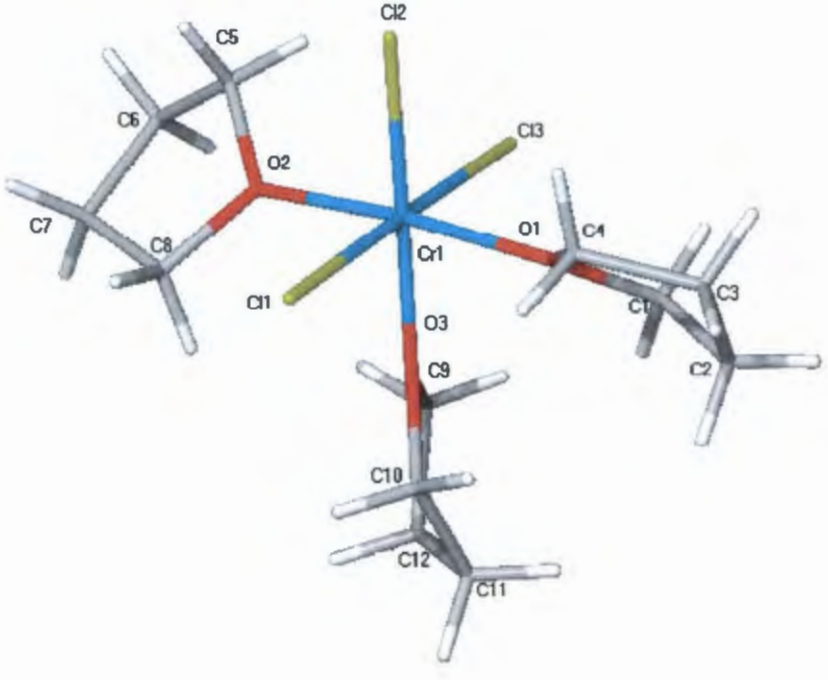

Figure 3.12 Our X-ray structure of $CrCl_3(thf)_3$. As noted before,[70] a *mer* stereochemistry is observed.

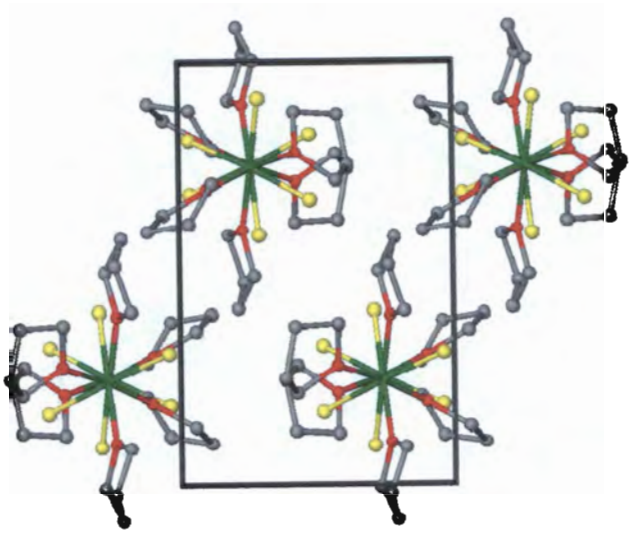

Figure 3.13 Crystal packing diagram of unit cell viewed along *l* axis. Invariance with respect to translation is seen clearly.

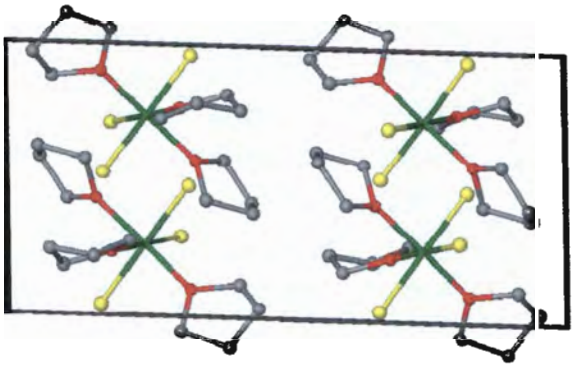

Figure 3.14 Crystal packing diagram of unit cell along *k* axis. Again invariance with respect to translation is observed.

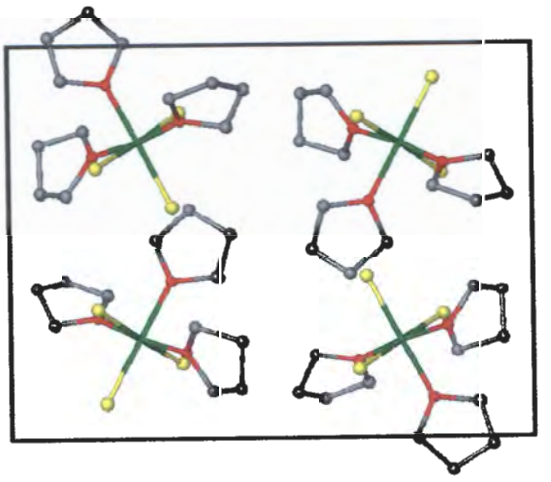

Figure 3.15 Crystal packing diagram of unit cell along *h* axis.

Atom	x	y	z	U(eq)
Cr(1)	2625(1)	7529(1)	2475(1)	16(1)
Cl(1)	391(1)	6876(1)	1670(1)	22(1)
Cl(2)	2919(1)	5903(1)	3123(1)	25(1)
Cl(3)	4786(1)	8272(1)	3272(1)	23(1)
O(1)	4263(2)	7173(1)	1603(1)	20(1)
O(2)	1013(2)	8051(1)	3287(1)	23(1)
O(3)	2324(2)	8986(1)	1876(1)	19(1)
C(4)	4230(3)	6204(2)	1096(1)	20(1)
C(11)	2375(3)	10201(2)	781(2)	34(1)
C(7)	-1125(3)	9006(2)	3923(1)	25(1)
C(3)	5797(3)	6266(2)	607(1)	26(1)
C(10)	2145(3)	10839(2)	1561(2)	30(1)
C(1)	5731(3)	7823(2)	1424(1)	25(1)
C(9)	2743(3)	10053(2)	2214(1)	24(1)
C(2)	6159(3)	7473(2)	580(1)	26(1)
C(8)	-563(3)	8622(2)	3101(1)	21(1)
C(6)	382(3)	8842(2)	4508(2)	38(1)
C(5)	1225(3)	7905(2)	4169(1)	29(1)
C(12)	1795(3)	9094(2)	1016(1)	28(1)

Table 3.4 Atomic coordinates (x 10^4) and equivalent isotropic displacement parameters (A^2 x 10^3) U(eq) is defined as one third of the trace of the orthogonalized U*ij* tensor.

Atoms	Bond lengths (Å)	
	This work	Cotton *et al.* [70]
Cr-Cl(1)	2.3202(6)	2.307(2)
Cr-Cl(2)	2.2921(6)	2.283(2)
Cr-Cl(3)	2.3131(6)	2.312(2)
Cr-O(1)	2.0308(14)	2.027(4)
Cr-O(2)	2.0030(15)	1.994(4)
Cr-O(3)	2.0700(14)	2.077(4)

Table 3.5 Comparison of some key bond lengths in our structure determination and that reported by Cotton *et al.* [70]

Atoms	Bonding Angle (°)	
	This work	Cotton *et al.*[70]
O(2)-Cr-O(1)	173.54(6)	172.5(1)
O(2)-Cr-O(3)	88.02(6)	86.5(1)
O(1)-Cr-O(3)	85.63(6)	86.0(1)
Cl(2)-Cr-O(3)	178.98(4)	179.8(1)

Table 3.6 Comparison of some bonding angles in our structure determination and that reported by Cotton *et al.* [70]

As expected, no hydrogen bonding is present. Besides minor differences in the values seen here (bond lengths and angles), there are no significant deviations from the published structure. Our complete data is listed in the appendix (A1), and does not warrant further discussion.

3.11 General conclusion

In this chapter, a series of model dinuclear Cr(III) complexes, and their synthesis was highlighted. In light of the intractable nature of these complexes, their lability and air-sensitivity, characterization was complicated. Although several techniques were attempted only some were successful. In all cases, the presence of the bridging halides was validated by the use of FT-IR. Although FAB-MS enabled identification of Cp-Cr fragments, the parent ion was undetected. Also,

MALDI-TOF MS failed. NMR spectroscopy was used with partial success in some of the complexes. Other techniques not investigated could have been atomic absorption (AA) spectroscopy, to determine the presence of Cr. Also, possibly, an ICP analysis could have been conducted on the complexes.

Other model compounds were also looked at, in particular that of Fe(II) sandwiches. The $co(_5Ph_4H)_2Fe$ was prepared, fully characterized, and studied by CV. A dramatic difference was noted in the half wave potential of ferrocene (the standard), and $(C_5Ph_4H)_2Fe$, highlighting the potential electronic influences of the bulky, arylated ligand.

Chapter 4

Catalytic Studies on Model Complexes and Cyclopentadienyl Ligands

"Education is what survives when what has been learned has been forgotten."

B. F. Skinner (1904 - 1990), New Scientist, May 21, 1964

4.1 Introduction and overview

The recent work by Mahomed *et al.* [42] has demonstrated the feasibility of the system discussed in this dissertation. It is possible to assess the catalytic activity and selectivity to various products (specifically 1-hexene) of new ligands (bulky cyclopentadienes) by combining them with a Cr source, a halogen source (see chapters 1 and 3) and an alkylating agent (triethylaluminium), together with pressurized ethene. A correlation between the catalytic activity of the model compounds themselves (See Chapter 3) with that of the ligands (along with the Cr source, TEA and halogen source) would suggest that the structure of the precursor, and active species, resembles that of the model complex. Unfortunately, due to time constraints, not all the ligands prepared could be screened for catalytic activity (with the Cr source and other compondents), and this work will follow in a publication after submission of this work. Here, three important catalytic results will be reported, and the link in reactivity and selectivity demonstrated for the model complex and the *in situ* system.[42]

Figures 4.1 and 4.2 show a schematic comparison of the approach by Mahomed *et al.*, and the approach using Cr model complexes, that possibly resemble or mimic the active precursor.

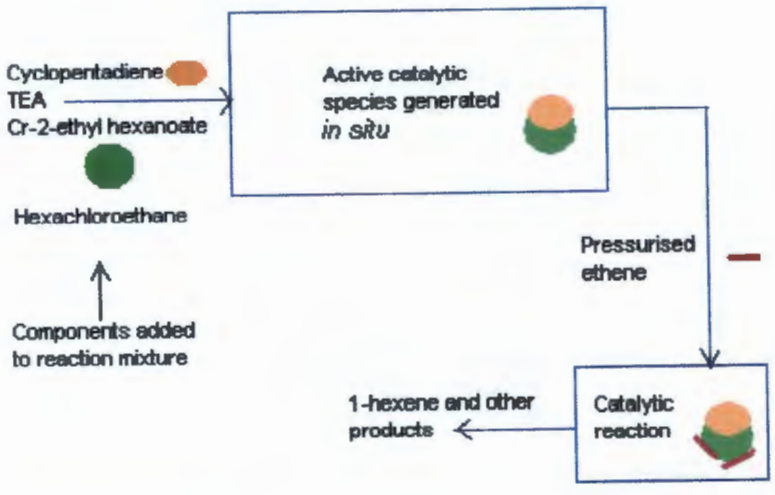

Figure 4.1 Schematic representation of the process by Mahomed *et al.*[11] The active species is generated *in situ* from several components.

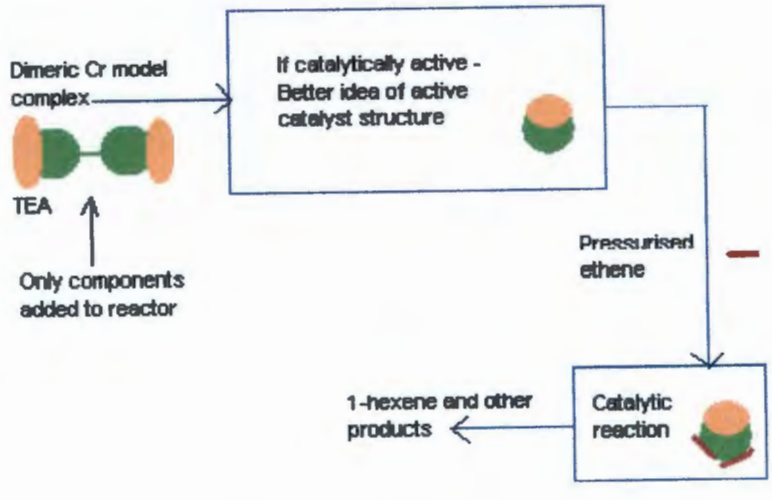

Figure 4.2 Schematic representation of our approach – generating an active catalytic species from a defined model complex viz. $[(C_5Ph_5)CrCl_2]_2$

4.2 Catalytic results

A Parr™ pressure reactor was used in all catalytic reactions. A Figure of such a reactor is presented in Figure 4.3.

Figure 4.3 Parr™ pressure reactor, with control unit, used in the catalytic testing.[71]

The details of the catalytic conditions, and work-up procedures are shown in the experimental chapter. A succinct summary of the three catalytic results performed on selected systems is shown here, and a discussion will follow.

Figure 4.1 shows a summary of the ethene uptake as a function of time, for each of the three catalytic runs conducted. The *in situ* system refers to that analogous to the recently published one by Mahomed *et al.* In this system, a combination of a halogen source (typically C_2Cl_6), a chromium source (usually Cr-2-ethyl hexanoate), protonated free ligand, and TEA are added to a reactor, and placed under a positive pressure of ethene. The model system is simply the model complex, $[(C_5Ph_5)CrCl_2]_2$ (**3.1**), combined with the same molar equivalent of TEA as with the *in situ* system, with the exact same reaction conditions and work-up.

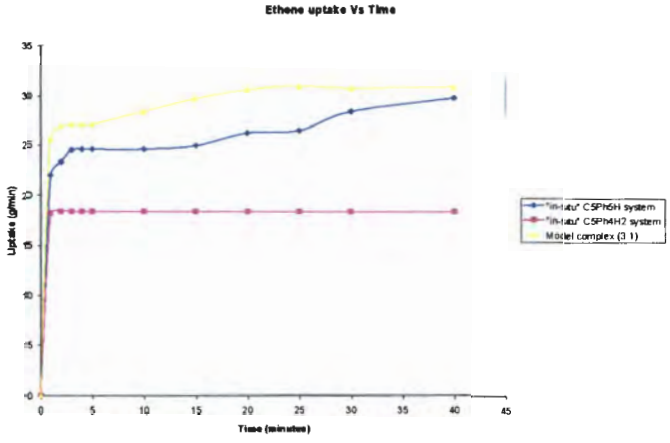

Figure 4.4 Summary of reaction/catalytic results. The "y-axis" refers to the total ethene uptake, determined by the decrease in total pressure in the reactor.

The GC chromatograms of each catalytic reaction mixture was analysed, and the details thereof are added in the experimental section, with a complete analysis of all products present, and their relative percentages. Here, the C-6 and 1-hexene selectivity will be focused on and presented, as this is the desired product in this catalytic reaction. Table 4.1 shows a summary of the C-6 and 1-hexene selectivities determined in each catalytic reaction.

Catalytic run	C-6 Selectivity (%)	1-Hexene selectivity (%)
C_5Ph_5H / Cr source /C_2Cl_6 /TEA / ethene	92.8	79.8
Model complex (**3.1**) / TEA / ethene	87.5	80.2
$C_5Ph_4H_2$ / Cr source /C_2Cl_6 /TEA / ethene	81.3	59.8

Table 4.1 Selectivities (C6 and 1-hexene) for each catalytic run.

Discussion and conclusion

Although only three key catalytic reactions were carried out, due to time constraints and resource availability, these three catalytic reactions have clearly demonstrated a key facet of this research project. Table 4.1 shows, that the selectivity towards 1-hexene and the C-6 selectivity for the system, C_5Ph_5H / Cr source /C_2Cl_6 /TEA / ethene (i.e. the system published by Mahomed *et al.*), and Model complex (**3.1**) / TEA / ethene (this work) are virtually the same. This indeed suggests that possibly, the reactive precursor in the Dixon system, resembles that of the key model complex prepared in this project. This is the first indication, catalytically, of the structure of the active catalytic precursor.

In light of this result, it would appear that the active catalytic species in the Dixon system, is similar in composition to that of the model complex (**3.1**). This suggests that the ligand is co-ordinated in a eta-5 fashion to the Cr(III) centre, and upon activation, yields a catalytically active complex. A mechanistic rationalization of this process, which at this stage remains speculative, but possible is presented in Scheme 4.1. This mechanism rationalizes the catalytic activity of the model complex, and in light of the similar reactivities towards 1-hexene and C-6 fragments of the

corresponding Dixon system, it seems possible, that a similar process takes place in that reaction, by generation of an analogous species, from the components *in situ*.

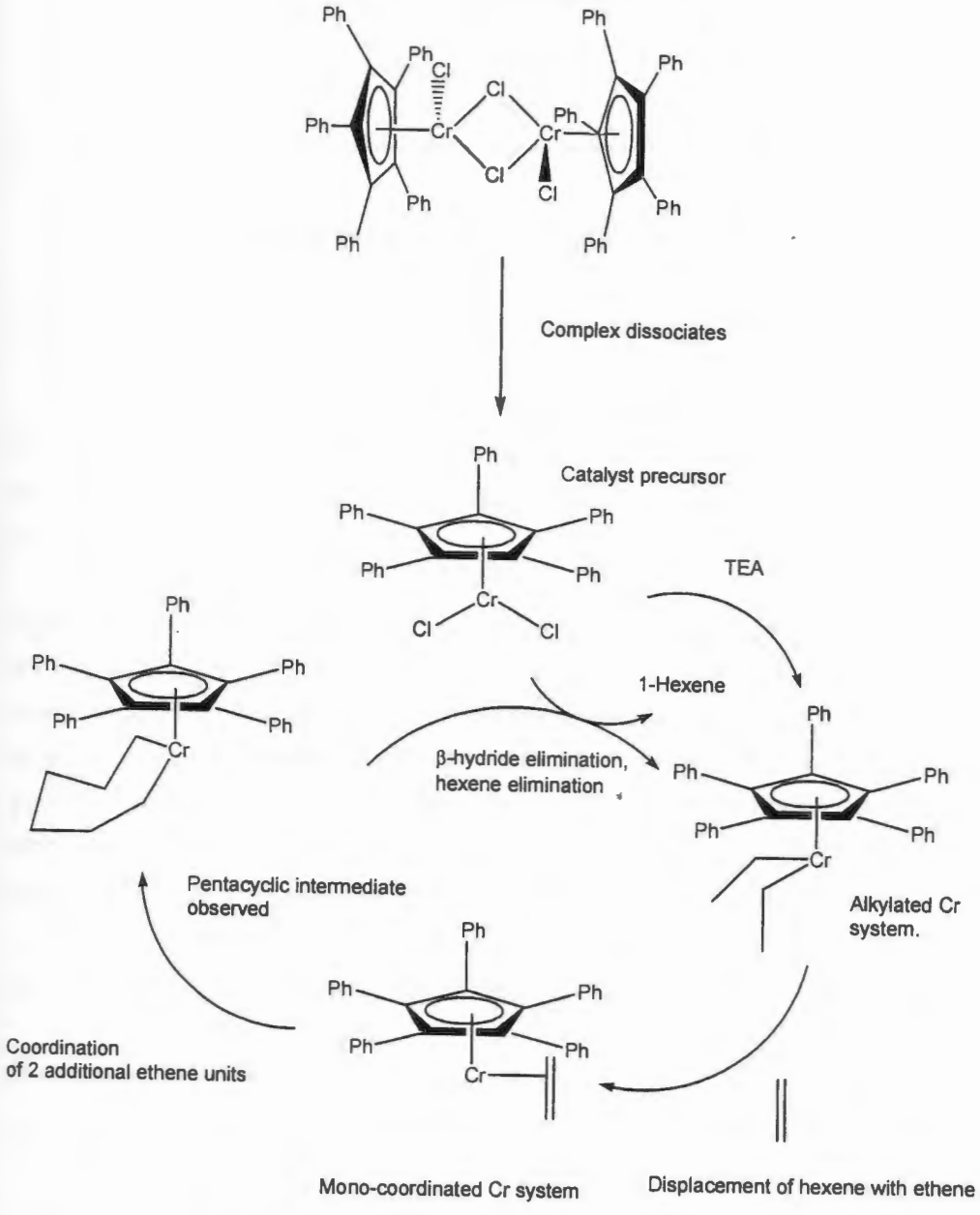

Scheme 4.1 Schematic representation of the possible reaction pathway in the catalytic trimerisation of ethene using model complex (**3.1**).

Chapter 5

Density Functional Theory and Transition State Theory : An Introduction [80]

"Do not worry about your difficulties in Mathematics. I can assure you mine are still greater."

Albert Einstein

5.1 Introduction and background to DFT (Density Functional Theory)

In addition to a synthetic and catalytic approach, a computational approach was also investigated in this project. Molecular modeling was employed as a tool to further understand the catalytic mechanism of ethene trimerisation, with our system. This chapter serves as a theoretical introduction and background to this method. DFT (Density Functional Theory) will briefly be discussed in addition to TS (Transition-state) theory, both of which are relevant in this project. *This introduction is based on (ref. 80).*

The fundamental departure point for the use of DFT in molecular modeling is the 1964 proof by Hohenberg and Kohn. [72] This fundamental proof demonstrates that the ground-state electronic energy is determined by electron density alone. The ultimate goal of DFT is to associate electron density with ground state energy,[73] as it has been demonstrated that each density yields different ground-state energies. The energy functional, as per the wave mechanical approach, can be separated into three components : Kinetic energy $T[\rho]$, nuclear-electronic attraction, $E_{ne}[\rho]$ and finally, electron-electron repulsion, $E_{ee}[\rho]$. Assuming the Born-Oppenheimer approximation holds, nuclear-nuclear attraction is held constant. Hartree-Fock theory dictates that the term $E_{ee}[\rho]$ can be further divided into a Coulombic component, $J[\rho]$, and an exchange component, $K[\rho]$.

The energy functional, $E_{TF}[\rho] = T_{TF}[\rho] + E_{ne}[\rho] + J[\rho]$, known as the Thomas-Fermi (TF) functional, constitutes the TF model (Thomas-Fermi). The largest shortcoming of the TF model is that molecules don't exist , as a result of the absence of bond-prediction. The basis of DFT use in computational chemistry was the 1965 introduction of orbitals by Kohn and Sham. [74] The kinetic energy component is inadequately represented by the TF model, while Kohn-Sham (KS) decomposes the kinetic energy into two components, a small correction terms, and one that can be calculated exactly. The principal key to the KS theory is the determining of kinetic energy making use of the assumption of non-interacting electrons. This energy is small, and is taken into

consideration by an exchange-correlation term, resulting in the generalized DFT expression (eq. 5.1).

$$E_{DFT}[\rho] = T_S[\rho] + E_{ne}[\rho] + J[\rho] + E_{XC}[\rho] \quad \text{(eq. 5.1)}$$

By equating E_{DFT} to the exact energy, the energy expression may be re-written in terms of E_{XC} after subtraction of the non-interacting kinetic energy, E_{ne}, and J terms, resulting in (eq. 5.2).

$$E_{XC}[\rho] = (T[\rho] - T_s[\rho]) + (E_{ee}[\rho] - J[\rho]) \quad \text{(eq. 5.2)}$$

The first term in (eq. 5.2) corresponds to the kinetic correlation energy, while the second term to that of potential correlation energy. The exchange energy is the largest contributor to E_{XC}, while the correlation energy contributes far less to E_{XC}. In DFT the total electronic density need only be considered. The major obstacle in this theory, however is finding a basis set of orthogonal (or orthonormal) orbitals that minimize the energy. By enforcing Langrange methods, and the use of $\mathbf{h}_{KS}$ (a one electron operator) , and a Lagrange multiplier diagonal, a set of *canonical* Kohn-Sham (KS) orbitals is produced. The result is the so-called pseudo-eigenvalue equations known as the Kohn-Sham (KS) equations. (eq. **5.3**)

$$\mathbf{h}_{KS}\,\phi i = \varepsilon_i\,\phi i \qquad \text{(eq. 5.3)}$$

Many similarities exist between DFT, wave mechanics and HF theory, but there is one critical difference. If $E_{XC}[\rho]$ was known exactly, then DFT would provide the exact total energy, inclusive of electron correlation. Consequently, DFT accommodates the computationally demanding correlation energy in wave mechanics at a computational effort similar to determining uncorrelated HF energy.

5.2 DFT Methods at a glance

5.2.1 Local Density Methods (LDA) and Local Spin Density Approximation (LSDA)

In Local density approximation (LDA), the electronic density is treated as a uniform gas, or at least a slowly varying density function. The Dirac formula generates the exchange energy for a uniform gas as (eq. 5.4),

$$\varepsilon_X^{LDA}[\rho] = -C_X\rho^{1/3} \quad \text{(eq. 5.4)}$$

Local Spin Density Approximation (LSDA) is more general, where α and β densities are unequal, and each individual density is raised to the power 4/3 in the integration, to yield (eq. 5.5).

$$\varepsilon_X^{LSDA}[\rho] = -2^{1/3} C_X [\rho_\alpha^{1/3} + \rho_\beta^{1/3}] \text{ (eq. 5.4)}$$

Despite the differences highlighted between LDA and LSDA above, for closed shell systems, the two methods can be employed interchangeably. Slater proposed a method [75] whereby the correlation energy is ignored, and this method can also be considered a LDA method. Monte-Carlo methods, have generated correlation energies of uniform electronic gasses, and it's use in DFT calculations extended by Vosko *et al.* [76], who generated a functional that enables interpolation between unpolarized and spin polarized limits (eq. **5.5**)

$$f(\zeta) = \frac{(1+\zeta)^{4/3} + (1-\zeta)^{4/3} - 2}{2(2^{1/3} - 1)} \qquad \text{(eq. 5.5)}$$

5.2.2 Generalised Gradient Approximation (GGA)

Assuming non ideality in the density of an electron gas, would enable more accurate energy determinations over LSDA (or LDA). This implies derivatives of density need to be found, and this method is commonly referred to as GGA, Generalised Gradient Approximation, or Gradient Corrected Approximation. Perdew and Wang (Acronym for algorithm PW86) [77] proposed changing the exchange energy expression for LSDA, by the addition of several exponential terms (eq. **5.6**).

$$\varepsilon_X^{PW86} = \varepsilon_X^{LDA} (1 + ax^2 + bx^4 + cx^6)^{1/15} \qquad \text{(eq. 5.6)}$$

In this expression, x, is a dimensionless variable relating to gradient, and a, b, and c suitable constants. The variable x is related to electron density by (eq. **5.7**)

$$x = \frac{|\nabla \rho|}{\rho^{4/3}} \qquad \text{(eq. 5.7)}$$

Another modification of LSDA exchange energy was made by Becke [78] in which the correct asymptotic behavior of the energy density is included (eq. **5.8**)

$$\varepsilon_X^{B88} = \varepsilon_X^{LDA} + \Delta \varepsilon_X^{B88} \text{ (eq. 5.8)}$$

where,

$$\Delta_x^{B88} = -\beta\rho^{1/3}\frac{x^2}{1+6\beta x\sinh^{-1}x} \quad \text{(eq. 5.8 b)}$$

β is determined from known data, and x is defined as in (Eq. **5.8**).

Other functionals exist which contain the derivatives of the orbitals, rather than the gradient (or derivative) of the overall density such an example is that proposed by Becke and Roussel (BR).[79] The BR functional is of the form (eq. **5.9**)

$$\varepsilon_x^{BR} = -\frac{2-2e^{-\alpha\beta}-\alpha\beta e^{-\alpha\beta}}{4\beta}$$

$$\alpha^3 e^{-\alpha\beta} = 8\pi\rho$$

$$\alpha(\alpha b-2) = \frac{\nabla^2\rho - 2D}{\rho}$$

$$D = \sum_i^N \left|\nabla\phi_i\right|^2 - \frac{(\nabla\rho)^2}{4\rho} \quad \text{(eq. 5.9)}$$

Such a functional is more computationally demanding, and results of comparable accuracy have been found for other less demanding methods.

It is worth noting, that it is possible to combine these methods into a "hybrid method". Examples of such hybrid methods are the Becke three parameter functional, or the Adiabatic Connection Model (ACM).

5.3 Computational Accuracy and Performance

Several methods for performing DFT calculations exist, and the performance, computational demands and accuracy need to be taken into consideration when deciding which method to employ. In the scope of this dissertation, a simple comparison of different methods will be presented and an in depth discussion omitted.

In the scope of this research project, it was decided to use the BLYP functional. Taking the factors of deviation, and computational accuracy into account, this proved the optimal choice for our modeling work.

Table 5.1 shows a comparison of different DFT methods. (Values are in kcal/mol).

DFT Method	Mean absolute deviation	Maximum absolute deviation
G2(MP2)	1.6	8.2
G2(MP2, SVP)	1.9	12.5
SVWN	90.9	228.7
BLYP	7.1	28.4
BPW91	7.9	32.2
B3LYP	3.1	20.1

Table 5.1 : Comparison of performance of different DFT methods.[80]

5.3 The transition state theory (TS)

Another important aspect in our modeling work was the determination of transition states between various species in the catalytic cycle under investigation. This section serves as an introduction to the theory of transition states, and theoretical background to this.

A loose definition of a TS (transition-state) is that of a species that "links" the low energy configurations of a reactant and product, being an "intermediate" energy maximum. A *true* transition state is one which is the energy maximum on the *lowest* energy reaction pathway (or surface) that links a reactant and product. This is represented in the two dimensional case for a hypothetical molecule in Figure 5.1. Although this is a simplified representation of the more realistic three dimensional energy surface, it demonstrates the point. The true TS is the energy maxima of the lowest possible energy surface linking reactant and product.

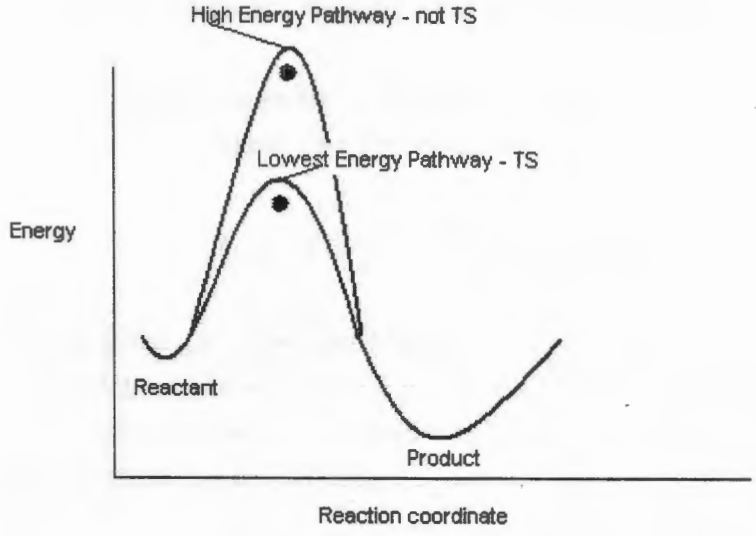

Figure 5.1 Two dimensional surface representing possible energy surfaces linking reactant and product.

TS theory is semi-classical, in the sense that the progression along the horizontal (reaction co-ordinate) axis is treated classically, while quantization of energy is taken into consideration in the vertical axis. (i.e. molecular partition functions apply, which take quantization into account). The macroscopic rate constant (assuming equilibrium between the reactant and TS) can be expressed as (eq. 5.10)

$$k = \frac{k_B T}{h} e^{-\Delta G^{\#} / RT} \qquad \textbf{(eq. 5.10)}$$

In this expression (5.10) $\Delta G^{\#}$ is the Gibbs free energy difference between the TS and the reactant and k_B is the Boltzmann's constant. As an aside, the TST expression only holds is "re-crossing" is permissible. This means that a molecule that passes into the TS can go back to the energy and structural configuration in reactant. This enables (occasionally) introduction of κ as a transmission co-efficient, and also allows introduction of Quantum mechanical tunneling. This tunneling effect is however usually ignored.

In TS theory, the field of statistical thermodynamics becomes important. This type of thermodynamics acts as the link between rigorous quantum mechanics and classical

thermodynamics, by enabling the introduction of quantization of energy. In this section, the mathematical framework will be kept at a minimum in the discussion of TST.

The total energy of a system is dependant on the energy by virtue of translation, rotation and vibration, and the electronic contribution. This is reflected in (eq. 5.11)

$$\varepsilon_{tot} = \varepsilon_{trans} + \varepsilon_{rot} + \varepsilon_{vib} + \varepsilon_{elec} \quad \text{(eq. 5.11)}$$

In statistical thermodynamics (as mentioned before), partition functions are made use of, to accurately determine the energy of a system microscopically. Each model of energy (translation, rotation, vibration and electronic) has a representative molecular partition function associated with it. In each case, this is represented as, (eq. 5.12)

$$q = \sum_{i=1}^{n} g_i e^{-\varepsilon_i / k_B T} \quad \text{(eq. 5.12)}$$

The partition function for one molecule is denoted q, g_i is the degeneracy factor, and the other variable hold the usual definition. The total partition function for N molecules is, (eq. 5.13)

$$Q = q^N \quad \text{(eq. 5.13).}$$

The *total* partition function for a system is the product of all partition functions (translation, rotation, vibration and electronic). The relation between the usual thermodynamic parameters of G (Gibbs Free energy), H (enthalpy), and S (entropy); and the partition functions is (for Free energy), (eq. 5.14)

$$G = H - TS = k_B T V \left(\frac{\partial \ln Q}{\partial V} \right)_T - k_B T \ln Q \quad \text{(eq. 5.14)}$$

where, Q is the total partition function.

It is these partition functions, that are used in the establishment of the TS energy, and it's thermodynamic energies. It is this theory that is used in the calculation of TS in molecular modeling, and was used as the mathematical framework in our calculations.

Chapter 6

Molecular Modeling studies on model CpCr(III) trimerisation system

"As far as the laws of mathematics refer to reality, they are not certain; and as far as they are certain, they do not refer to reality."
Albert Einstein

6.1 Introduction to molecular modeling

Other than a recent study by Janse van Rensberg *et al.* [81] which highlights a DFT study of a pyrrole Cr system (The Phillips System), theoretical studies of ethene trimerisation systems thus far, have been restricted to tantalum[82] and titanium. [83, 84] In light of this, it was decided to carry out DFT (Density functional theory) calculations [85] on a simple, representative CpCr system, containing a Cp ring (Cp = C_5H_5) and a Cr centre with a view of establishing the rate determining step, and to gain understanding of the catalytic process. This would hence enable a better understanding of the catalytic cycle of ethene trimerisation, and possibly enable improvement and tailoring of the catalysts themselves, with the CpCr system under investigation.

This chapter will detail our molecular modeling efforts on the system $CpCrCl_2$ which could act as a mechanistic model for the Cp^bCrCl_2 (Cp^b = bulky cyclopentadiene) catalyst (See Chapter 4). Firstly, determination of geometry optimized structures will be discussed, then calculations of transition states will be highlighted. The role of the alkylating agent will be mentioned in terms of the effects on energy (free and enthalpic), and finally a short discussion on the possible role of the phenyl rings on the energy of the geometry optimized species will be discussed.

6.2 Finding minimum energy configurations of molecules

The first step in elucidating the cycle using a simple model complex, was identifying the *global* energy minima of geometry optimized molecules, which would be the reactants and/or products in each step of the process. Based on the findings in the catalysis (Chapter 4) and the EPR studies in Chapter 3, a reasonable assumption, that the precursor is a monomeric Cr(III) complex was made. In light of this, the starting point in our MM (molecular modeling) study was to use a $CpCrR_2$ (R = alkyl (methyl)) as the catalyst precursor species. Figure 6.1 shows a hypothetical one dimensional free energy surface of a hypothetical molecule, with two minima: one being a *local* minimum the other the *global* minimum of the molecule.

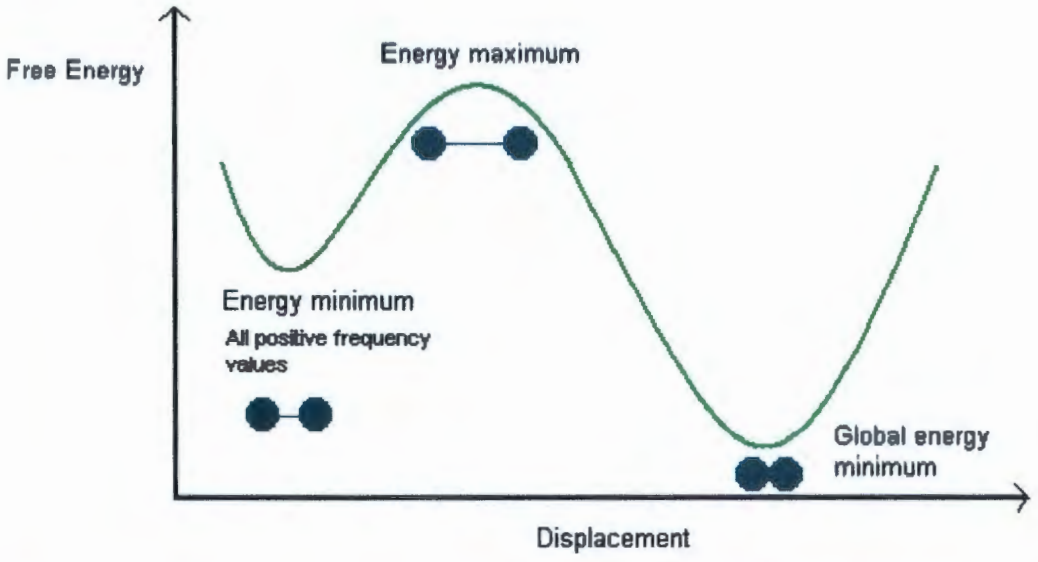

Figure 6.1 Schematic representation of free energy surface of a molecule in one dimension.

The energy of each species thought to be involved in the trimerisation process was minimized and frequencies of the species determined. The nature and structure of each species was based on the experimental data obtained through the catalytic studies of the ligands, as well as the Cr(III) model complexes, as well as the spectroscopic evidence (EPR and NMR) obtained earlier. Due to computational restrictions, a model Cr(III) precursor, namely $CpCrCl_2$ was used in the calculations. The addition of several phenyl rings would markedly increase the computational time required for a geometry optimization procedure. The process of alkylation (activation) through TMA (Trimethyl aluminium) was looked at in addition to the metallacyclic pathway that has been proposed before for the catalysis.

Scheme 6.1 shows a schematic representation of the process investigated, starting from the dialkylated Cr(III) complex. Each species is numbered, and corresponds to the species discussed in the rest of this chapter. The transition states that were calculated are also shown here.

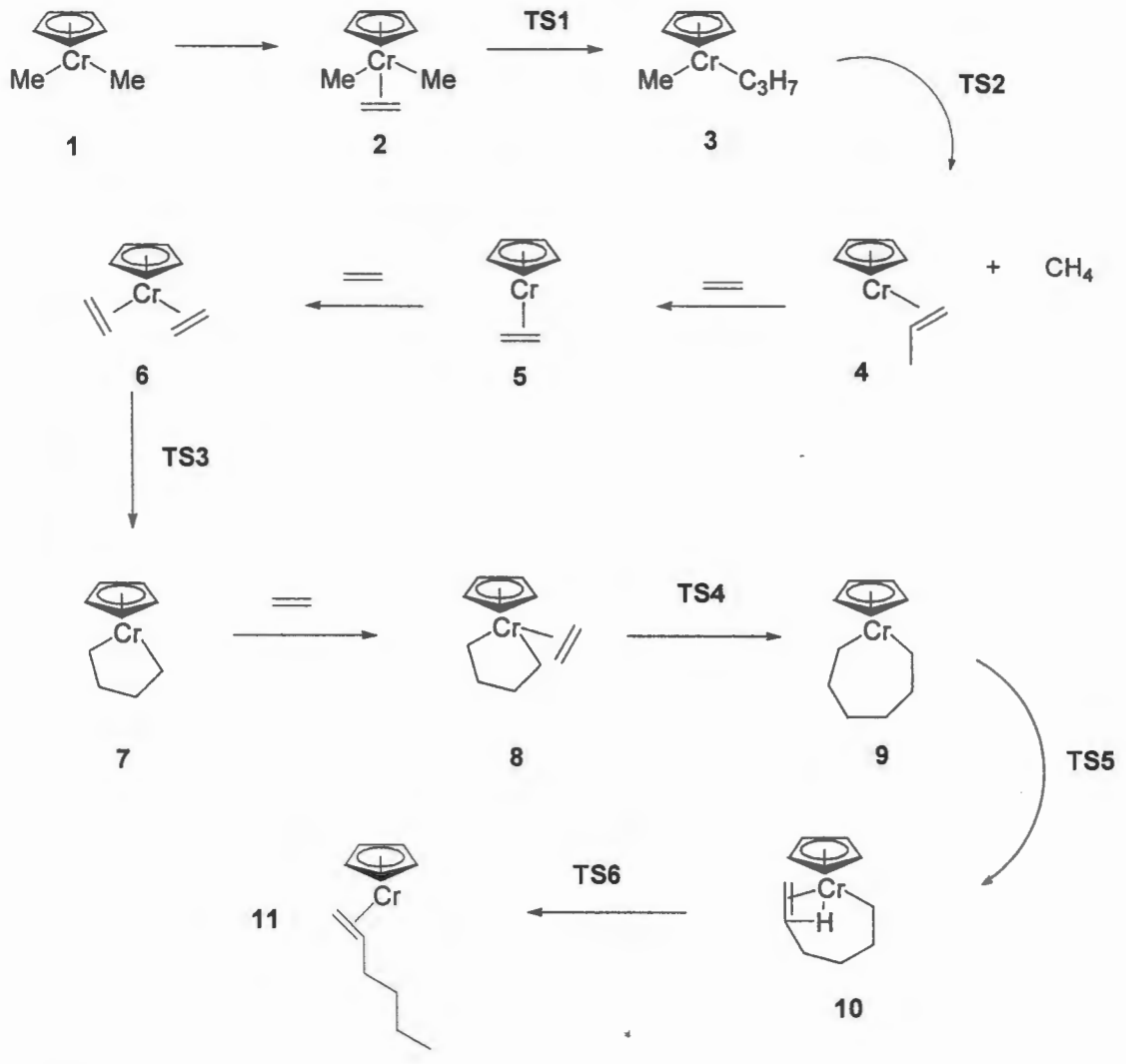

Scheme 6.1 Schematic representation of all species investigated using DFT methods. The numbering Scheme for species and transition states used in this section is shown.

6.2.1 DFT (Density functional theory) approach.

A Geometry optimization procedure was used to identify the stationery points of all species in question using Materials studio BLYP functionality. A DND numerical basis set was used for all atoms, and Zero point energies (ZPEs) and thermal corrections were obtained by vibrational analysis to convert electronic energies into free energies at 1 atm , 298 K (G_{298}). A point on a potential energy surface of a molecule is a *true* minimum if it is not a saddle point, and no imaginary values are obtained in a vibrational (frequency) analysis of that species. An additional criterion that needs to be fulfilled is that of having the gradient of the energy surface equal to

zero. Furthermore, convergence to a geometry optimized structure of a species is reached when the criterion,

$$\varepsilon(N) - \varepsilon(N-1) < \alpha \quad \text{(C 1)}$$

(where ε(N) is the energy of the species at optimization step N; α, an arbitrarily small energy value), is satisfied. A general profile of such a procedure is shown in Figure 6.2. In this example the species CpCr(heptacycle)Cl was optimized using the BFGS algorithm[86] (BLYP functional) and a DND basis set. It is clearly seen in this example, as is the case with all optimizations, that the optimization algorithm is complete when criterion (C 1) is fulfilled. Another output generated by Materials Studio is that reflecting the change in displacement, and the maximum force (Figure 6.3) which are also required for the optimization criterion to be reached successfully.

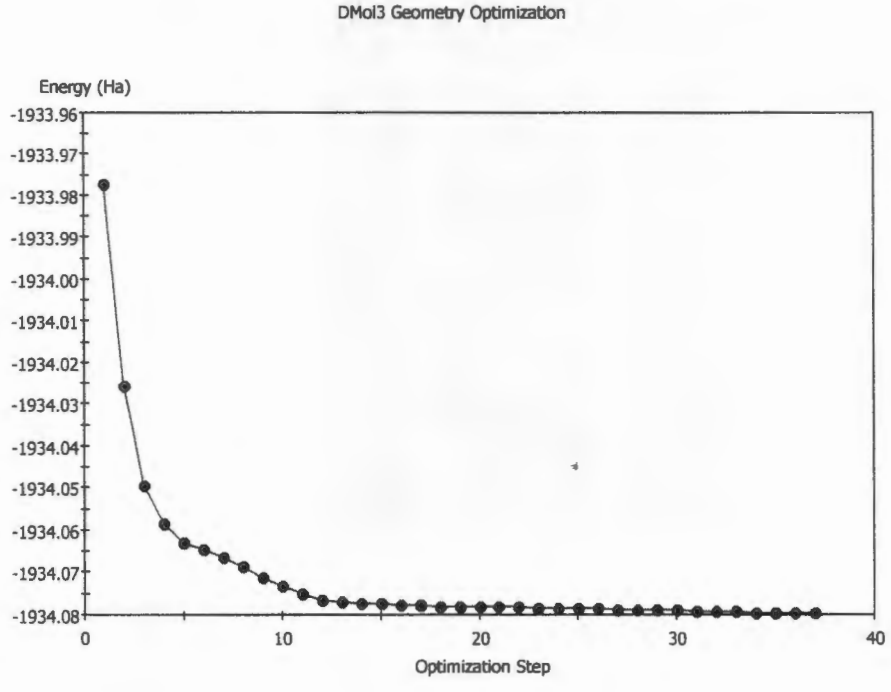

Figure 6.2 Familiar energy profile of geometry optimization (Energy in Ha).

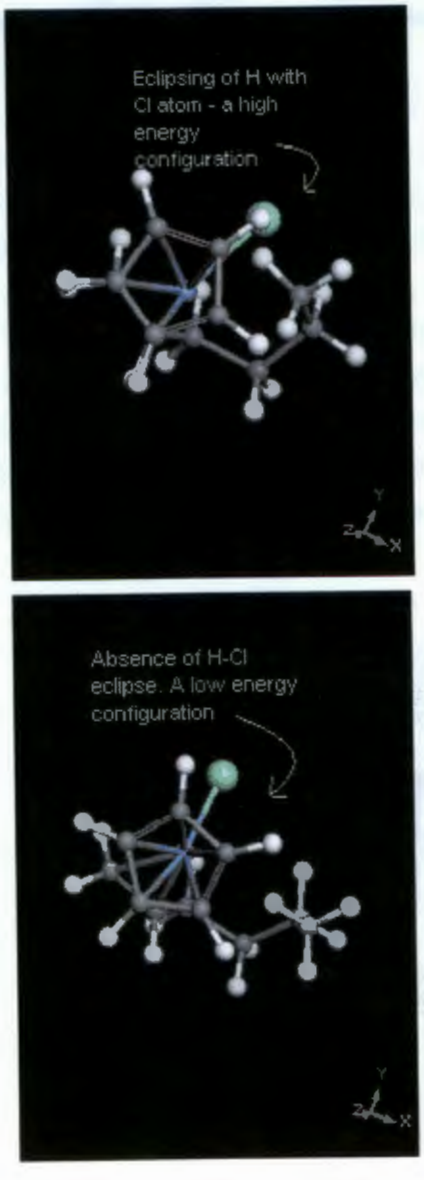

Figure 6.4 Comparison of the structures of a saddle point (top) with that of a true energy minimum (bottom). (Species CpCrCl[heptacycle]).

6.2.2 Catalyst precursor activation.

Calculations representing this step in the process were not carried out. Ideally, this transformation is represented by $CpCrCl_2$ to $CrCrR_2$, mediated through the alkylating agent (AlR_3). This will be looked at in the future.

6.2.3 Catalyst precursor generation (neglecting the role of the alkylating agent).

In the preliminary investigation, the role of the alkylating agent was neglected in order to generate a preliminary model for the process. Starting from the species $CpCrMe_2$ (**1**), where Me is reperesentative of the alkylating agent used in the activation (In the case of activating with TEA, ethyl groups would be present), a series of optimizations was conducted. Coordination of ethene takes place into the $CpCrMe_2$ species to form $CpCrMe_2(C_2H_4)$ (**2**), in contrast to the findings with the Ta system. [82] The next species to form is the CpCr(Me)(Pr) (**3**), which subsequently undergoes β hydride transfer, and through an agostic mediated shift the species $CpCr(C_3H_6)$ (**4**) with methane as a side product results. This observation is in accordance with the Ta system. [82] Species (**4**) is thought to be the precursor responsible for the trimerisation of ethene. The optimized structure of each species, including bond angles and lengths, with Free energy values are represented in Figure 6.4.

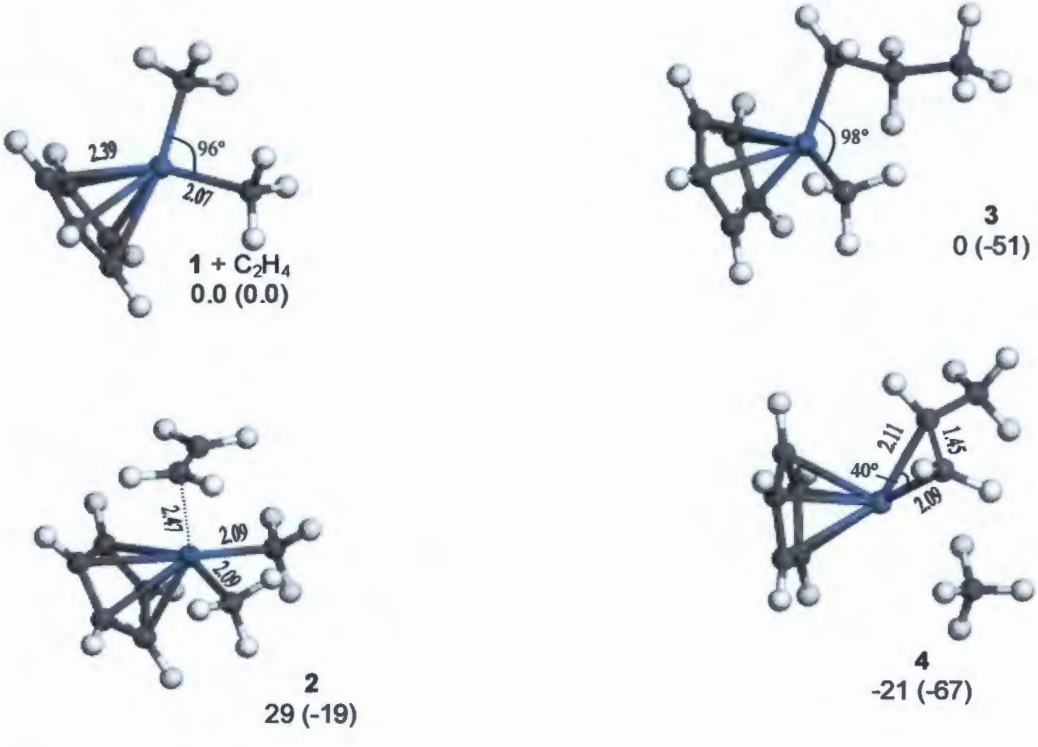

Figure 6.4: BLYP optimized stationary structures (ΔG_{298}) for the generation of the catalyst precursor; ZPE corrected values (ΔE_0) in parentheses. Energies in kJ/mol, distances in Å.

6.2.4 The catalytic process.

Starting from species (**4**) displacement of the propene with ethene proceeds favorably resulting in $CpCr(C_2H_4)$ (**5**). In view of the electronic deficiency of the Cr centre in (**5**), another ethene co-ordination is possible, resulting in the species, $CpCr(C_2H_4)_2$ (**6**). At this stage, it is possible for a coupling reaction to take place, between the co-ordinated ethenes to form the chromapentacycle, $CpCr(C_4H_8)$ (**7**). Again insertion of ethene is possible, to form the species $CpCr(C_4H_8)(C_2H_4)$ (**8**). Insertion of the ethene into the already existing pentacycle is possible, resulting in a so called heptacycle $CpCr(C_6H_{10})$ (**9**). After beta hydride transfer, the product 1-hexene is formed, and the initial precursor species re-generated. The computed free energy values for each species in it's geometrically optimized orientation (stationary structure) as well as the enthalpic values are shown in Figure 6.5.

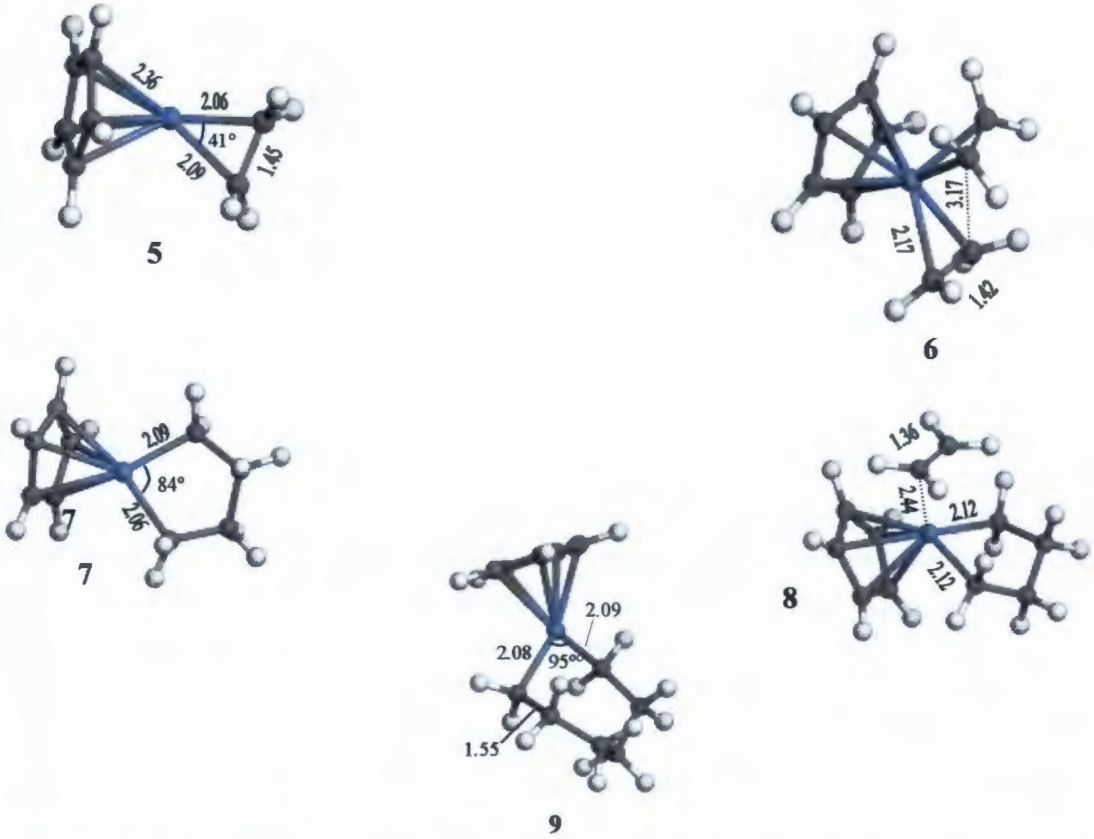

Figure 6.5 BLYP DND optimized stationary structures of all species involved in CpCr catalytic cycle.

Species	Relative Calculated Free Energy (kJ.mol^{-1})(ΔG_{298})	ZPE (Zero potential corrected energy) (kJ.mol^{-1})
1	0	0
2	29	-19
3	0	-51
4	-21	-67
5	0	0
6	-5	-56
7	-3	-54
8	31	-71
9	16	-87
10	-1	-106
11	-10	-111

Table 6.1 Comparison of BLYP calculated energy parametrers for stationary optimized structures.

6.3 Transition state (TS) searches

6.3.1 DFT Approach

The background theory of transition states was highlighted in Chapter 5. In our system, transition state searches (TSS) were conducted at each stage of the catalytic process. The Materials Studio algorithms employed were LST / GC / QST (Linear synchronous transit – Quadratic synchronous transit) on Materials Studio. A TS (C*) is determined between a reactant (A) and a product (B) by generating a "trajectory file" in Materials Studio. The trajectory file is a pre-requisite for a TS search to take place, and is a crude representation of the pathway of the reaction from reactant (A) to product (B). An abridged example of such a document (frame by frame) is shown in Figure 6.4.

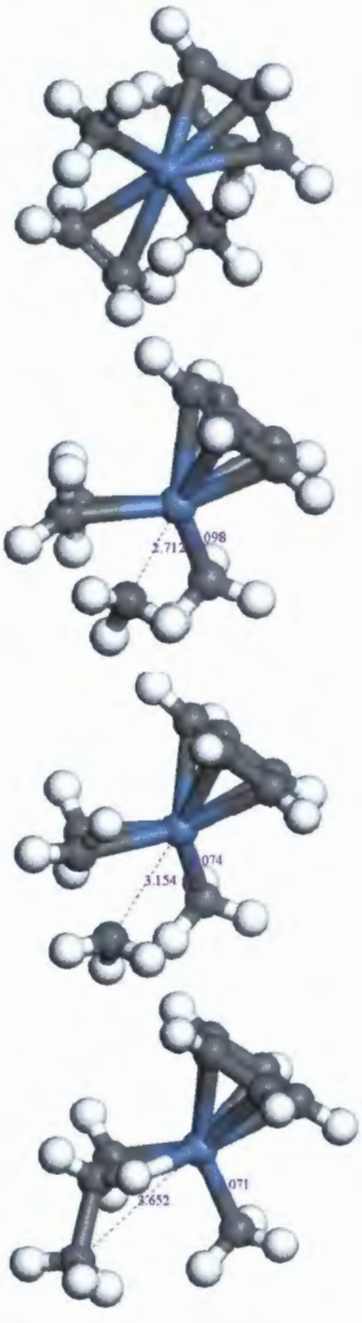

Figure 6.4 Example of Trajectory TS document for a transition state. The 1st frame (previous page, top) represents the dimethyl-alkene CpCr (**2**). The second frame shows dissociation of the methyl group with the Cr centre, This migration continues (frame 3) with the distance between the methyl and Cr centre increasing gradually. Finally, bonding to the β C commences, in frame 4, and the agostic shift is induced.

The LST algorithm determines a crude structural representation and energy value of the TS (C*), and this is subsequently refined by the QST algorithm. Convergence (using C1) generally implies determination of the TS. In general, the free energy of the TS is higher than that of the reactant or product.

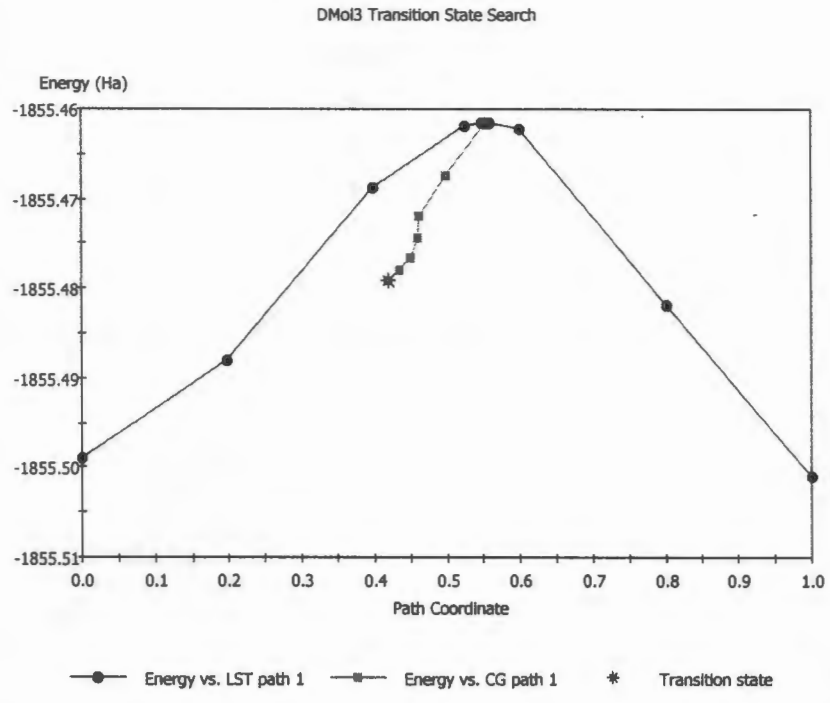

Figure 6.5 Representation of QST/CQ/LST TS search on Materials Studio.

A summary of the TS searches conducted using the above algorithm is summarized in Table 6.2.

The existence of a transition state can be verified by a frequency analysis of the structure thought to be a transition state. An actual transition state structure only has *one* imaginary frequency (or negative frequency) and the presence of more or none of these imaginary frequencies implies the structure is not a real transition state. Other structures on the potential energy surface, around the transition state can similar in structure, but are not the transition state. All species thought to be transition states were subsequently checked using this frequency analysis, and in each case only one imaginary frequency value was returned.

Reactant	Product	Transition State
Catalyst precursor generation		
2	3	TS1
3	4	TS2
Catalytic trimerisation	7	TS3
6	9	TS4
8	10	TS5
9	11	TS6
10		

Table 6.4 Summary of TS searches on Materials Studio.

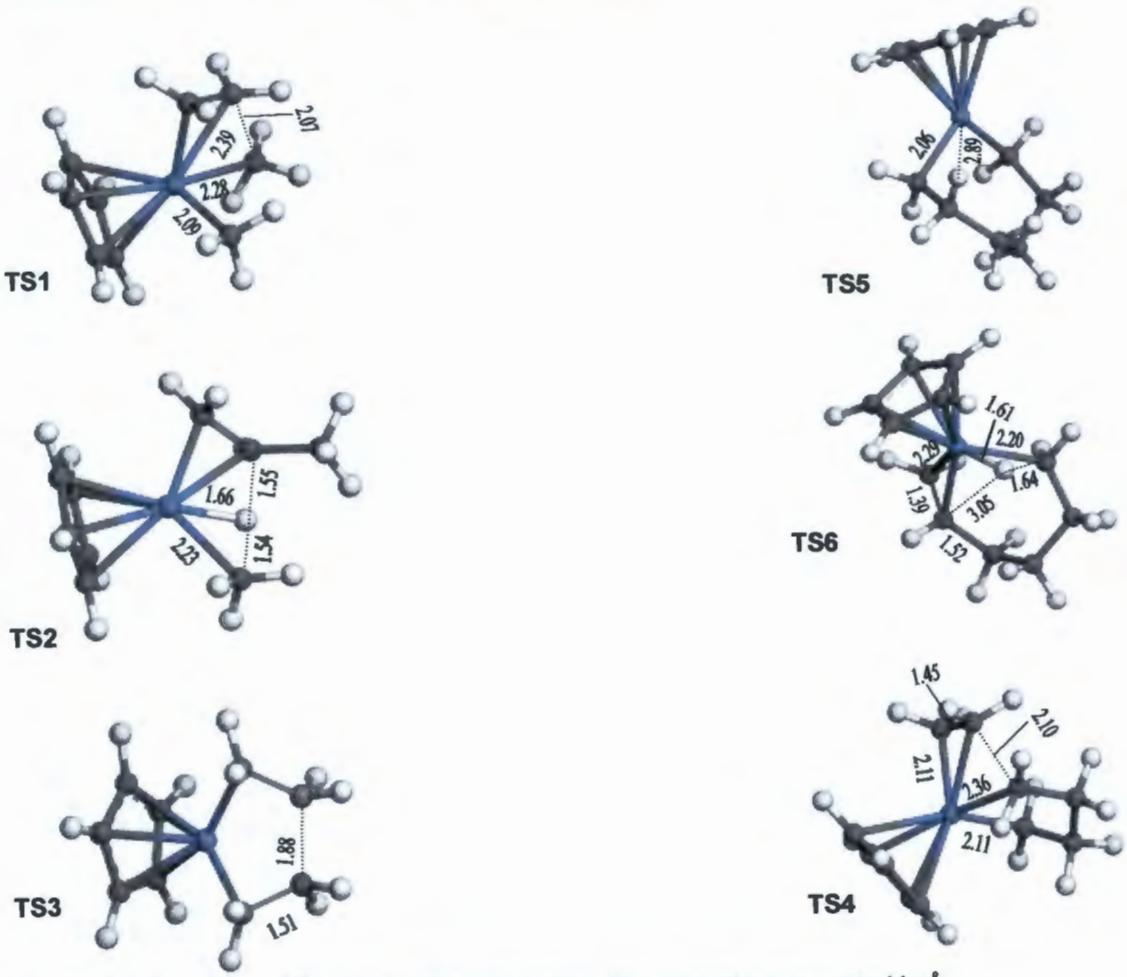

Figure 6.6 Summary of Transition state structures. Bond lengths are quoted in Å.

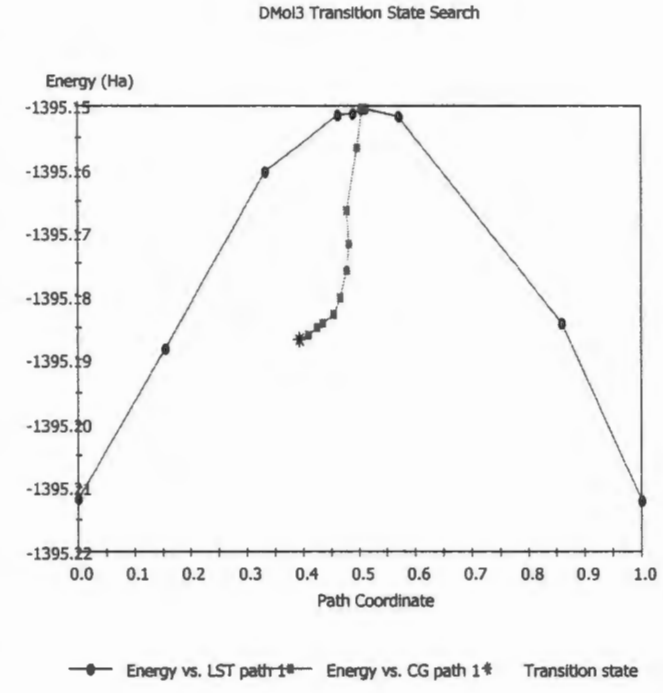

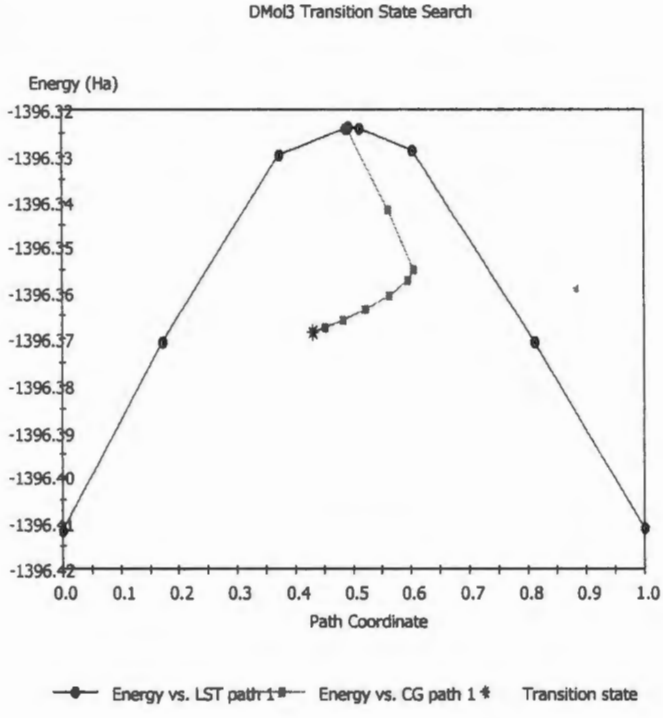

Figure 6.7 LST/CG/QST TS search Material Studio outputs. **TS1** (top) **TS2** (Bottom)

Transition State	Computed Free Energy (kJ.mol^{-1}) (ΔG_{298})	ZPE (Zero potential corrected energy) (kJ.mol^{-1})
Catalyst precursor generation		
TS1	95	42
TS2	70	21
Catalytic trimerisation		
TS3	58	5
TS4	55	-18
TS5	27	-74
TS6	87	-18

Table 6.3 Summary of calculated parameters for Transition states.

6.3.2 Transition states in the catalyst precursor generation step

Between species (**2**) and (**3**) our calculated TS (**TS1**) shows a bond distance of 2.07 Å between the carbon atom of the one methyl group and the one carbon atom of the coordinated ethane. Subsequent bond formation between these two atoms can be imagined to take place in light of the close proximity of the atoms, resulting in (**3**). The calculated distance in (**TS2**) between the hydride and the β carbon of the coordinated propene is 1.55 Å, however, the distance between the hydride and the carbon atom of the Cr-Me is slightly less at 1.54 Å. The result is that preferential association of the hydrogen (of the hydride) with the Me group takes place to form the complex (**4**) with methane as side product.

6.3.3 Transition states in the catalytic process

If the assumption of ligand exchange of ethene with the coordinated propene in (**4**) (which is in accordance with the Ta system), [82] is made, species (**5**) results. The electron deficient species (**5**) can accommodate an additional ethene resulting in (**6**). (**TS3**) results between (**6**) and (**7**). Closer inspection of the calculated (**TS3**) reveals co-planarity of the ethene units, and a short distance of 1.88 Å between the carbon atoms which readily couple to form (**7**). Addition of ethene to the electron deficient (**7**) results in (**8**). Between (**8**) and (**9**) the calculated (**TS4**) demonstrates the close proximity (2.10 Å) of the ethene carbon atom with that of the carbon atom bonded to the Cr centre. This readily facilitates insertion of the ethene into the existing pentacycle to form (**9**).

In contrast to the finding for the Ta system, [82] conversion of (**9**) to (**11**)is not a one step process. A so-called Nudged elastic Band calculation (NEB)[87] reveals the presence of another intermediate (**10**) along this reaction pathway, by passing through (**TS5**). The calculated structure of (**TS5**) reveals a distance of 2.89 Å between the β hydrogen and the Cr centre. This facilitates the existence of (**10**) as an "agostic" intermediate. On proceeding from (**10**) to (**11**) a high energy transition state (**TS6**) is passed through. The agostic hydride proceeds closer to the α carbon on the other side of the metallacyclic ring (1.64 Å) compared with 3.05 Å distance between the β carbon and the hydride. This facilitates the eventual formation of (**11**), which is analogous with the original precursor (**4**), and ethene displacement of the coordinated hexene results in (**5**) and 1-hexene as product.

6.4 The role of the alkylating agent

In most of our calculations, the effect of the alkylating agent (acting as the "anionic" fragment) was neglected. Work done by Janse van Rensberg *et al.*, on the pyrrole chromium system, has however demonstrated very little deviation from the relative energy values of , in their case, a hapto-pyrrole-Cl chromium model, and that of a hapto-pyrrole-($ClAlMe_3$) chromium model, the latter being the more realistic model. This has also been shown to be true for the sigma pyrrole case, of this system also. In light of this observation, it should then be possible to calculate the energies of a model with only one chlorine ligand, that can be assumed to be energetically similar to that of the $ClAlMe_3$ analogue, while dramatically reducing the time required for the calculation. In our case, two key steps, with high energy barriers were looked at, with a view of observing the effect of the addition of the Cl ligand on the energy of the model.

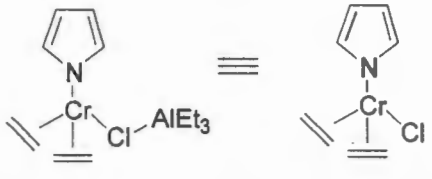

Figure 6.8 It has been shown that the relative energies of the above (and related structures) in the ethene trimerisation are virtually identical.

In our case, the two key steps investigated were that of the formation of TS2, and TS6, with the addition of the Cl ligand, which was omitted before. These were chosen in light of their high energies, which could hinder the pathway of the catalytic process. In turn a comparison could be looked at between the energies of the model without the Cl (simulating the anionic fragment), and that containing the Cl, with respect to the energies of the respective transition states. It must be

made clear at this point, that the addition of the Cl ligand (simulating the presence of the alkylating agent) changes the oxidation state of the Cr atom from Cr(III) to Cr(IV).

Geometry optimizations were done, as before, except for the addition of Cl on structures (**6**), (**7**), (**10**) and (**11**) (see above models). These results will be omitted, and reported in a publication in preparation. All structures were optimized successfully (with the Cl ligand) and for simplicity for the rest of the discussion called (**6'**), (**7'**), (**10'**) and (**11'**), where these structures are virtually identical to structures (**6**), (**7**), (**10**) and (**11**), except for the addition of a single Cl stom onto the Cr centre.

Then, in an analogous was as before, the transition states were found between (**6'**) and (**7'**), and (**10'**) and (**11'**) respectively, designated (**TS3'**) and (**TS6'**). As before, the TS was verified by performing a frequency calculation, and verifying the existence of only one negative frequency value. This was successful in both cases. The structures of these transition states are shown below.

Figure 6.9 Structure of (**TS2'**). Again, proximity of the two coupling carbon atoms is noted. The oxidation state of the Cr is four here.

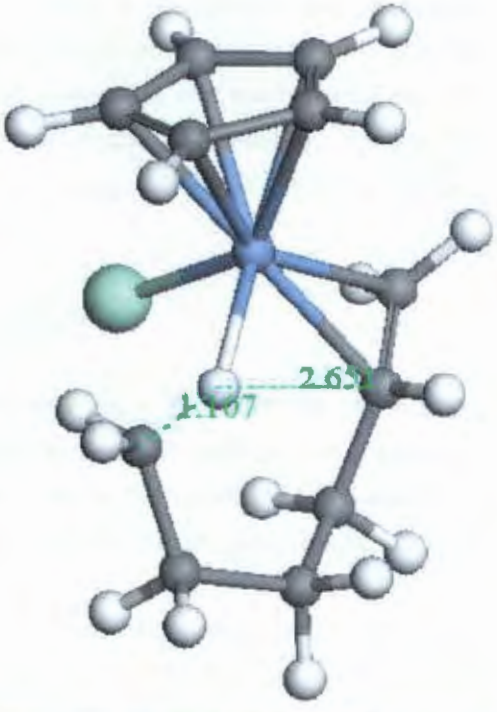

Figure 6.10 Structure of (**TS6'**). The agostic transition state is noted, as before, as the β hydride transfer occurs to form the hexene co-ordinated product. Again the oxidation state of the Cr is four.

The electronic energies of the transition states are shown below in Table 6.4.

Transition state	Electronic Energy (Ha)
TS2 Cr(III)	-1395.187
TS2' Cr(IV)	-1855.479
TS6 Cr(III)	-1473.808
TS6' Cr(IV)	-1933.853

Table 6.4 Comparison of transition state electronic energies between transition states with and without the Cl ligand respectively.

A dramatic difference in the transition state energy is noted in each case, between the system with the Cl ligand and without. In each case, the transition state of the system that contains Cl as a ligand (representing the presence of the anionic fragment), dramatically stabilizes the transition state, by being much lower in energy than without. This indeed shows the necessity for an

alkylaluminium reagent to be added to the catalytic mixture, to ensure the formation of species that allow a lower and more favorable reaction pathway. The absence of an alkylaluminium reagent, results in transition states that are much higher in energy, than the corresponding chlorinated analogues. In other words, this tentatively shows the pathway with the Cl ligand (Cr(IV)) is far more realistic and reasonable than the Cr(III) pathway.

6.5 The role of the phenyl groups

In all the calculations conducted in this project – the role of the phenyl rings was neglected due to the computational demands that would be required in the case of their inclusion. However, to gain insight into their possible role in the trimerisation process, some preliminary work was done on monophenyl Cp Cr systems and will be discussed below.

To probe the effect of having a phenyl Cp system, on the free energy of some model complexes, $PhCpCr(C_2H_4)$, $PhCpCr(C_2H_4)_2$ and $PhCpCr(C_2H_4)_3$ were compared with the non phenyl analogues, i.e. $CpCr(C_2H_4)$ $CpCr(C_2H_4)_2$ and $CpCr(C_2H_4)_3$. Here the free energies of the geometry optimized stationary structures were computed and compared to observe possible trends in binding energies of ethene and other parameters.

A selection of the BLYP optimised stationary structures is presented below. In each case a discussion of the features of the optimized structure, with some parameters in highlighted.

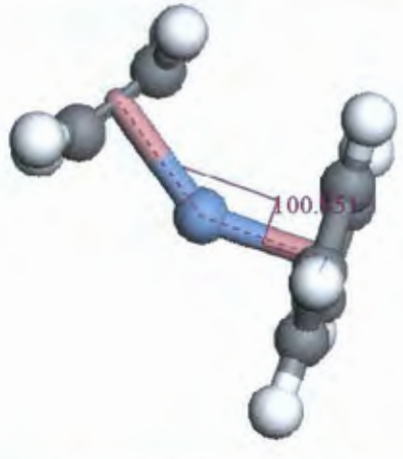

Figure 6.11 BLYP stationary structure of $CpCr(C_2H_4)$. A torsion angle of 100.8° is noted between the coordinated ethene and the Cp ring. This species is highly idealized, as it represents a highly electon deficient complex, unlikely to exist in solution.

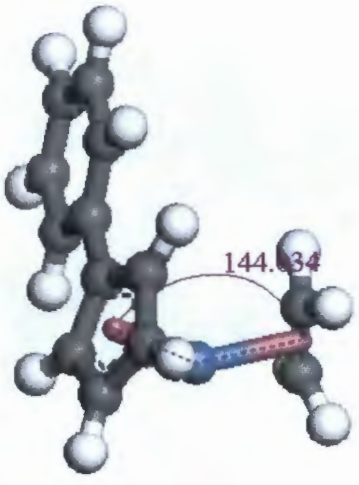

Figure 6.12 BLYP stationary structure of PhenylCpCr(C_2H_4) (Phenyl analogue of Figure 6.8). Near coplanarity with the phenyl and Cp ring is noted. A 144° bond angle is noted between the ethene centre and that of the Cr.

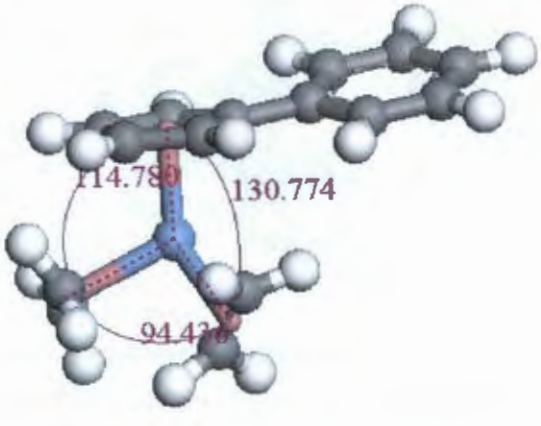

Figure 6.13 BLYP stationary structure of PhenylCpCr(C_2H_4)$_2$. This species represents the second alkene coordination. Asymmetry is noted with respect to the coordination of the respective ethene units.

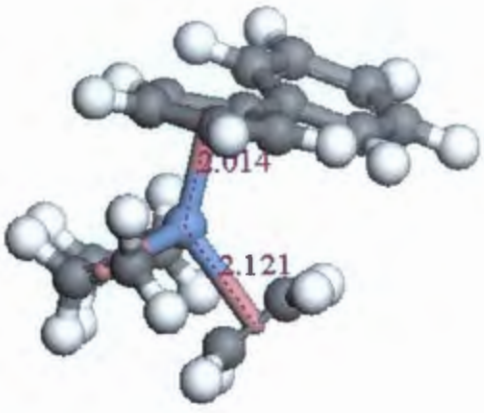

Figure 6.14 BLYP stationary structure of PhenylCpCr(C_2H_4)$_3$. Near eclipsing of two ethene ligands results in a high energy configuration, which is ultimately unfavorable.

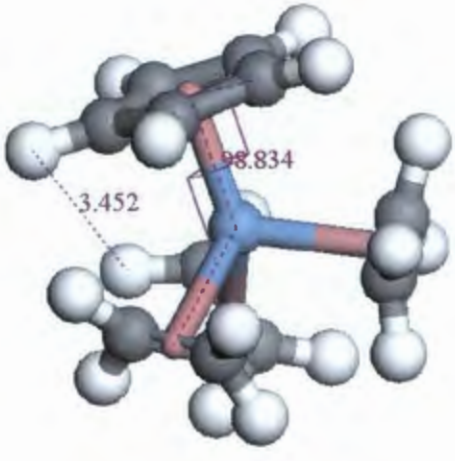

Figure 6.15 BLYP stationary structure of CpCr(C_2H_4)$_3$. Distance between Cp ring and one of the coordinated ethene ligands shows a possible steric congestion. This too is energetically unfavorable.

Thermodynamic parameters (Free energy at 298 K, ZPE) for each optimized structure was calculated and tabulated.

cies	Electronic Energy (Ha)	Correction to G_{298} ($kj.mol^{-1}$)	Conversion to (Ha)	Total(G_{298}) (Electronic energy+Free energy)	Corrected for C_2H_4	Relative corrected values (to CpCr or CpPhCr)
nyl Cp Cr	-1469.008531	76.5	0.121770689	-1468.886761	-1704.512076	0
nyl Cp $_2H_4$)	-1547.63682	106.3	0.169205546	-1547.467615	-1704.551158	-0.039082151
nyl Cp $_2H_4)_2$	-1626.233314	138.7	0.220779014	-1626.012535	-1704.554307	-0.042231191
nyl Cp $_2H_4)_3$	-1704.806531	170.944	0.272104166	-1704.534427	-1704.534427	-0.022351147
r	-1237.99826	30.355	0.048318291	-1237.949942	-1473.575257	0
$r(C_2H_4)$	-1316.602173	60.864	0.096881715	-1316.505291	-1473.588835	-0.013577884
$r(C_2H_4)_2$	-1395.200441	92.626	0.147439632	-1395.053001	-1473.594773	-0.019515675
$r(C_2H_4)_3$	-1473.775843	125.604	0.199933146	-1473.575909	-1473.575909	-0.000652269
C_2H_4	-78.5691503	17.2	0.027378508	-78.54177179		

e 6.5 Summarized thermodynamic parameters for all BLYP stationary species expressed finally as cted values in each case to CpCr or PhCpCr respectively.

ugh previous calculations demonstrate a stepwise addition of ethene ligands to the chromium centre, with ral intermediate species between each ethene coordination, the point of these geometry optimizations was ly to compare stepwise ethene binding energy, assuming sequential addition of ethene ligands to the mium centre. It could be argued that this negates the value of these calculations, however, as a preliminary stigation into the thermodynamic differences in the phenyl Cp Cr against the CpCr system, it has shown natic differences in associated free energies, of all species as a direct consequence of the phenyl ring.

exact effect of having several more phenyl rings remains to be investigated, and certainly, by the addition ur more phenyl rings to result in the realistic system investigated in other areas of this thesis, more putational time makes this exercise problematic in the near future.

mparison, however, of each species shows a marked effect on the sequential binding energy of each ne ligand. This is most dramatically reflected graphically (Figure 6.13).

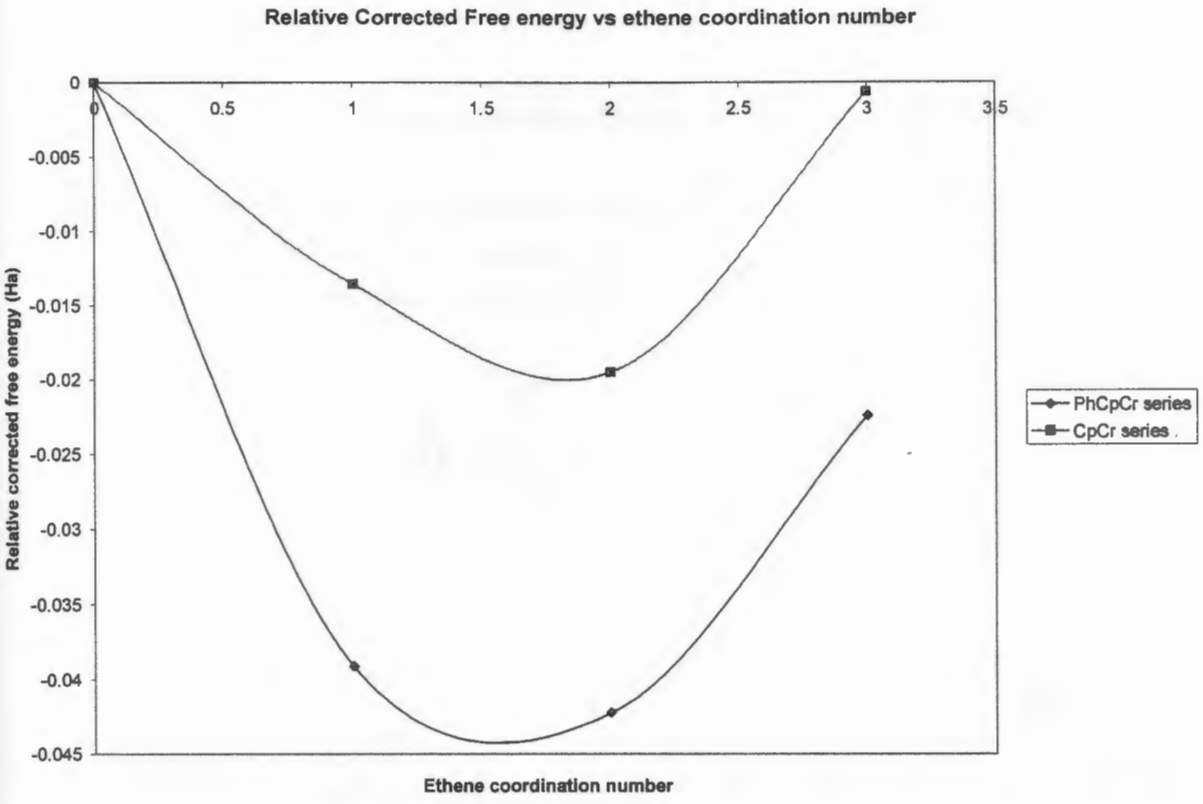

Figure 6.16 Graph demonstrating dramatic difference in Free energy with the addition of one phenyl ring to the Cp ligand. This trend is followed with all species investigated. (the data points have been connected to demonstrate the trend clearly [iv]).

Figure 6.16 demonstrates a much greater free binding energy for the phenyl CpCr system, compared with the CpCr system, at each sequential addition of another ethene ligand. In both cases, the addition of a third ethene ligand, sequentially without any intermediate process (such as coupling to form a metallacycle) results in a lower free binding energy. In both cases, a maximum binding energy is reached upon coordination of the second ethene ligand, which is lowered substantially when a third ethene ligand is added to the Cr centre. This can be explained in terms of the electronic saturation of the Cr centre, and possible steric encumbrances. However, the free binding energy in all cases is higher in the PhCpCr case. This can again be rationalized by arguing a degree of electron density withdrawal from the Cr centre (which has been experimentally validated by cyclic voltametry studies – see Chapter 3). This results in a highly electron deficient Cr centre (in the PhCpCr case), even more so than the CpCr case. These

[iv] Of course, it is incorrect to connect these data points, as ethene coordination is a discrete variable, this has been done here to demonstrate a point.

preliminary calculations consequently establish a thermodynamic role of the phenyl ring(s) in the catalyst.

6.6 Free energy profile of catalyst precursor generation and catalytic cycle.

In summary, this section provides the free energy pathways of each discussed step in the catalytic reaction studied, as free energy surfaces. In light of previous discussion (in the above sections) further discussion is omitted in this section.

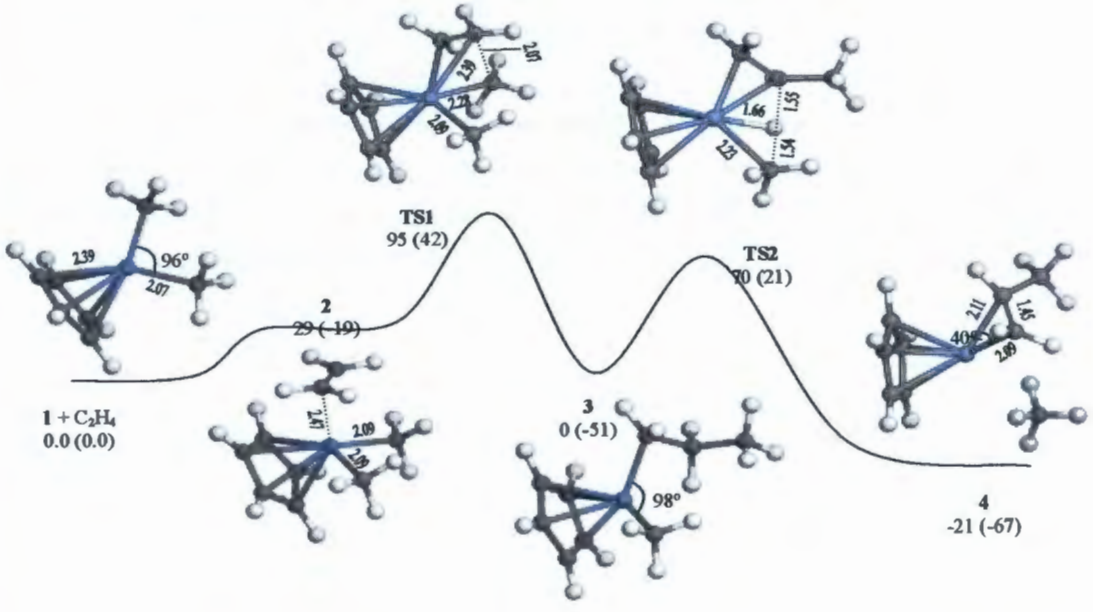

Figure 6.17 Overall reaction preview : neglecting phenyl groups and the alkylaluminium reagent.

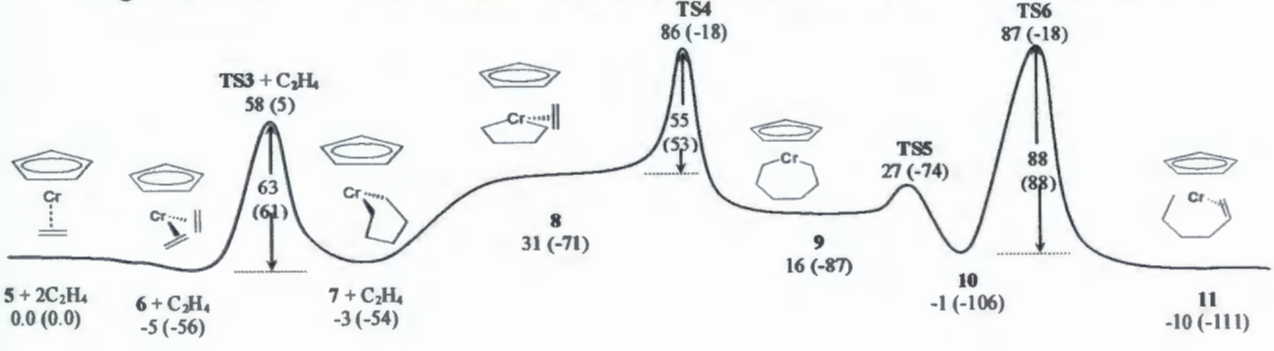

Figure 6.18 Catalytic reaction : neglecting phenyl groups and presence of the alkylaluminium reagent.

6.7 Discussion and conclusion of DFT work

The DFT investigation of this catalytic process has demonstrated several key limiting steps. Although a simple cyclopentadienyl system was used as a model in this investigation, it has enabled a better understanding of the observed selectivities to 1-hexene in the bulky cyclopentadienyl system. Ideally, this sequence of calculations should be repeated for a more bulky phenylated cyclopentadienyl Cr system (which again is the system which experimentally shows high selectivities to 1-hexene) , but in light of computational demands for such a large system, this is unrealistic at this time with available resources.

The role of the alkylaluminium reagent was also highlighted in this work. The presence thereof in the catalytic process dramatically reduces the energy of the corresponding transition states in a system that lacks the reagent, which would allow the catalytic reaction to occur more readily. More work quantifying the role of this more clearly would need to be done in the future.

Chapter 7

Conclusions, Discussion and Future Work.

"The future, according to some scientists, will be exactly like the past, only far more expensive."

John Sladek

7.1 Brief summary of thesis results : global perspective

In this project, a multidisciplinary approach was utilized to gain insight into the ethene trimerisation process, catalysed by bulky cyclopentadieneyl Cr(III) species. This has proved most valuable, since an approach from a synthetic point of view (the synthesis of known and new ligand systems), in addition to Cr(III) model complexes that are catalytically active, shed light on the fundamental chemistry of the process. Testing the catalytic activity (i.e. an approach from a catalytic point of view) shed light on the activity of these complexes, which enabled a tentative understanding of the various effects (steric and electronic) on the catalytic activity of the ligands and complexes. The third approach employed, the molecular modeling investigation, yielded insights into the energetic and thermodynamic considerations in the overall process. Although the system used in this part of the investigation was a highly simplified system of the more realistic phenylated systems, it did succeed in opening a pathway for additional and future studies in this area.

In order to appreciate the global perspective of these three approaches, it is important to see them as linked, and part of a global picture. Each technique complimented the other, and a more realistic perspective of the process was gained.

7.2 The synthetic approach in a "nut shell"

Being one of the corner stones of the project, a series of new and known bulky cyclopentadiene ligands was prepared, and fully characterized using the standard spectroscopic techniques. Several routes were looked at to synthesise these cyclopentadiene ligands and the one which proved most successful was that of using tetracyclone as starting material, and reaction with a lithium or Grignard reagent. Other routes were explored in addition, such as that of using a symmetrical alkyne and performing lithium mediated dimerisation. This route was partially successful, but limited by the nature of the alkyne. It was found that dimerisation would not

proceed if there was no aromatic group present on either side of the triple bond. A third route, which made use of Cp_2ZrCl_2 as starting material, and source of cyclopentadiene yielded one known "super-bulky" cyclopentadiene in high yields. In addition to preparing ligands, selected Cr(III) dimeric complexes were also prepared as possible model complexes or precursors for the trimerisation. These complexes were prepared using one of two routes: using the potassium or sodium salt form of the ligand, and reacting it with $CrCl_3(thf)_3$ to form the dimeric complexes of the type, $[(C_5Ar_nH_{6-n})CrCl_2]_2$. Characterization by the usual means was employed, but was found to be problematic in terms of elemental analysis, as has been reported in the literature. New EPR spectroscopy was conducted on two of these complexes, $[(C_5Ph_5)CrCl_2]_2$ and $[(C_5Ph_4H)CrCl_2]_2$ in weakly coordinating CH_2Cl_2. It was found that the resulting EPR spectrum is that of a mononuclear Cr(III) species, with a spin of 3/2 (in each case), with characteristic signals at g = 4 and g = 2. This indicated a subtle solution dissociation equilibrium between the dimeric parent complex, and mononuclear species. This study revealed subtle dissociation chemistry of these complexes, which were later shown to be catalytically active. This valuable EPR investigation also shed light on possible solvent effects, and fundamentally revealed solution behavior of the dimers.

One Fe(II) model complex, i.e. $(C_5Ph_4H)_2Fe$ was synthesized to probe possible electronic influences of the phenyl rings on the metal centre. The cyclic voltammogram of $(C_5Ph_4H)_2Fe$ was compared with that of $(C_5H_5)_2Fe$ and a dramatic shift was noted. This study revealed that the phenyl rings "withdraw" electon density from the metal centre, making is more "electropositive". This study shed light on the electronic influences of the phenyl rings on the metal centre, and indeed, possibly on the catalytic activity.

7.3 The catalytic studies in a "nut shell"

Although our catalytic studies were limited, we were able to show activity of a dinuclear model complex, viz. $[(C_5Ph_5)CrCl_2]_2$, which was very similar in activity to that of the Cr-2-ethyl hexanoate/TEA / hexachloroethane/Cp system. This tentatively demonstrated the formation of the same catalytically active species in both systems, and in light of the clearly defined structure of the model complex, it is possible to speculate as the structure of the active catalytic species. This would most likely take the form of a mono nuclear Cr(III) species, with co-ordinated Cp i.e. $CpCrX_2$, where X = Cl in our case.

7.4 The molecular modeling investigation in a "nut shell"

Starting from a representative model compound, i.e. $CpCrMe_2$ the generation of the catalytically active precursor was looked at, in addition to the catalytic cycle, to generate 1-hexene as product. A full array of DFT calculations was performed, using "Materials Studio" as program. Each species thought to be involved in the process was minimized using a geometry optimization procedure. Transition states were also calculated in each step of the process. Reasonable comparisons with our calculations and similar Ta and Ti systems can be made. Calculations looking into the effect of one phenyl ring on the free-energy of the stationary species, $PhCpCr(C_2H_4)_n$ and $CpCr(C_2H_4)_n$, n = 1, 2, 3 was also looked at, to tentatively evaluate the effect(s) of one phenyl ring on the thermodynamic parameters. It was found (as complimented by our CV studies) that the phenyl ring acts as "an electon withdrawing agent" rendering the metal centre more electrophillic. A higher free energy of binding of ethene is noted in each case (for the species $PhCpCr(C_2H_4)_n$ compared with the species, $CpCr(C_2H_4)_n$). Thirdly, the effect of including the alkylating agent was looked at. In this case similar simplifications was made as with the previously published Phillips system, and simulated by adding one Cl ligand to the Cr(III) centre. Two key steps, that showed high free energy barriers of activation was looked at, and in these cases the energy was reduced dramatically by the addition of this one Cl atom to the Cr centre. This hence shed light on the role and necessity of having an alkylating agent present in the catalytic mixture (realistically TEA – triethyl aluminium).

7.5 Future work

Although this project looked at several key features of the catalytic process, more work can be carried out in the future on all these fronts.

7.5.1 Additional Synthetic work

Firstly, establishing the quantitative role of the phenyl rings on the Cp nucleus can be investigated further. This would mean synthesizing ligands of the type $C_5Ph_nH_{6-n}$ (n = 1,2,3), and testing them for catalytic activity with a Cr source (as per the Mahomed system) as ethene trimerisation catalyst precursors. Making the corresponding dinuclear chromium complexes of these new ligands would also be a possibility.

More bulky cyclopentadienyl ligands can be prepared that contain electron donating and withdrawing groups. This will enable more understanding of the electronic effects of substituents on the ligand in the trimerisation process

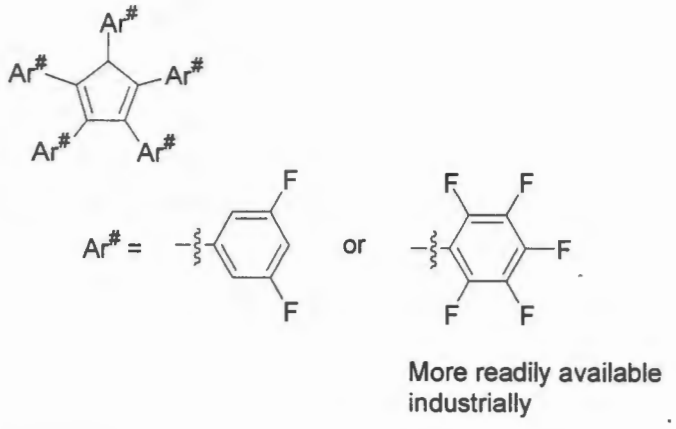

More readily available industrially

Figure 7.1 Possible future target(s) – ligands with electron withdrawing groups.

Other even bulkier substituents can be attached also to look at the exact steric requirements of the ligands in the trimerisation. This can be achieved by tailoring and modifying the Pd route used in this project,[40] and possibly preparing more exotic and bulky (super-bulky) ligand systems.

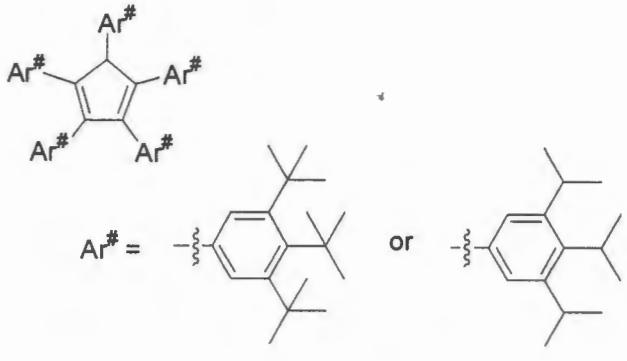

Figure 7.2 "Super-bulky" ligands, other possible future targets that will help in the understanding of the steric parameters in this trimerisation process.

Also, other model compounds, resembling other key intermediates in the process can be synthesized to further validate their presence in the catalytic reactions. For example, Bulky analogues of Jolly type metallacycles can be prepared and tested for catalytic activity. This will validate their presence and role in the catalytic process. It should also be possible to conduct

isotope-labeling studies on this system, as was done with a diphosphine system by Agapie *et al.* [15]

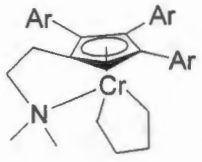

Ar = Any aromatic or substituted aromatic group

Figure 7.3 A metallacyclic system, a bulkier analogue of those studied by Jolly *et al.*, another possible future target.

7.5.2 Additional Catalytic work

All the other ligands prepared in this dissertation, and new ones will ultimately be tested for catalytic activity and selectivity to various products. The use of other solvents, in the trimerisation process, can also be looked at including the use of strongly donating, and/or weakly donating solvents. This could aid in understanding the role of the solvent in the process better. This will shed additional light on the requirements and parameters controlling selectivity to 1-hexene and other products.

7.5.3 Additional Molecular Modeling

Here, additional work on the effect(s) of the alkylating agent (typically triethyl aluminium) can be looked at more closely. In addition, the effect of more phenyl rings (as opposed to only one looked at in this thesis) attached to the Cp nucleus can be looked at with a view of establishing thermodynamic trends. The activation of the precursor that was neglected in this project can also be investigated.

Chapter 8

Experimental

"Science may set limits to knowledge, but should not set limits to imagination."
Bertrand Russell (1872 - 1970)

8.1 General experimental details

All reactions (unless otherwise stated) were carried out using standard Schlenk-line techniques.[88] [89] A Braun Unilab Glovebox under N_2 at a positive pressure of 200 mbar was used for the manipulation and preparation of samples for analysis. Argon gas was purified through columns of active molecular sieves (5 Å) and BASF catalyst before use on the Schlenk line. Syringes were stored at 60 °C and all other glassware at 200 °C for 2 h. Before use, the glassware was heated under vacuum with a hot gun, and cooled under vacuum to room temperature.

8.2 Solvents and materials

All solvents were distilled prior to use by literature methods. [90] Typically, solvents were stored in Teflon sealed storage vessels. Table 8.1 summarises the drying agents and procedures used in the purification of used solvents.

Solvent	Drying Agent	Distillation	Colour
Benzene-d_6	Na / K alloy	Vacuum Transfer	None
Chloroform-*d*	CaH_2	Vacuum Transfer	None
Dichloromethane	CaH_2	Yes	None
Diethylether	Na / tetraglyme[v]	Yes	Blue[vi]
Heptane	Na	Yes	None
Methanol	Mg turnings / I_2	Yes	None
Pentane	Na / tetraglyme	Yes	Blue
Tetrahydrofuran	Na / tetraglyme	Yes	Blue
Toluene	Na	Yes	None

Table 8.1 Purification of solvents

[v] This is a high boiling point ether.
[vi] This blue colour acts as an indicator of active sodium.

1,2,3,4,5-pentaphenylcyclopenta-1,3-diene and 1,2,3,4-tetraphenylphenylcyclopenta-1,3-diene was purchased from Aldrich and used without further purification. 3,5-dimethyl-1-bromobenzene was obtained from Lancaster and used as received. Tri-*t*-butyl-phosphine was purchased from Aldrich and used as received, and stored in the glove box. $Pd(OAc)_2$ was purchased from Aldrich and used as received. *n*-BuLi was purchased from Aldrich and transferred via cannula to a Teflon sealed storage vessel for use. *n*-Hexyllithium was purchased from Acros Organics as a 33 % wt. solution in *n*-hexane and used without further purification. All other chemicals were obtained commercially (Aldrich) and unless otherwise stated, used without further purification, unless stated in Table 8.1. Air-sensitive compounds were stored under N_2 or in the glove-box.

8.3 Instrumentation

Melting points were determined on the Kofler hotstage microscope (Reichart Thermovar) and are uncorrected. Three measurements were taken, and averaged. Microanalysis data was obtained from the University of Cape Town's Microanalytical Laboratory using a Carlo Erba EA1108 elemental analyser. In some cases oxidant, V_2O_5 was added to the sample. Infrared Spectra were recorded on a Perkin-Elmer 1000 FT-IR spectrometer, at the University of Cape Town, in solution cells with NaCl windows unless otherwise stated. FT-IR spectra of the model complexes were carried out at the University of Pretoria in KBr pellets (mid-infrared region) or in polyethylene pellets (far infrared region). All data are given in wavenumbers (cm^{-1}). NMR Spectra were recorded on a Varian Unity-400 spectometer (^1H, ^{13}C), or on a Mercury 300 spectometer (^1H, ^{13}C). Mass spectrometry of the ligands was carried out using Fast atom bombardment mass spectrometry (FAB-MS), at the Lund Chemical Centre, Lund, Sweden using a JEOL SX-102 instrument. In general this was done at a temperature of 4 °C, using direct inlet, and a 0 % cut level. Isotopic distribution patterns were checked against theoretical distributions.

Electron spin resonance spectroscopy (EPR) was also conducted at the Lund Chemical Centre, Lund, Sweden. Spectra were recorded in 1 mm quartz tubes (100 kHz modulation frequency at an amplitude of 0.005–0.08 mT, microwave effect 0.4–1.6 mW), and irradiation was performed by the 50 W high-pressure Hg lamp from Bruker (ER 202) with a filter with cutoff at 430 nm.

Gas Chromatography (GC), on the catalytic mixtures was conducted on a HP 5890 Series II Gas Chromatograph fitted with a PONA (Crosslinked Methyl Siloxanes) capillary column (50 m × 0.20 mm × 0.5 m). Flame Ionisation detection (FID) was used.

Cyclic Voltametry (CV) was carried out using a BAS-100B electrochemical analyzer in a one compartment-three-electrode system. Ag/Ag^+ (0.01 M) was used as reference electrode, while

platinum wire was used as the auxiliary electrode. A platinum disc was used as the working electrode. The supporting electrolyte was tetrabutylammonium perchlorate (0.1 M) in acetonitrile (dry). The solutions were saturated with argon through bubbling argon through the solution for 5 minutes before each CV data run. The working electrode was polished after each data run.

X-ray diffraction data was collected at 113 K using a Nonius Kappa CCD with 1.5 kW graphite-monochromated Mo radiation. Data collection strategy was evaluated using COLLECT.[91] Several sets of data were collected with both 360° ϕ and Ω scans to collect the cusp data. The structure was solved and refined using SHELX97. [92]

DFT calculations were carried out using Materials Studio™ (Accelrys Inc.) and the calculations were performed using the "Erica" or "Disa" server at the University of Cape Town's Department of Chemical Engineering.

8.4 Experimental details pertaining to Chapter 2

Synthesis of $Li_2C_4Ph_4$ (2.1)

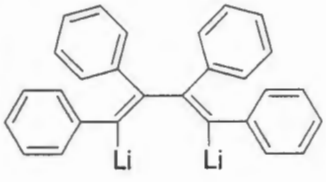

This reaction was carried out under argon, in light of the reactivity of lithium with nitrogen at ambient temperatures. A centrifuge tube was charged with diphenylacetylene (1.02 g, 5.60 mmol), lithium metal (0.05g, 7.20 mmol) and THF (5 cm^3) and stirred at room temperature overnight. A red solution is seen to develop after *ca.* 3 h of stirring indicating dimerisation. The solvent was subsequently removed to yield a yellow solid as the crude product. The solid was washed with pentane (3 x 10 cm^3) using centrifuge techniques, each time removing the supernatant liquid with a syringe. The product was isolated as a bright yellow solid in low yields and partially characterized by ^1H NMR (0.70 g, 34 %). δ_H (400 MHz, C_6D_6) 6.62 – 7.12 (20 H, m, 20 Ar*H*), 1.04 (m, THF (co-ordinated to Li)), 3.15 (m, THF (co-ordinated to Li)).

Synthesis of 1,2,3,4,5 pentaphenyl cyclopenta-1,3-diene (2.2)

A procedure similar to the literature procedure was followed.[34] α,α–Dibromotoluene (0.90 g, 5.70 mmol) was added to a suspension of (**2.1**) in Et_2O (15 cm^3) at – 10 °C. The reaction was allowed to warm up to room temperature and stirred for 24 h. The

reaction was opened to the atmosphere at this time. Water (30 cm^3) was added to the reaction mixture, and extracted with diethylether (3 x 30 cm^3). The collected organic fractions were rinsed with water (3 x 30 cm^3) and brine (3 x 30 cm^3). The organic fraction was dried over anhydrous Na_2SO_4 overnight. The mixture was filtered, and the solvent removed *in vacuo.* The crude product was dissolved in a minimum volume of boiling toluene and cooled to -15 °C overnight. A pale yellow solid was obtained as the pure product from the above recrystallisation. Since this is a known compound, only ^1H NMR and m.p. was carried out. (0.170 g, 7 %). m.p. 247 - 249 °C (lit. 255 °C [34]); δ_H (300 MHz, C_6D_6) 6.81 – 7.62 (25 H, m, 5 Ph*H*), 5.03 (1 H, s, Cp*H*).

Synthesis of 1,1 dibromoheptane

A route similar to the literature procedure was followed.[35] 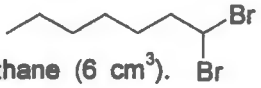

Triphenylphosphite (3.72 g, 12 mmol) was dissolved in dry dichloromethane (6 cm^3). Bromine liquid (1.92 g, 12 mmol) was added drop- wise to the mixture at 0 °C through a rubber septum. After complete addition of the bromine, the mixture was taken down to -15 °C. An orange colour was noted at this time. The aldehyde, heptanal (0.86 cm^3, 6.10 mmol) was added drop-wise through a rubber septum to the mixture at -15 °C. The reaction mixture was warmed to 0 °C and filtered through a column of alumina, and a extraction from Et_2O followed. A short-path distillation was carried out to purify the product. NMR analysis confirmed the structure of the compound.

Synthesis of 1,2,3,4-tetraphenyl cyclopenta-1,3-diene (2.3).

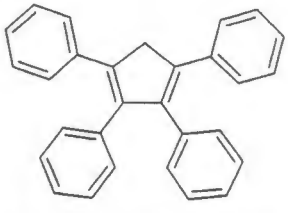

Similar methodology was used as in the preparation of (**2.2**) Dibromomethane (5.70 mmol) was added to a suspension of (**2.1**) in Et_2O (15 cm^3) at – 10°C. The reaction was allowed to warm up to room temperature and stirred for 24 h. The reaction was opened to the atmosphere at this time. Water (30 cm^3) was added to the reaction mixture, and extracted with diethylether (3 x 30 cm^3). The collected organic fractions were rinsed with water (3 x 30 cm^3) and brine (3 x 30 cm^3). The organic fraction was dried over anhydrous Na_2SO_4 overnight. The mixture was filtered, and the solvent removed *in vacuo.* The crude product was dissolved in a minimum volume of boiling toluene and cooled to -15 °C overnight. A pale yellow solid was obtained at the pure product. Since this is a known compound, only ^1H NMR and m.p. was conducted, and compared with a commercial sample. (0.165 g, 10 %). m.p. 185-186 °C (Lit. 181 °C [93]); δ_H (400 MHz, C_6D_6), 6.98 – 7.26 (20 H, m, 4 Ph*H*), 4.05 (2 H, s, 2 Cp*H*).

Synthesis of $Na[C_5Ph_4H]$ (2.4).

The literature procedure was used.[50] The solid, (**2.3**) (0.20 g, 0.54 mmol) and NaH (0.03 g, 1.08 mmol) was added made up to a suspension in THF (5 cm^3) in a centrifuge tube and refluxed overnight. A cold-finger reflux condenser was used for convenience. Bubbles of H_2 gas were liberated during the reflux indicating that the reaction was taking place. The solvent was removed *in vacuo* to yield a yellow solid as crude product. This solid was washed with pentane (3 x 10 cm^3) using centrifuge techniques, and the supernatant fluid removed each time. The resulting solid was dried *in vacuo* to yield an off-white solid as the pure product in good yields. Due to the pyrophoric nature of this compound, only ^1H NMR data was collected. (0.43 mmol, 80 %). δ_H (400 MHz, C_6D_6) 6.85 – 7.25 (20 H, m, 4 Ph*H*), 3.70 (1 H, s, Cp*H*).

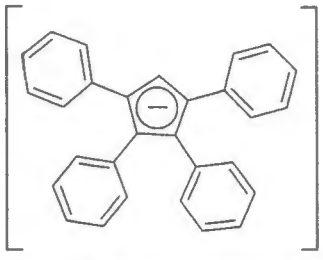

Synthesis of 5-^{t}butyl-1,2,3,4-tetraphenylcyclopenta-1,3-diene (2.5)

The compound, 1,2,3,4-tetraphenylcyclopenta-1,3-dienone (2.00g, 5.20 mmol) was made up to a suspension in diethyl ether (10 cm^3) and cooled to -78 °C. *tert*-butyl lithium (1.6 M hexanes) (3.85 cm^3, 6.50 mmol) was added drop-wise to the suspension. An immediate colour change from purple to yellow was noted. The temperature was held at -78 °C for two hours, and allowed to warm up to ambient temperatures. A further 16 hours of stirring at ambient temperatures was followed by removal of the solvent *in vacuo*. A brown syrup-like residue remained. Acetic Acid (10 cm^3) and aqueous HBr (40 % in water) (1.8 cm^3) was added to the syrup-like residue and brought to reflux for 0.5 h. Zn dust (1.40 g, 21.40 mmol) was added to the boiling mixture while refluxing continued for a further 5 h. During this time additional HBr (aq) was added (1.4 cm^3). A further 16 h of refluxing followed, after which the mixture was cooled to room temperature and diluted with 250 cm^3 $CHCl_3$. The organic fraction was separated from the aqueous fraction and rinsed with a solution of $NaHCO_3$ (3 x 250 cm^3), water (3 x 250 cm^3) and brine (3 x 250 cm^3). The organic fraction was dried over $MgSO_4$ overnight, after which the solvent was removed *in vacuo*. Purification of the crude product by column chromatography followed. Silica gel was used as stationary phase, made up as a slurry with the eluent, $CHCl_3$: hexane (1 : 5). The crude product was dissolved in the minimum eluent and transferred to the column. The first band to elute was the desired product. Removal of the eluent *in vacuo* yielded a light yellow solid. Recrystallisation from $CHCl_3$/hexane afforded a white powder-like solid as product. (0.54 g, 24 %) mp (200 – 204 °C), (Found: C, 92.09; H, 6.24% $C_{33}H_{30}$ requires C, 92.91; H, 7.09%; M^+ =

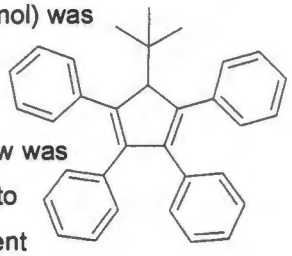

427); δ_H(300 MHz, $CDCl_3$) 6.59 – 7.26 (20 H, m, 20 Ar*H*), 4.48 (1 H, s, Cp*H*), 1.28 (9 H, br s, 3 CH_3); $\delta_{C\{H\}}$ (76 MHz, $CDCl_3$) 138.0 – 143.0 (5 C, Cp(C)), 125.0 – 131.4 (24 C, Ar(C)), 67.25 , 62.94, 38.3; m/z 387, 279, 154, 136, 77, 57, 39.

Synthesis of 5 - ^{n}butyl-1,2,3,4-tetraphenylcyclopenta-1,3-diene (2.6)

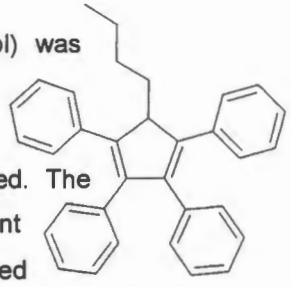

The compound, 1,2,3,4-tetraphenylcyclopenta-1,3-dienone (2.00g, 5.20 mmol) was made up to a suspension in diethyl ether (10 cm^3) and cooled to -78 °C. *n*-butyl lithium (1.6 M hexanes) (4.33 cm^3, 6.50 mmol) was added dropwise to the suspension. An immediate colour change from purple to yellow was noted. The temperature was held at -78 °C for two hours, and allowed to warm to ambient temperatures. A further 16 hours of stirring at ambient temperatures was followed by removal of the solvent *in vacuo*. A brown syrup-like residue remained. Acetic Acid (10 cm^3) and aqueous HBr (40 % in water) (1.8 cm^3) was added to the syrup-like residue and brought to reflux for 0.5 h. Zn dust (1.40 g, 21.40 mmol) was added to the boiling mixture while refluxing continued for a further 5 h. During this time additional HBr (aq) was added (1.4 cm^3). A further 16 h of refluxing followed, after which the mixture was cooled to room temperature and diluted with 250 cm^3 $CHCl_3$. The organic fraction was rinsed with a solution of $NaHCO_3$ (3 x 250 cm^3), water (3 x 250 cm^3) and brine (3 x 250 cm^3). The organic fraction was dried over $MgSO_4$ overnight, afterwhich solvent was removed *in vacuo*. Purification of the crude product by column chromatography followed. Silica gel was used as stationary phase, made up as a slurry with the eluent, $CHCl_3$: hexane (1 : 5). The crude product was dissolved in the minimum eluent and transferred to the column. The first band to elute was the desired product (a yellow band). Removal of the eluent *in vacuo* yielded a light yellow solid. Recrystallisation from $CHCl_3$/hexane afforded a light yellow needles as product. (0.56 g, 25 %), mp (163 – 166 °C), (Found : C, 92.48; H, 7.44% $C_{33}H_{30}$ requires C, 92.46; H, 7.54 %, M^+ = 426); ν_{max}/cm^{-1} (in dichloromethane) 2954 (C-H), 2934 (C-H), 2875, 2355, 1606 (Aromatic), 1497 (Aromatic), 1469, 1380; δ_H(300 MHz, $CDCl_3$) 7.02 – 7.26 (20 H, m, 20 Ar-*H*), 4.30 (1 H, t, ^3J (HH) = 4.7 Hz, Cp*H*), 1.77 (2 H, m, CpCH_2), 1.00 – 1.02 (4 H, m, $CpCH_2CH_2CH_2$), 0.64 (3 H, t, ^3J(HH) = 6.84 Hz, CH_3); $\delta_{C\{H\}}$ (76 MHz, $CDCl_3$) 136.4 – 145.3 (5 C, Cp(C)), 126.3 – 130.2 (Ar(C)), 54.8, 28.6, 24.7, 22.7, 13.76; m/z 426 (M^+), 383, 377, 339, 307, 289, 276, 252, 215 ($CpPh_2^+$), 165, 154, 136, 91, 69, 55, 41, 27.

Synthesis of 5 - ^{n}hexyl-1,2,3,4-tetraphenylcyclopenta-1,3-diene (2.7)

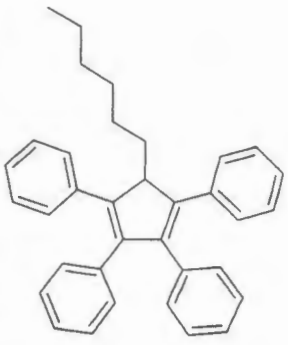

The compound, 1,2,3,4-Tetraphenylcyclopenta-1,3-dienone (8.00g, 20.80 mmol) was made up to a suspension in diethyl ether (40 cm^3) and cooled to -78 °C. *n*-hexyl lithium (33 % wt in hexanes) (10.6 cm^3) was added drop wise to the suspension. An immediate colour change from purple to yellow was noted upon completion of the addition. The temperature was held at -78 °C for two hours, and allowed to warm up to ambient temperatures. A further 16 hours of stirring at ambient temperatures was followed by removal of the solvent *in vacuo*. A brown syrup-like residue remained. Acetic Acid (40 cm^3) and aqueous HBr (40 % in water) (7.2 cm^3) was added to the syrup-like residue and brought to reflux for 0.5 h. Zn dust (5.60 g, 85.61 mmol) was added to the boiling mixture while refluxing continued for a further 5 h. During this time additional HBr (aq) was added (5.6 cm^3). A further 16 h of refluxing followed, after which the mixture was cooled to room temperature and diluted with 2 L $CHCl_3$. The organic fraction was rinsed with a solution of $NaHCO_3$ (3 x 1 L), water (3 x 1 L) and brine (3 x 1 L). The organic fraction was dried over $MgSO_4$ overnight, afterwhich solvent was removed *in vacuo*. Purification of the crude product by column chromatography followed. Silica gel was used as stationary phase, made up as a slurry with the eluent, $CHCl_3$: hexane (1 : 5). The crude product was dissolved in the minimum eluent and transferred to the column. The first band to elute was the desired product (a yellow band). Recrystallisation from $CHCl_3$/MeOH afforded a light yellow needle-like solid as product. (2.47 g, 26 %), mp (125 – 127 °C), (Found : C, 92.48; H, 7.44% $C_{35}H_{34}$ requires C, 92.46; H, 7.54 %, M^+ = 454); ν_{max}/cm^{-1} (in $CHCl_3$) 2976 (C-H), 2926 (C-H), 2866, 1956, 1823, 1759, 1908, 1498 (Aromatic), 1151, 1046; δ_H (300 MHz; C_6D_6) 7.03 – 7.15 (20 H, m, 20 Ar-*H*), 4.25 (1 H, t, ^3J(HH) = 4 Hz, Cp*H*) 1.70 (2 H, m , $CpCH_2$), 0.9 – 1.04 (8 H, m, $CpCH_2CH_2CH_2CH_2CH_2CH_3$), 0.69 (3 H, t, ^3J(HH) = 6.5 Hz, CH_3); $\delta_{c\{H\}}$ (76 MHz; C_6D_6), 135.6 – 138.4 (Cp(C)) 125.6 – 130.2 (Ar(C)), 61.9, 54.8, 31.1, 28.9, 22.4, 13.9; m/z 454 (M^+), 383, 370 ($CpPh_4^+$), 326, 289, 276, 265, 215 ($CpPh_2^+$), 154, 136, 91, 89, 77, 51, 39, 31.

Synthesis of 5- (1-propenyl)-1,2,3,4 tetraphenylcyclopenta-1,3-diene (2.8)

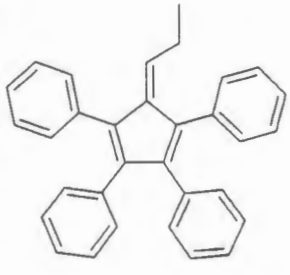

The compound, 1,2,3,4-Tetraphenylcyclopenta-1,3-dienone (4.00g, 10.40 mmol) was made up to a suspension in diethyl ether (20 cm^3) and cooled to 0°C. Allyl Grignard (37.00 cm^3, 13.00 mmol) was added drop wise to the suspension. An immediate colour change from purple to yellow was noted. The temperature was held at -78 °C for two hours, and allowed to warm up to ambient temperatures. A further 16 hours of stirring at ambient temperatures was followed by removal of the solvent *in vacuo*. A brown syrup-like residue remained. Acetic Acid (20 cm^3) and aqueous HBr (40 % in water) (3.6 cm^3) was added to the syrup-like residue and brought to reflux for 0.5 h. Zn

dust (2.80 g, 42.80 mmol) was added to the boiling mixture while refluxing continued for a further 5 h. During this time additional HBr (aq) was added (2.8 cm^3). A further 16 h of refluxing followed, after which the mixture was cooled to room temperature and diluted with 500 cm^3 $CHCl_3$. The organic fraction was rinsed with a solution of $NaHCO_3$ (3 x 500 cm^3), water (3 x 500 cm^3) and brine (3 x 500 cm^3). The organic fraction was dried over $MgSO_4$ overnight, afterwhich solvent was removed *in vacuo*. Purification of the crude product by column chromatography followed. Silica gel was used as stationary phase, made up as a slurry with the eluent, $CHCl_3$: hexane (1 : 5). The crude product was dissolved in the minimum eluent and transferred to the column. The first band to elute was the desired product (a bright orange band). Removal of the eluent *in vacuo* followed by recrystallisation from $CHCl_3$/hexane afforded a bright orange powder as pure product. R_f ($CHCl_3$: hexane (5 : 25) = 0.81; (0.25 g, 23%), mp = 150 – 153 °C, (Found; C, 91.68; H, 6.04% $C_{32}H_{26}$ requires C, 93.62, H, 6.38, M^+ = 410); ν_{max}/cm^{-1} (in $CHCl_3$) 3031 (C-H), 2965 (C-H), 2872, 1961 (Aromatic), 1885, 1810, 1624, 1598 (Aromatic), 1492 (Aromatic), 1452, 1331, 1265, 1107, 1020; δ_H (300 MHz, $CDCl_3$) 6.87 – 7.29 (20 H, m, 20 Ar*H*), 6.41 (1 H, t ^3J (HH) = 7.7 Hz, CpC*H*CH_2), 2.05 (2 H, t), 1.65 (1 H, dd ^3J (HH) = 1.83 Hz), 0.89 (3 H, t, ^3J (HH) = 8 Hz, CH_3); $\delta_{C\{H\}}$ (76 MHz, $CDCl_3$) 126.3 – 131.7 (20 C, Ar(C)), 23.4 (1 C, *C*H); m/z 410 (M^+), 307, 289, 215 (CPh_2^+),178, 154, 136, 89, 77, 69, 55, 41, 27.

Synthesis of 5-ethyl-1,2,3,4-tetraphenylcyclopenta-1,3-diene (2.9)

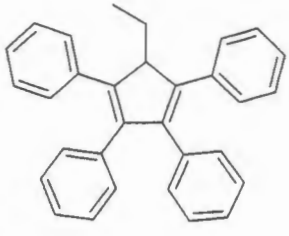

Although the target 5-vinyl-1,2,3,4-tetraphenyl cyclopenta 1,3 diene was attempted using this route, from spectroscopic evidence, (**2.9**) was isolated. Tetracyclone (C_5Ph_4O) (3.21 g, 8.35 mmol) was made up to a suspension in Et_2O (16 cm^3) at 0 °C. Vinyl magnesium bromide (10 cm^3, ca. 1.0 M) was added dropwise to the suspension at 0 °C. The solution was stirred at 0 °C for 2 h. and then at room temperature for a further 16 h. The solvent was removed *in vacuo* to afford a brown tar-like residue. Acetic Acid (16 cm^3) and HBr (aq.) (3 cm^3) was added to the residue and brought to reflux for a period of 0.5 h. Over an additional period of 5 h refluxing continued with addition of Zn dust (2.4 g) added in small portions over that period. After the addition was complete, a further 16 h reflux period followed. The mixture was allowed to cool to room temperature, and $CHCl_3$ (500 cm^3) was added to the crude mixture. The organic phase was extracted with a $NaCO_3$ solution (3 x 100 cm^3), water (3 x 100 cm^3) and brine (3 x 100 cm^3). The resulting organic phase was dried over $MgSO_4$ overnight and filtered. Purification of the crude product by column chromatography followed. Silica gel was used as stationary phase, made up as a slurry with the eluent, $CHCl_3$: hexane (1 : 5). The crude product was dissolved in the minimum eluent and transferred to the

column. The first band to elute was the desired product (a yellow band). Removal of the eluent *in vacuo and* recrystallisation from chloroform at -15 °C overnight yielded a light yellow solid as product. (1.25 mmol, 14 %), mp (164 – 167 °C), δ_H (400 MHz, $CDCl_3$) 7.09 – 7.22 (20 H, m, 20 Ar*H*), 4.25 (1 H, t, Cp*H*), 1.85 (2 H, m, CpCH_2), 0.51 (3 H, t, $CpCH_2CH_3$); $\delta_{c\{H\}}$ (100.6 MHz, $CDCl_3$)127.6 – 130.2 (Ar(C)), 55.5, 22.3, 7.5; m/z 398 (M^+), 307, 289, 154, 136, 107, 77 (Ph^+), 63, 39, 27 $(C_2H_5 - 2\ H)^+$.

Synthesis of 1,2,3,4,5-penta-(3,5 dimethyl phenyl) cyclopenta-1,3-diene (2.10)

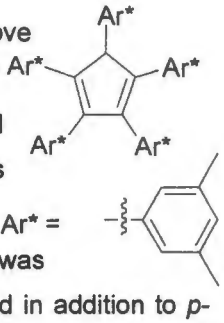

The literature procedure, reported by Giesbrecht *et al.*. was followed.[40] In a glove box Cp_2ZrCl_2 (0.58 g, 2.00 mmol), 3,5-dimethyl-1-bromobenzene (4.44 g, 24.00 mmol), Cs_2CO_3 (7.82 g, 24.00 mmol), $Pd(OAc)_2$ (0.11 g, 0.50 mmol) and *t*-Bu_3P (0.11 g, 0.50 mmol) was added to a schlenk tube. DMF (50 cm^3) was added to the mixture, and stirred at 130 °C (reflux temperatures) for 24 h. During this time, the formation of a creamy white slurry is noted. The mixture was cooled to room temperature, and exposed to air. CH_2Cl_2 (150 cm^3) was added in addition to *p*-toluenesulfonic acid (9.12 g, 48.00 mmol). This mixture was subsequently stirred at room temperature for 15 minutes and passed through a column of silica gel yielding a brown solution. The coloumn was rinsed with additional CH_2Cl_2 and DMF until washings were colourless. Removal of the solvent *in vacuo* resulted in a tar-like solid as crude product. Dissolution of the solid in $CHCl_3$ and subsequent extraction with a solution of $NaHCO_3$ (3 x 150 cm^3), and saturated brine (3 x 150 cm^3) was followed by drying the organic layer over $MgSO_4$. The solvent was removed *in vacuo* and the residue washed with hexane until washings were colourless. The solid was noted to be partially soluble in hexane, and caution was taken in this step. The solid was dried *in vacuo* affording a pale off white solid as (**2.10**). Characterisation by ^1H NMR was conducted to confirm the structure of the compound, and compared with literature.[41] (1.85 g, 79 %), m.p 203 – 206, δ_H (400 MHz, $CDCl_3$) 6.67 – 6.81 (15 H, m, 15 Ar*H*), 5.00 (1 H, s, Cp*H*), 2.06 – 2.20 (30 H, m, 10 CH_3).

8.5 Experimental details pertaining to Chapter 3

Synthesis of $[(\eta^5\text{–}C_5Ph_5)Cr_2Cl_2]_2$ (3.1)

$CrCl_3(thf)_3$ (0.20 g, 0.54 mmol) was added to (**2.4**) (0.25 g, 0.54 mmol) in a centrifuge tube. Toluene (8 cm^3) was added to the mixture, and brought to reflux for 24 h. The mixture was allowed to cool to room temperature and the mixture centrifuged. The supernatant fluid was syringed into another centrifuge tubes, and the solvent removed *in* vacuo. The resulting solid was washed with pentane (3 x 15 cm^3) and each time the supernatant was removed via syringe. The resulting solid was dried *in vacuo* to yield an olive green solid as product in high yield. (0.39 g, 86 %); m.p. 337 – 339 °C (Lit. 330 °C). (Found **(with oxidant)**; C, 71.62; H, 4.16 %; Found **(without oxidant)** C, 68.41; H, 3.76 %; $C_{70}H_{50}Cr_2Cl_4$ requires C, 73.95, H, 4.43, M^+ = 1136.95) ν_{max}/cm^{-1} (KBr pellets / polyethylene pellets) 3059 (C-H), 3026 (C-H) , 1619 (Aromatic), 1600 (Aromatic), 1578 (Aromatic), 1499, 1488, 1443, 1417, 1185, 1157, 1073, 1027, 549 (Cr-Cl terminal), 442 (Cr-Cl terminal), 416 (Cr-Cl terminal), 350 (Cr-Cl terminal), 317 (Cr-Cl terminal), 297 (Cr-Cl bridging), 227 (Cr-Cl bridging), 208 (Cr-Cl bridging), 189 (Cr-Cl bridging), 151 (Cr-Cl bridging); δ_H (300 MHz, benzene-d_6) 6.89 – 7.15 (50 H, m, 50 Ar*H*); $\delta_{C\{H\}}$ (75.4 MHz, benzene-d_6) 126.8 , 127.1, 128.8, 128.9, 129.5, 130.5; (EPR analysis CH_2Cl_2 glass at 5 K, 9.622 GHz, power = 1 mW) 1756 G (*g* (orthogonal) = 3.92) , 3457 G (*g* (parallel) = 1.99); m/z 532 [$(C_5Ph_5)CrCl^+$], 445 ($C_5Ph_5^+$), 363, 289, 154, 136, 77 (Ph^+), 39.

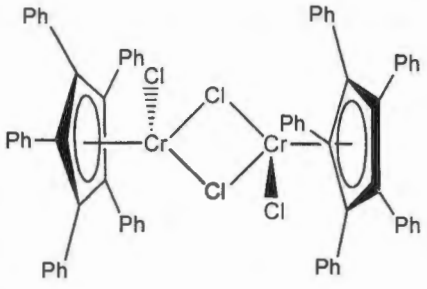

Alternative synthesis of $[(\eta^5\text{–}C_5Ph_5)Cr_2Cl_2]_2$ (3.1)

$KN(TMS)_2$ (0.13g, 0.64 mmol) was added to a pre-weighed centrifuge tube in the glove-box. C_5Ph_5H (0.27 g, 0.61 mmol) was added to the centrifuge tube in addition to toluene (5 cm^3). The mixture was stirred at a temperature of 70 °C for 2 hours, during which the product, $K[C_5Ph_5]$, was seen to form as a bright yellow solid. The solvent was removed *in vacuo*, and the crude $K[C_5Ph_5]$ washed with pentane (3 x 10 cm^3) using centrifuge techniques to afford the pure $K[C_5Ph_5]$ as product, confirmed by ^1H NMR spectroscopy. $CrCl_3(thf)_3$ (**3.3**) (0.22 g, 0.61 mmol) was added to the salt, in addition to toluene (5 cm^3). The mixture was stirred at a temperature of 70 °C for 4 hrs. During this time a colour change from pink to green-blue was noted. The reaction was stopped, centrifuged, and the supernatant fluid syringed off into another pre-weighed centrifuge tube. The original centrifuge tube was rinsed with toluene (2 x 5 cm^3), each time centrifuging and removing the supernatant fluid, and adding it to the second centrifuge tube. The solvent was removed *in vacuo* and the crude product washed with pentane (3 x 10 cm^3), each time centrifuging and removing the supernatant fluid. The resulting purified product was dried *in vacuo* overnight to

afford the product as a green solid. The product was confirmed by mp determination, and IR spectroscopy analysis, and compared with the above route.

Synthesis of $[(\eta^5\text{–}C_5Ph_4H)Cr_2Cl_2]_2$ (3.4)

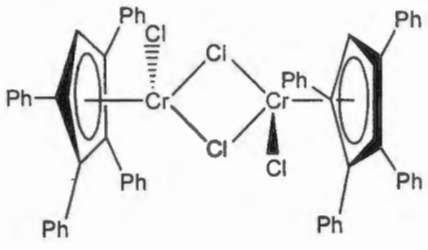

$CrCl_3(thf)_3$ (0.16 g, 0.43 mmol) was added to (**2.4**) (0.17 g, 0.43 mmol) in a centrifuge tube. Benzene (7 cm^3) was added to the mixture, and brought to reflux for 24 h. After ca. 2 h the mixture turns bright green. The mixture was allowed to cool to room temperature and centrifuged. The supernatant fluid was syringed over into another centrifuge tube and the solvent removed *in vacuo* resulting in a green solid as crude product. The solid was washed with pentane (3 x 15 cm^3) and each time the supernatant fluid was removed via syringe. The resulting solid was dried *in vacuo* to yield a light green solid as product in moderate yield. (0.24 g, 60 %), mp 335 – 340 °C; (Found; C, 71.94; H, 3.42% $C_{58}H_{42}Cr_2Cl_4$ requires C, 70.74; H, 4.30 % 6.38, M^+ = 984.76); ν_{max}/cm^{-1} (KBr pellets / polyethylene pellets) 3055 (C-H) , 2955 (C-H), 1599 (Aromatic), 1442, 1262, 1186, 1076, 1030, 919, 858, 770, 699, 521 (Cr-Cl terminal), 458 (Cr-Cl terminal), 321 (Cr-Cl terminal), 229 (Cr-Cl bridging), 206 (Cr-Cl bridging), 187 (Cr-Cl bridging), 155 (Cr-Cl bridging); δ_H (300 MHz, toluene-d_8) 6.51 – 7.51 (40 H, m, Ar*H*), Cp*H* not observed in this chemical shift range; (EPR analysis CH_2Cl_2 glass at 5 K, 9.622 GHz, power = 1 mW) 1776 G (*g* (orthogonal) = 3.87), 3403 G (*g* (parallel)= 2.02); m/z 526, 456 $[(C_5Ph_4H)CrCl]^+$; 400, 370 ($C_5Ph_4^+$), 302, 289, 191, 178, 136, 73, 43, 28.

Synthesis of $CrCl_3(thf)_3$ (3.3)

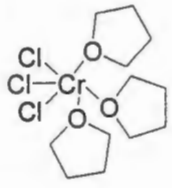

The literature procedure was used in this synthesis.[51] $CrCl_3(H_2O)_6$ (1.59 g, 5.95 mmol) was stirred with excess $SOCl_2$ (10 cm^3). The mixture was brought to reflux for 3 h, during which a grey colour was noted. This procedure was undertaken dehydrate the hydrated chromium adduct. THF (excess) (1.72 g, 23.80 mmol) was added dropwise to the solution, uponwhich a bright purple-pink adduct in formed as product. IR spectroscopy was conducted to confirm the structure. (1.68 g, 73 %), ν_{max}/cm^{-1} 857, 1016.

Synthesis of $K[C_5Ar^*_5]$ where Ar = $C_6H_4Me_2$ (3.7)

$KN(TMS)_2$ (0.10 g, 0.69 mmol) was weighed out in a glove-box and (**2.10**) (0.38 g, 0.65 mmol). THF (10 cm^3) was added, and the mixture stirred at room temperature for 3 h. As the reaction proceeded, a white precipitate is noted, being the solid product. The crude product was rinsed with pentane (3 x 15 cm^3) using centrifuge techniques, and dried *in vacuo* for 2 h, to afford a white solid as product. No characterization was conducted on this compound in light of its pyrophoric nature. Based on the colour, the product was assumed to be acceptable for use in the preparation of complex (**3.6**).

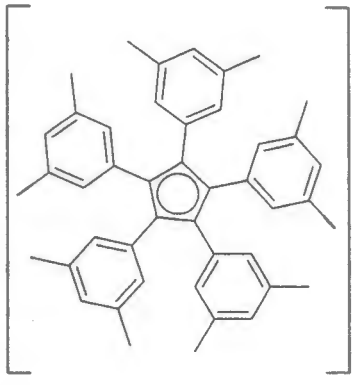

Synthesis of $[(\eta^5-C_5Ar_5^*)CrCl_2]_2$ (3.6)

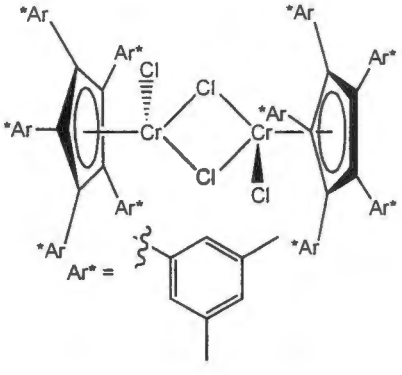

(2.10) (0.75 g, 1.28 mmol) was dissolved in THF (15 cm^3). $KN(TMS)_2$ was dissolved in THF (5cm^3) and the two solutions added. A creamy white precipitate was immediately formed (**3.7**) and the solutions were allowed to stir for 2 h at room temperature. (**3.3**) (0.49g, 1.30 mmol) was added to the solution, and an immediate colour change to dark-blue was noted (probably the THF adduct monomer). Upon stirring, the solution thinned and the creamy white precipitate disappeared. After stirring for 3 h the mixture was centrifuged, and the blue solution isolated. The THF was removed *in vacuo* and rinsed with pentane (3 x 10 cm^3) using centrifuge techniques, each time removing the supernatant liquid. The purified product was dried *in vacuo* at 50 °C for several hours, to afford an olive green powder as product. (0.24 g, 60 %), mp 365 – 370 °C (dec); (complex too labile for elemental analysis); ν_{max}/cm^{-1} (KBr pellets / polyethylene pellets) 3007 (C-H stretch vibration), 2957 (C-H stretch vibration), 2916 (C-H stretch vibration), 2861 (C-H stretch vibration), 1599 (Aromatic), 1446 (Aromatic), 1404 (Aromatic), 1376, 1255, 1039 (C-C), 847, 757, 723, 699, 537 (Cr-Cl terminal), 452 (Cr-Cl terminal), 317 (Cr-Cl terminal), 227 (Cr-Cl bridging), 207(Cr-Cl bridging), 191(Cr-Cl bridging), 149 (Cr-Cl bridging). δ_H (300 MHz, toluene-d_8) 6.38 – 6.99 (30 H, m, 30 Ar**H*), 1.88 – 1.98 (60 H, m, CH_3).

Synthesis of $(C_5Ph_4H)_2Fe$ (3.8)

A similar procedure prescribed in the literature was followed. [67] **(2.3)** (0.57 g, 1.54 mmol) and benzene (5 cm^3) was stirred at room temperature. *n*-BuLi (1.29 cm^3, 2.00 mmol (1.6 M in hexane)) was added dropwise to the solution. An immediate white slurry-like precipitate is seen forming. The reaction was stirred for 1 h. and the solvent removed *in vacuo*. The white solid, (Li $[C_5Ph_4H]$), was dried under high vacuum overnight. Ethereal $FeCl_2$ (0.097 g, 0.77 mmol) was added to the white solid in addition to THF (10 cm^3). The mixture was stirred at room temperature over night. The solvent was removed *in vacuo*, and boiling toluene (80 cm^3) added to the residue in air. The mixture was rapidly filtered, the volume of the solvent reduced *in vacuo*, and the solution cooled at – 15 °C overnight. A red solid recrystallised out of solution, was filtered and rinsed with pentane to yield a red air stable solid as product. (0.28 g, 46 %), (Found; C, 87.69; H, 5.53% $(C_5Ph_4H)_2Fe$ requires C, 87.65; H, 5.33 % , M^+ = 794.80); δ_H (300 MHz, benzene-d_6) 6.80 – 7.29 (40 H, m, 40 Ar*H*), 5.65 (2 H, s, Cp*H*); $\delta_{C\{H\}}$ (300 MHz, toluene-d_8) 135.9, 132.8, 129.9, 128.3, 128.0, 127.9, 127.7, 127.4, 126.8; m/z 795 (M^+), 391, 369 ($C_5Ph_4^+$), 307, 289, 154, 136, 89, 77, 39.

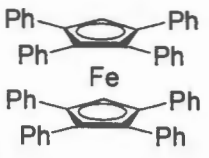

8.6 Catalytic reaction conditions and work-up (Chapter 4)

In the case of the 1,2,3,4,5-pentaphenylcyclopenta-1,3-diene Mahomed *et al.* system (the *in situ*) system, a typical catalytic procedure was as follows:

A Schlenk tube was charged with 1 molar equivalent of Cr-2-ethylhexanoate (14.8 mg, 0.021 mmol), 3 molar equivalents of hexachloroethane (15 mg, 0.063 mmol) and C_5Ph_5H (1,2,3,4,5-pentaphenylcyclopenta-1,3-diene) (9.5 mg, 0.021 mmol). Dried cyclohexane (20 cm^3) was added to the Schlenk tube, and stirred for 15 minutes. Next, 45 molar equivalents of triethylaluminium (TEA) (1.6 M, 0.6 cm^3, 0.95 mmol) was added to the Schlenk tube. An immediate colour change from bottle green to brown was noted. The mixture was transferred to a nitrogen saturated, 1 L Parr™ pressure reactor, and an additional 100 cm^3 cyclohexane added to the reactor. The reactor was placed under a *ca.* 400 psi ethene pressure (and then sealed off), with the overhead stirring unit set at 1600 rpm, the ethene uptake noted, by noting the pressure decrease. After 45 minutes, the reactor was cooled to ambient temperatures, and spiked with internal standard, nonane (2.44 g). The reactor was opened to the atmosphere, and a random sample passed through cotton-wool and injected into the GC for analysis. See full product distribution in appendix A2.

In the case of the 1,2,3,4-tetraphenylcyclopenta-1,3-diene Mahomed *et al.* system (the *in situ*) system, a typical catalytic procedure was as follows:

A Schlenk tube was charged with 1 molar equivalent of Cr-2-ethylhexanoate (14.8 mg, 0.021 mmol), 3 molar equivalents of hexachloroethane (15 mg, 0.063 mmol) and $C_5Ph_4H_2$ (1,2,3,4-tetraphenylcyclopenta-1,3-diene) (7.7 mg, 0.021 mmol). Dried cyclohexane (20 cm^3) was added to the Schlenk tube, and stirred for 15 minutes. Next, 45 molar equivalents of triethylaluminium (TEA) (1.6 M, 0.6 cm^3, 0.95 mmol) was added to the Schlenk tube. An immediate colour change from bottle green to brown was noted. The mixture was transferred to a nitrogen saturated, 1 L Parr™ pressure reactor, and an additional 100 cm^3 cyclohexane added to the reactor. The reactor was placed under a *ca.* 400 psi ethene pressure (and then sealed off), with the overhead stirring unit set at 1600 rpm, the ethene uptake noted, by noting the pressure decrease. After 45 minutes, the reactor was cooled to ambient temperatures, and spiked with internal standard, nonane (3.07 g). The reactor was opened to the atmosphere, and a random sample passed through cotton-wool and injected into the GC for analysis. See full product distribution in appendix A2.

In the case of the catalytic testing of the model complex, $[(C_5Ph_5)CrCl_2]_2$ the following procedure was used:

A Schlenk tube was charged with 1 molar equivalent of $[(C_5Ph_5)CrCl_2]_2$ (11.76 mg, 0.021 mmol), Dried cyclohexane (20 cm^3) was added to the Schlenk tube, and stirred for 15 minutes. Next, 45 molar equivalents of triethylaluminium (TEA) (1.6 M, 0.6 cm^3, 0.95 mmol) was added to the Schlenk tube. An immediate colour change from olive green to brown was noted. The mixture was transferred to a nitrogen saturated, 1 L Parr™ pressure reactor, and an additional 100 cm^3 cyclohexane added to the reactor. The reactor was placed under a *ca.* 400 psi ethene pressure (and then sealed off), with the overhead stirring unit set at 1600 rpm, the ethene uptake noted, by noting the pressure decrease. After 45 minutes, the reactor was cooled to ambient temperatures, and spiked with internal standard, nonane (3.01 g). The reactor was opened to the atmosphere, and a random sample passed through cotton-wool and injected into the GC for analysis. See full product distribution in appendix A2.

Chapter 9

References

"There is no mistaking a real book when one meets it. It is like falling in love."
Christopher Morley (1890 - 1957), O Magazine, December 2003

1. G. Natta, *Angew. Chem.,* 1956, **68** , 393, and references therein.

2. G.W. Coates, *J. Chem. Soc. Dalton Trans.*, 2002, 467, and references therein.

3. P. Cossee, *J. Cat.,* 1964, **3**, 80.

4. C. P. Casey, T. Lee, A. Tunge and D. W. Carpenetti (II), *J. Am. Chem. Soc.,* 2001, **123**, 10762.

5. C. M. Killian, L. K. Johnson and M. Brookhart, *Organometallics,* 1997, **16**, 2005, and references therein.

6. P.J. Flory, *J. Am. Chem. Soc.,* 1940, **62**, 1661.

7. M. Brookhart, *J. Am. Chem. Soc.*, 1995, **117**, 1137.

8. W. K. Reagan, T. M. Pettijohn, J. W. Freeman and E. A. Benham, Phillips Petroleum Company, U.S. Pat. 5786431, July 28, 1998.

9. A. Carter, S. A. Cohen, N. A.Cooley and A. Murphy, *Chem. Comm.,* 2002, 858.

10. J. W. Deckers, B. Hessen and J. H. Teuben, *Organometallics*, 2002, **21**, 5122.

11. J. Dixon and A. Bollmann, 1999-2002, unpublished results.

12. H. Yang, H. Kim, J. Lee, H. Paik and H. G. Jang, *App. Cat.,* 2000, **193**, 29.

13. R. Emrich, O. Heinemann, P. W. Jolly, C. Kruger and G. P. J. Verhovnik, *Organometallics,* 1997, **16**, 1511.

14. O. Heinemann, P. W. Jolly, C. Kruger and G. P. J. Verhovnik, *J. Organomet. Chem.,* 1998, **553**, 477.

15. T. Agapie, S. J. Schofer, J. A. Labinger and J. E. Bercaw, *J. Am. Chem. Soc.,* 2004, **126**, 1304.

16 . A. Carter, S. A. Cohen, N. A. Cooley, A. Murphy, J. Scutt and D. F. Wass, *Chem. Comm,,* 2002, 858.

17. D. S. McGuinness, P. Wassercheid, W. Keim, D. Morgan, J. T. Dixon, A. Bollmann, H. Maumela, F. Hess and U. Englert, *J. Am. Chem. Soc.,* 2003, **125**, 5272.

18. T. Monoi and Y. Sasaki, *J. Mol. Cat. A : Chemical.*, 2002, **187**, 135.

19. D. H. Morgan, S. L. Schwikkard, J. T. Dixon, J. J. Nair and R. Hunter, *Adv. Synth. Cat.*, 2003, **345**, 939.

20. R. D. Kohn, M. Haufe, G. Kociok-Kohn, S. Grimm, P. Wasserscheid and W. Keim, *Angew. Chem. Int. Ed.*, 2000, **39**, 4337.

21 T. J. Kealy and P. L. Pauson, *Nature*, 1951, **168**, 632.

22. G. Wilkinson, M. Rosenblum, M. C. Whiting and R. B. Woodward, *J. Am. Chem. Soc.*, 1952, **74**, 2125.

23. R. B. Woodward, M. Rosenblum and M. C. Whiting, *J. Am. Chem. Soc.*,1952, **74**, 3458.

24. P. Beagley, M. A. L. Blackie, K. Chibale, C. Clarkson, J. R. Moss and P. J. Smith, *J. Chem. Soc., Dalton Trans.*, 2002, 4426.

25. See as a recent example : B. Hessen, *J. Mol. Cat. A : Chemical.*, 2004, **213**, 129.

26. See for example : *Inorganic Chemistry* (3rd edition), D. F. Shriver, P. W. Atkins, Oxford University Press, Oxford, 1999.

27. As a good reference : *Metallocenes, an introduction to sandwich complexes*, N. J. Long, Blackwell Science, Oxford, 1998.

28. R. B. King and M. B. Bisnette, *J. Organomet. Chem.*, 1967, **8**, 287.

29. See for example : E. J. Miller, S. J. Landon and T. B. Brill, *Organometallics*, 1985, **4**, 533.

30. M. O. Albers, D. C. Liles, D. J. Robinson, A. Shaver, E. Singleton and M. B. Wiege, *Organometallics*, 1986, **5**, 2321.

31.C. Janiak, and H. Schumann in: *Advances in Organometallic Chemistry*, Ed. F. G. A. Stone, R. West, Academic Press Inc., San Diego, 1995, Vol. **33**, 291

32 M. J. Heeg, C. Janiak, J. J. Zuckerman, H. Schumann and W. F. Manders, *J. Organomet. Chem.*, 1984, **106**, 4259.

33. R. J. Hoobler, M. A. Hutton, M. M. Dillard, M. P. Castellani, A. L. Rheingold, A. L. Rieger, P. H. Rieger, T. C. Richards and W. E. Geiger, *Organometallics*, 1993, **12**, 116.

34. E. H. Braye, W. Hubel and I. Caplier, *J. Am. Chem. Soc.*, 1961, **83**, 4406.

35. R. W. Hoffmann and P. Bovicelli, *Synthesis*, 1990, 657.

36. H. Sittzmann, *Z. Naturforsch.*, 1989, 1293

37. L. D. Field, K. M. Ho, C. M. Lindall, A. F. Masters and A. G. Webb, *Aust. J. Chem.*, 1990, **43**, 281.

38. K. Ziegler and B. Schnell, *Just. Lieb. Ann. Chem.*, 1925, **445**, 266.

39. C. Janiak, H. Schumann, C. Stader, B. Wrackmeyer and J.J. Zuckerman, *Chem. Ber.,* 1988, **121**, 1745.

40. G. R. Giesbrecht, J. C. Gordon, D. L. Clark and B. L. Scott, *J. Chem. Soc.,Dalton Trans.,* 2003, 2658.

41. G. Dyker, J. Heiermann, M. Miura, J. I. Inoh, S. Pivsa-Art, T. Satoh and M. Nomura, *Chem. Eur. J.,* 2000, **6**, 3426.

42. H. Mahomed, A. Bollmann, J. T. Dixon, V. Gokul, L. Griesel, C. Grove, F. Hess, H. Maumela, L. Pepler, *App. Cat. A: General,* 2003, **255**, 355.

43. O. Heinemann, P. W. Jolly, C. Kruger and G. P. J. Verhovnik, *J. Organomet. Chem.,* 1998, **553**, 477.

44. G. J. P. Britovsek, V. C. Gibson and D. F. Wass, *Angew. Chem. Int. Ed.,* 1999, **38**, 428.

45. F. J. Karol, G. L. Karapinka, C. Wu, A. W. Dow, R. N. Johnson, W. L. Carrick, *J. Pol. Sc.,* 1972, **10**, 2621.

46. K. H. Theopold, *Chemtech,* 1997, 26.

47. K.H. Theopold, *Eur. J. Inorg. Chem.,* 1997, 15.

48. M. Bastian, D. Morales, R. Poli, P. Richard and H. Sitzmann, *J. Organomet. Chem.,* 2003, (**654**), 109.

49. M. A. Hutton, J. C. Durham, R. W. Grady, B. E. Harris, C. S. Jarrel, J. M. Mooney and M. P. Castellani, *Organometallics,* 2001, **20**, 734.

50. R. J. Hoobler, M. A. Hutton, M. M. Dillard, M. P. Castellani, A. L. Rheingold, A. L. Rieger, P. H. Rieger, T. C. Richards and W. E. Geiger, *Organometallics,* 1993, **12**, 116.

51. J. Shamir, *Inorg. Chim. Acta,* 1989, **156**, 163.

52. O. M. Heigl, E. Herdtweck, S. Grasser, F. H. Kohler, W. Strauss and H. Zeh, *Organometallics,* 2002, **21**, 3572.

53. *Laboratory Methods in Vibrational Spectrosocpy*, Ed. H. A. Willis, J. H. van der Maas and R. G. J. Miller, John Wiley & Sons Ltd., Toronto, 1987.

54. *Metal-Ligand and Related Vibrations*, Ed. D. M. Adams, Edward Arnold Publishers Ltd., London, 1966.

55. A useful text : *Electron Spin Resonance, elementary theory and applications,* J. E. Wertz and J. R. Bolton, Chapman and Hall, London, 1986.

56. *Advanced inorganic chemistry,* fifth ed., F. A. Cotton and G. Wilkinson, John Wiley and Sons, Toronto, 1988.

57. R. Poli, *Private communication.*

58. K. P. Bryliakov, M. V. Lobanova and E. P. Talsi, *J. Chem. Soc., Dalton Trans.,* 2002, 2263.

59. N. Shaham, H. Cohen, D. Meyerstein and E. Bill, *J. Chem. Soc., Dalton Trans.,* 2002, 3082.

60. S. P. Mattamana and R. Poli, *Organometallics,* 1997, **16**, 2427.

61. O. M. Heigl, E. Herdtweck, S. Grasser, F. H. Kohler, W. Strauss and H. Zeh, *Organometallics,* 2002, **21**, 3572.

62. F. H. Kohler, J. Lachmann, G. Muller, H. Zeh, H. Brunner, J. Pfauntsch and J. Wachter, *J. Organomet. Chem.,* 1989, **365**, C16.

63. D.S. Richeson, J. F. Mitchell and K. H. Theopold, *Organometallics,* 1989, **8**, 2570.

64. P. Wei and D. W. Stephan, *Organometallics,* 2003, **22**, 1712

65. M. Castellani, Private Communication.

66. As an example: M. Enders, P. Fernandez, S. Mihan, H. Pritzkow, *J. Organomet. Chem.,* 2003, **687**, 125.

67. M. P. Castellani, J. M. Wright, S. J. Geib, A. L. Rheingold, W. C. Trogler, *Organometallics,* 1986, **5**, 1116.

68. M. P. Castellani, S. J. Geib, A. L. Rheingold and W. C. Trogler, *Organometallics,* 1987, **6**, 1703.

69. H. Schumann, A. Lentz, R. Weimann and J. Pickardt, *Angew. Chem. Int. Ed,* 1994, **33**, 1731

70. F. A. Cotton, S. A. Duraj, G. L. Powell and W. J. Roth, *Inorg. Chim. Acta,* 1986, **113**, 81.

71. Figure taken from http://www.parrinst.com.

72. P. Hohenberg and W. Kohn, *Phys. Rev.*, 1964, B864

73. E. J. Baerends and O. V. Gritsenko, *J. Chem. Phys.,* 1997, **101**, 5383.

74. W. Kohn, L. J. Sham, *Phys. Rev.,* 1965, **140**, A1133.

75. J. C. Slater, *Phys. Rev.,* 1951, **81**, 385.

76. S.J. Vosko, L. Wilk and M. Nusair, *Can. J. Phys.,* 1980, **58**, 1200.

77. J. D. Perdew and Y. Wang, *Phys. Rev.,* B, 1986, **33**, 8800.

78. A. D. Becke, *Phys. Rev.,* B, 1988, **38**, 3098.

79. A. D. Becke and M. R. Roussel, *Phys. Rev. A.,* 1989, **39**, 3761.

80. *Introduction to Computational Chemistry,* Frank Jensen, John Wiley and Sons, Chichester, 1999.

81. W. J. Janse van Rensberg, C. Grove, J. P. Steynberg, K. B. Stark, J. J. Huyser and P. J. Steynberg, *Organometallics,* 2004, **23**, 1207.

82. Z. X. Yu and K. N. Houk, *Angew. Chem. Int. Ed.,* 2003, **42**, 808.

83. A. N. J. Blok, A. W. Gal and P. H. M. Budzelaar, *Organometallics,* 2003, **22**, 2564.

84. T. J. M. de Bruin, L. Magna, H. Toulhoat and P. Raybaud, *Organometallics,* 2003, **22**, 3404.

85. All calculations were performed with the DMol^3 program : Dmol^3 (Version 2.2), B. Delley, *J. Chem. Phys.,* 1990, **92**, 508.

86 . See for example : R. Kari, *J. Quantum. Chem.,* 1984, **25**, 321.

87. See for example : P. Maragakis, S. A. Andreev, Y. Brumer, D. R. Reichman, E. Kaxiras, *J. Chem. Phys.,* 2002, **1170**, 4651.

88. As a good reference : *Experimental Organometallic Chemistry – a practicum in synthesis and characterization.* Ed. A. L. Wayda and M. Y. Darensbourg, ACS Symposium Series, 1985.

89. Private communications : Dr. Reinout Meijboom, Dr M. J. Overett, *University of Cape Town.*

90. D. D. Perin and W. L. F. Armarego, *Purification of Laboratory Chemicals,* Pergamon Press, 1988.

91. COLLECT, Data Collection Software, BV Nonius, Delft, The Netherlands, 2000.

92. G.M. Sheldrick, SHELX97, Program for Solving Crystal Structures, University of Gottingen, Gottingen, Germany, 1997.

93. Melting point taken from Aldrich catalogue, 2004.

Appendices

A1 : Appendix A – X-ray Crystal data (additional information)

Empirical formula	C_{12} H_{24} Cl_3 Cr O_3
Formula weight	374.66
Temperature	113(2) K
Wavelength	0.71073 A
Crystal system, space group	Monoclinic, P21/c
Unit cell dimensions	a = 8.01240(10) Å alpha = 90 deg. b = 12.44290(10) Å beta = 92.6030(10) deg. c = 16.3678(5) Å gamma = 90 deg.
Volume	1630.14(6) A^3
Z, Calculated density	4, 1.527 Mg/m^3
Absorption coefficient	1.194 mm^-1
F(000)	780
Crystal size	0.20 x 0.15 x 0.15 mm
Theta range for data collection	4.30 to 26.75 deg.
Limiting indices	-10<=h<=10, -15<=k<=15, -20<=l<=20
Reflections collected / unique	44881 / 3457 [R(int) = 0.0301]
Completeness to theta =	26.75 99.4 %
Max. and min. transmission	0.8413 and 0.7962
Refinement method	Full-matrix least-squares on F^2
Data / restraints / parameters	3457 / 0 / 173
Goodness-of-fit on F^2	1.048
Final R indices [I>2sigma(I)]	R1 = 0.0332, wR2 = 0.0803
R indices (all data)	R1 = 0.0405, wR2 = 0.0853

Extinction coefficient	0.0022(8)
Largest diff. peak and hole	1.644 and -0.525 e.A^-3

Table 1 Crystal data and structure refinement for $CrCl_3(thf)_3$

	x	y	z	U(*eq*)
Cr(1)	2625(1)	7529(1)	2475(1)	16(1)
Cl(1)	391(1)	6876(1)	1670(1)	22(1)
Cl(2)	2919(1)	5903(1)	3123(1)	25(1)
Cl(3)	4786(1)	8272(1)	3272(1)	23(1)
O(1)	4263(2)	7173(1)	1603(1)	20(1)
O(2)	1013(2)	8051(1)	3287(1)	23(1)
O(3)	2324(2)	8986(1)	1876(1)	19(1)
C(4)	4230(3)	6204(2)	1096(1)	20(1)
C(11)	2375(3)	10201(2)	781(2)	34(1)
C(7)	-1125(3)	9006(2)	3923(1)	25(1)
C(3)	5797(3)	6266(2)	607(1)	26(1)
C(10)	2145(3)	10839(2)	1561(2)	30(1)
C(1)	5731(3)	7823(2)	1424(1)	25(1)
C(9)	2743(3)	10053(2)	2214(1)	24(1)
C(2)	6159(3)	7473(2)	580(1)	26(1)
C(8)	-563(3)	8622(2)	3101(1)	21(1)
C(6)	382(3)	8842(2)	4508(2)	38(1)
C(5)	1225(3)	7905(2)	4169(1)	29(1)
C(12)	1795(3)	9094(2)	1016(1)	28(1)

Table 2 Atomic coordinates (x 10^4) and equivalent isotropic displacement parameters (A^2 x 10^3) for $CrCl_3(thf)_3$ U(eq) is defined as one third of the trace of the orthogonalized Uij tensor.

Cr(1)-O(2)	2.0030(15)
Cr(1)-O(1)	2.0308(14)
Cr(1)-O(3)	2.0700(14)
Cr(1)-Cl(2)	2.2921(6)
Cr(1)-Cl(3)	2.3131(6)
Cr(1)-Cl(1)	2.3202(6)
O(1)-C(4)	1.463(2)
O(1)-C(1)	1.468(2)
O(2)-C(5)	1.457(2)
O(2)-C(8)	1.469(2)
O(3)-C(12)	1.458(2)
O(3)-C(9)	1.471(2)
C(4)-C(3)	1.521(3)

C(4)-H(4A)	0.99
C(4)-H(4B)	0.99
C(11)-C(12)	1.509(3)
C(11)-C(10)	1.521(4)
C(11)-H(11A)	0.99
C(11)-H(11B)	0.99
C(7)-C(8)	1.515(3)
C(7)-C(6)	1.521(3)
C(7)-H(7A)	0.99
C(7)-H(7B)	0.99
C(3)-C(2)	1.530(3)
C(3)-H(3A)	0.99
C(3)-H(3B)	0.99
C(10)-C(9)	1.512(3)
C(10)-H(10A)	0.99
C(10)-H(10B)	0.99
C(1)-C(2)	1.504(3)
C(1)-H(1A)	0.99
C(1)-H(1B)	0.99
C(9)-H(9A)	0.99
C(9)-H(9B)	0.99
C(2)-H(2A)	0.99
C(2)-H(2B)	0.99
C(8)-H(8A)	0.99
C(8)-H(8B)	0.99
C(6)-C(5)	1.469(4)
C(6)-H(6A)	0.99
C(6)-H(6B)	0.99
C(5)-H(5A)	0.99
C(5)-H(5B)	0.99
C(12)-H(12A)	0.99
C(12)-H(12B)	0.99

O(2)-Cr(1)-O(1)	173.54(6)
O(2)-Cr(1)-O(3)	88.02(6)
O(1)-Cr(1)-O(3)	85.63(6)
O(2)-Cr(1)-Cl(2)	92.00(5)
O(1)-Cr(1)-Cl(2)	94.37(5)
O(3)-Cr(1)-Cl(2)	178.98(4)
O(2)-Cr(1)-Cl(3)	89.12(5)
O(1)-Cr(1)-Cl(3)	89.57(4)
O(3)-Cr(1)-Cl(3)	89.17(4)
Cl(2)-Cr(1)-Cl(3)	91.85(2)
O(2)-Cr(1)-Cl(1)	89.21(5)
O(1)-Cr(1)-Cl(1)	91.80(4)
O(3)-Cr(1)-Cl(1)	88.15(4)
Cl(2)-Cr(1)-Cl(1)	90.83(2)
Cl(3)-Cr(1)-Cl(1)	176.89(2)
C(4)-O(1)-C(1)	109.56(15)

C(4)-O(1)-Cr(1)	125.66(12)
C(1)-O(1)-Cr(1)	124.68(12)
C(5)-O(2)-C(8)	109.05(15)
C(5)-O(2)-Cr(1)	124.57(12)
C(8)-O(2)-Cr(1)	126.38(12)
C(12)-O(3)-C(9)	109.39(16)
C(12)-O(3)-Cr(1)	124.08(12)
C(9)-O(3)-Cr(1)	126.31(12)
O(1)-C(4)-C(3)	105.25(16)
O(1)-C(4)-H(4A)	110.7
C(3)-C(4)-H(4A)	110.7
O(1)-C(4)-H(4B)	110.7
C(3)-C(4)-H(4B)	110.7
H(4A)-C(4)-H(4B)	108.8
C(12)-C(11)-C(10)	102.21(19)
C(12)-C(11)-H(11A)	111.3
C(10)-C(11)-H(11A)	111.3
C(12)-C(11)-H(11B)	111.3
C(10)-C(11)-H(11B)	111.3
H(11A)-C(11)-H(11B)	109.2
C(8)-C(7)-C(6)	104.90(18)
C(8)-C(7)-H(7A)	110.8
C(6)-C(7)-H(7A)	110.8
C(8)-C(7)-H(7B)	110.8
C(6)-C(7)-H(7B)	110.8
H(7A)-C(7)-H(7B)	108.8
C(4)-C(3)-C(2)	103.13(17)
C(4)-C(3)-H(3A)	111.1
C(2)-C(3)-H(3A)	111.1
C(4)-C(3)-H(3B)	111.1
C(2)-C(3)-H(3B)	111.1
H(3A)-C(3)-H(3B)	109.1
C(9)-C(10)-C(11)	102.11(19)
C(9)-C(10)-H(10A)	111.3
C(11)-C(10)-H(10A)	111.3
C(9)-C(10)-H(10B)	111.3
C(11)-C(10)-H(10B)	111.3
H(10A)-C(10)-H(10B)	109.2
O(1)-C(1)-C(2)	104.00(17)
O(1)-C(1)-H(1A)	111
C(2)-C(1)-H(1A)	111
O(1)-C(1)-H(1B)	111
C(2)-C(1)-H(1B)	111

H(1A)-C(1)-H(1B)	109
O(3)-C(9)-C(10)	104.92(17)
O(3)-C(9)-H(9A)	110.8
C(10)-C(9)-H(9A)	110.8
O(3)-C(9)-H(9B)	110.8
C(10)-C(9)-H(9B)	110.8
H(9A)-C(9)-H(9B)	108.8
C(1)-C(2)-C(3)	101.88(18)
C(1)-C(2)-H(2A)	111.4
C(3)-C(2)-H(2A)	111.4
C(1)-C(2)-H(2B)	111.4
C(3)-C(2)-H(2B)	111.4
H(2A)-C(2)-H(2B)	109.3
O(2)-C(8)-C(7)	104.81(16)
O(2)-C(8)-H(8A)	110.8
C(7)-C(8)-H(8A)	110.8
O(2)-C(8)-H(8B)	110.8
C(7)-C(8)-H(8B)	110.8
H(8A)-C(8)-H(8B)	108.9
C(5)-C(6)-C(7)	103.5(2)
C(5)-C(6)-H(6A)	111.1
C(7)-C(6)-H(6A)	111.1
C(5)-C(6)-H(6B)	111.1
C(7)-C(6)-H(6B)	111.1
H(6A)-C(6)-H(6B)	109
O(2)-C(5)-C(6)	103.88(19)
O(2)-C(5)-H(5A)	111
C(6)-C(5)-H(5A)	111
O(2)-C(5)-H(5B)	111
C(6)-C(5)-H(5B)	111
H(5A)-C(5)-H(5B)	109
O(3)-C(12)-C(11)	104.53(18)
O(3)-C(12)-H(12A)	110.8
C(11)-C(12)-H(12A)	110.8
O(3)-C(12)-H(12B)	110.8
C(11)-C(12)-H(12B)	110.8
H(12A)-C(12)-H(12B)	108.9

Table 3 Bond lengths [A] and angles [deg] for $CrCl_3(thf)_3$

U11	U22	U33	U23	U13	U12

Cr(1)	14(1)	17(1)	16(1)	-3(1)	0(1)	1(1)
Cl(1)	17(1)	26(1)	21(1)	-6(1)	0(1)	-3(1)
Cl(2)	24(1)	21(1)	30(1)	4(1)	4(1)	4(1)
Cl(3)	19(1)	26(1)	24(1)	-5(1)	-6(1)	1(1)
O(1)	17(1)	18(1)	25(1)	-7(1)	5(1)	-4(1)
O(2)	20(1)	35(1)	15(1)	-3(1)	-3(1)	12(1)
O(3)	24(1)	16(1)	17(1)	-2(1)	-4(1)	-1(1)
C(4)	21(1)	17(1)	21(1)	-4(1)	3(1)	-1(1)
C(11)	40(1)	32(1)	30(1)	8(1)	0(1)	-2(1)
C(7)	20(1)	30(1)	25(1)	-5(1)	2(1)	4(1)
C(3)	26(1)	26(1)	27(1)	-4(1)	8(1)	2(1)
C(10)	28(1)	20(1)	41(1)	4(1)	0(1)	-1(1)
C(1)	17(1)	26(1)	33(1)	-6(1)	5(1)	-7(1)
C(9)	25(1)	16(1)	31(1)	-5(1)	1(1)	-2(1)
C(2)	23(1)	29(1)	28(1)	1(1)	7(1)	-5(1)
C(8)	16(1)	26(1)	21(1)	0(1)	0(1)	6(1)
C(6)	39(1)	51(2)	25(1)	-3(1)	2(1)	9(1)
C(5)	31(1)	44(1)	13(1)	0(1)	-2(1)	13(1)
C(12)	38(1)	28(1)	18(1)	2(1)	-8(1)	-1(1)

Table 4 Anisotropic displacement parameters (A^2 x 10^3) for $CrCl_3(thf)_3$. The anisotropic displacement factor exponent takes the form: -2 pi^2 [h^2 a*^2 U11 + ... + 2 h k a* b* U12]

	x	y	z	U(*eq*)
H(4A)	3217	6191	727	23
H(4B)	4245	5551	1441	23
H(11A)	1680	10496	318	41
H(11B)	3560	10194	633	41
H(7A)	-2089	8579	4097	30
H(7B)	-1449	9773	3897	30
H(3A)	5593	5971	50	31
H(3B)	6733	5871	884	31
H(10A)	2831	11500	1574	36
H(10B)	958	11034	1620	36
H(1A)	6667	7678	1824	30
H(1B)	5462	8599	1435	30
H(9A)	3963	10121	2327	29
H(9B)	2167	10178	2728	29
H(2A)	7347	7615	478	32
H(2B)	5444	7836	155	32
H(8A)	-1403	8134	2838	25
H(8B)	-385	9238	2731	25
H(6A)	1120	9481	4517	46

H(6B)	33	8696	5069	46
H(5A)	2423	7893	4345	35
H(5B)	697	7228	4342	35
H(12A)	566	9032	941	34
H(12B)	2322	8536	682	34

Table 5 Hydrogen coordinates (x 10^4) and isotropic displacement parameters (A^2 x 10^3) for $CrCl_3(thf)_3$

O(2)-Cr(1)-O(1)-C(4)	-139.0(5)
O(3)-Cr(1)-O(1)-C(4)	-127.99(16)
Cl(2)-Cr(1)-O(1)-C(4)	50.98(15)
Cl(3)-Cr(1)-O(1)-C(4)	142.81(15)
Cl(1)-Cr(1)-O(1)-C(4)	-39.99(15)
O(2)-Cr(1)-O(1)-C(1)	45.2(6)
O(3)-Cr(1)-O(1)-C(1)	56.13(16)
Cl(2)-Cr(1)-O(1)-C(1)	-124.90(16)
Cl(3)-Cr(1)-O(1)-C(1)	-33.07(16)
Cl(1)-Cr(1)-O(1)-C(1)	144.13(16)
O(1)-Cr(1)-O(2)-C(5)	-126.3(5)
O(3)-Cr(1)-O(2)-C(5)	-137.21(18)
Cl(2)-Cr(1)-O(2)-C(5)	43.81(18)
Cl(3)-Cr(1)-O(2)-C(5)	-48.01(18)
Cl(1)-Cr(1)-O(2)-C(5)	134.62(18)
O(1)-Cr(1)-O(2)-C(8)	54.6(6)
O(3)-Cr(1)-O(2)-C(8)	43.68(16)
Cl(2)-Cr(1)-O(2)-C(8)	-135.30(16)
Cl(3)-Cr(1)-O(2)-C(8)	132.87(16)
Cl(1)-Cr(1)-O(2)-C(8)	-44.50(16)
O(2)-Cr(1)-O(3)-C(12)	-123.98(16)
O(1)-Cr(1)-O(3)-C(12)	57.25(16)
Cl(2)-Cr(1)-O(3)-C(12)	-33(3)
Cl(3)-Cr(1)-O(3)-C(12)	146.88(16)
Cl(1)-Cr(1)-O(3)-C(12)	-34.70(16)
O(2)-Cr(1)-O(3)-C(9)	61.92(15)
O(1)-Cr(1)-O(3)-C(9)	-116.85(16)
Cl(2)-Cr(1)-O(3)-C(9)	153(3)
Cl(3)-Cr(1)-O(3)-C(9)	-27.22(15)
Cl(1)-Cr(1)-O(3)-C(9)	151.20(15)
C(1)-O(1)-C(4)-C(3)	1.8(2)
Cr(1)-O(1)-C(4)-C(3)	-174.60(13)
O(1)-C(4)-C(3)-C(2)	-25.2(2)
C(12)-C(11)-C(10)-C(9)	40.7(2)
C(4)-O(1)-C(1)-C(2)	22.9(2)
Cr(1)-O(1)-C(1)-C(2)	-160.66(14)
C(12)-O(3)-C(9)-C(10)	10.0(2)
Cr(1)-O(3)-C(9)-C(10)	-175.16(13)
C(11)-C(10)-C(9)-O(3)	-31.4(2)
O(1)-C(1)-C(2)-C(3)	-37.7(2)

C(4)-C(3)-C(2)-C(1)	38.7(2)
C(5)-O(2)-C(8)-C(7)	10.8(2)
Cr(1)-O(2)-C(8)-C(7)	-169.98(14)
C(6)-C(7)-C(8)-O(2)	12.5(2)
C(8)-C(7)-C(6)-C(5)	-31.0(3)
C(8)-O(2)-C(5)-C(6)	-30.7(3)
Cr(1)-O(2)-C(5)-C(6)	150.10(17)
C(7)-C(6)-C(5)-O(2)	37.4(3)
C(9)-O(3)-C(12)-C(11)	15.9(2)
Cr(1)-O(3)-C(12)-C(11)	-159.11(15)
C(10)-C(11)-C(12)-O(3)	-35.1(2)

Table 6 Torsion angles [deg] for $CrCl_3(thf)_3$

D-H...A	d(D-H)	d(H...A)	d(D...A)	<(DHA)

Table 7 Hydrogen bonds for $CrCl_3(thf)_3$ [A and deg.].

Appendix A2 – Full Tabulated product distribution of catalytic reactions

A2.1 In-situ system – Cr-2-ethyl hexanoate, C_2Cl_6, TEA, C_5Ph_5H, ethene

Batch Trimerisation Run	**C_5Ph_5H system**		**2/7/2003**		
Combined fractions					
Compounds in liquid phase	**GC Area**	**Corrected Area**	**Mass %**	**Mass (g)**	**Internal std**
C-2	804	804	0.01	0.02	
C-4 (olefins + butane)	4654	4654	0.08	0.12	
C-5 (olefin + OH + pentane)	1592	1592	0.03	0.04	
C-6 (branched olefins + n-hexane)	0	0	0.00	0.00	
C-6 (internal n-olefins)	153740	153740	2.75	4.02	
C-6 (methylene-cyclopentane, cyclohex)	3371	3371	0.06	0.09	
C-6 (methyl-cyclopentane)	0	0	0.00	0.00	
1-Hexene	620385	620385	11.09	16.21	
EtOH (RF = 0.46)	0	0	0.00	0.00	
C-3 OH (RF = 0.60)	0	0	0.00	0.00	
C-7 (olefins + parafins + n-heptane)	0	0	0.00	0.00	
Cyclohexane	4355805	4660711.35	83.29	121.75	
C-8 (olefin + parafin + n-heptane)	2784	2784	0.05	0.07	
C-9 (olefin)	0	0	0.00	0.00	
Nonane	93478	93478	1.67	2.44	2.4419
C-10 (olefin + paraffin + n-decane)	50561	50561	0.90	1.32	
C-11 (olefin)	0	0	0.00	0.00	
C-12 (olefin)	0	0	0.00	0.00	
Heavies	3830	3830	0.07	0.10	
Unknown	0	0	0.00	0.00	
Total	**5291004**	**5595910**	**100**	**146.18**	
Liquid product area	**841721**				

Product	**Mass (g)**	**Mass (%)**	
Polimeric product	0.097	0.44	pol. estmtd.
Liquid product	21.99	99.56	

Catalyst performance			**Selectivity (%)**
Cr (mmole)	0.0207		
Cr (g)	0.0011	C-6	92.8
Activity (g Product/g Cr/h)	39978	1-Hexene	79.8
Tot. Activity (g liq. + g pol./g Cr/h)	40155		
Cat. Concentration (mmol/L)			

	Mass (g)
Ethylene in (massflowmeter)	

Total mass in (gas + liquid)	124.19
Total liquid out	146.18

A2.2 System : $[(C_5Ph_5)CrCl_2]_2$, TEA, ethene

Batch Trimerisation Run Combined fractions	**dinuclear model Complex**		**2/7/2003**		
Compounds in liquid phase	**GC Area**	**Corrected Area**	**Mass %**	**Mass (g)**	**Internal std**
C-2	2916	2916	0.04	0.05	
C-4 (olefins + butane)	51791	51791	0.77	0.82	
C-5 (olefin + OH + pentane)	1899	1899	0.03	0.03	
C-6 (branched olefins + n-hexane)	0	0	0.00	0.00	
C-6 (internal n-olefins)	180923	180923	2.68	2.87	
C-6 (methylene-cyclopentane, cyclohex)	3085	3085	0.05	0.05	
C-6 (methyl-cyclopentane)	0	0	0.00	0.00	
1-Hexene	744975	744975	11.04	11.80	
EtOH (RF = 0.46)	0	0	0.00	0.00	
C-3 OH (RF = 0.60)	0	0	0.00	0.00	
C-7 (olefins + parafins + n-heptane)	0	0	0.00	0.00	
Cyclohexane	5132778	5492072.46	81.35	87.00	
C-8 (olefin + parafin + n-heptane)	4260	4260	0.06	0.07	
C-9 (olefin)	0	0	0.00	0.00	
Nonane	190182	190182	2.82	3.01	3.0126
C-10 (olefin + paraffin + n-decane)	71570	71570	1.06	1.13	
C-11 (olefin)	0	0	0.00	0.00	
C-12 (olefin)	0	0	0.00	0.00	
Heavies	7344	7344	0.11	0.12	
Unknown	0	0	0.00	0.00	
Total	**6391723**	**6751017**	**100**	**106.94**	
Liquid product area	**1068763**				

Product	**Mass (g)**	**Mass (%)**	
Polimeric product	0.097	0.57	pol. estmtd.
Liquid product	16.93	99.43	

Catalyst performance			**Selectivity (%)**
Cr (mmole)	0.0207		
Cr (g)	0.0011	C-6	87.5
Activity (g Product/g Cr/h)	30782	1-Hexene	80.2
Tot. Activity (g liq. + g pol./g Cr/h)	30958		
Cat. Concentration (mmol/L)			

	Mass (g)
Ethylene in (massflowmeter)	
Total mass in (gas + liquid)	90.01
Total liquid out	106.94

A2.1 In-situ system – Cr-2-ethyl hexanoate, C_2Cl_6, TEA, $C_5Ph_4H_2$, ethene

Batch Trimerisation Run Combined fractions	$C_5Ph_4H_2$ system		2/7/2003		
Compounds in liquid phase	**GC Area**	**Corrected Area**	**Mass %**	**Mass (g)**	**Internal std**
C-2	10565	10565	0.17	0.21	
C-4 (olefins + butane)	12125	12125	0.20	0.25	
C-5 (olefin + OH + pentane)	248	248	0.00	0.01	
C-6 (branched olefins + n-hexane)	0	0	0.00	0.00	
C-6 (internal n-olefins)	133113	133113	2.17	2.70	
C-6 (methylene-cyclopentane, cyclohex)	4476	4476	0.07	0.09	
C-6 (methyl-cyclopentane)	0	0	0.00	0.00	
1-Hexene	204371	204371	3.33	4.14	
EtOH (RF = 0.46)	0	0	0.00	0.00	
C-3 OH (RF = 0.60)	0	0	0.00	0.00	
C-7 (olefins + parafins + n-heptane)	0	0	0.00	0.00	
Cyclohexane	5189354	5552608.78	90.45	112.44	
C-8 (olefin + parafin + n-heptane)	3628	3628	0.06	0.07	
C-9 (olefin)	0	0	0.00	0.00	
Nonane	151546	151546	2.47	3.07	3.0689
C-10 (olefin + paraffin + n-decane)	63105	63105	1.03	1.28	
C-11 (olefin)	0	0	0.00	0.00	
C-12 (olefin)	0	0	0.00	0.00	
Heavies	3301	3301	0.05	0.07	
Unknown	0	0	0.00	0.00	
Total	**5775832**	**6139087**	**100**	**124.32**	
Liquid product area	**434932**				

Product	**Mass (g)**	**Mass (%)**	
Polimeric product	0.097	1.09	pol. estmtd.
Liquid product	8.81	98.91	

Catalyst performance			**Selectivity (%)**
Cr (mmole)	0.0207		
Cr (g)	0.0011	C-6	81.3
Activity (g Product/g Cr/h)	16014	1-Hexene	59.8
Tot. Activity (g liq. + g pol./g Cr/h)	16190		
Cat. Concentration (mmol/L)			

	Mass (g)
Ethylene in (massflowmeter)	
Total mass in (gas + liquid)	115.51

Total liquid out	124.32